DEPARTMENT OF CIVIL ENGINEERING
UNIVERSITY OF SOUTHERN CALIFORNIA

DEPENDENCE OF PSEUDO RELATIVE VELOCITY SPECTRA OF STRONG MOTION ACCELERATION ON THE DEPTH OF SEDIMENTARY DEPOSITS

by

M.D. Trifunac and V.W. Lee

Report No. CE 79-02

A Report on the Research Conducted Under a Contract
from the U.S. Nuclear Regulatory Commission

Los Angeles, California

February, 1979

ABSTRACT

Reports on the observed damage caused by destructive earthquake ground motion and numerous instrumented studies have shown that the nature of strong shaking is influenced by the local site conditions. While the manner of characterization of these effects and the choice of their physical "basis" still represents a topic associated with many uncertainties, it has become possible, during the past several years, to improve the description of these effects empirically. This report presents some recent accomplishments in the analysis of these effects by focusing on the dependence of Pseudo Relative Velocity spectrum amplitudes on the "size" of local geologic inhomogeneities. It presents the empirical scaling functions of these spectra in terms of (a) magnitude and epicentral distance, or (b) Modified Mercalli Intensity at the site. It also considers differences between horizontal and vertical ground motions, dependence of amplitudes on depth of alluvium deposits beneath the site and the distribution of spectral amplitudes about the empirical scaling functions.

INTRODUCTION

Numerous recent studies have shown that the site conditions contribute significantly to the changes of amplitude (Trifunac and Brady, 1975; Trifunac, 1976; 1979; Trifunac and Anderson, 1977; 1978a,b; Trifunac and Lee, 1978) and of duration (Trifunac and Westermo, 1976; 1977; Westermo and Trifunac, 1978; 1979) of strong earthquake ground motion. There is little doubt now that in the linear response range, wave amplitudes with periods longer than about 0.3 sec are amplified as they propagate through "softer" geologic deposits. Amplitudes appear to be attenuated, though not significantly, for periods shorter than about 0.3 sec, thus leading to larger amplitudes of strong shaking for high frequency at igneous rock sites.

As in other wave propagation phenomena, the amplitudes of strong earthquakes waves once emitted from the source depend mainly on the variation of impedance and on the "size" of the inhomogeneities encountered along the propagation path. If the impedance jump across a discontinuity is large and if the size of the inhomogeneity is comparable to or greater than the wavelength of incident motion, major reflections and scattering will result in significant changes in the observed amplitudes of motion. Since the strong earthquake shaking of interest to earthquake engineering falls in the frequency range from about 0.1 Hz to about 20 Hz and since the seismic wave velocity near the earth's surface is in the range from about 0.1 km/sec to about 3 km/sec, it is seen that the corresponding wavelengths are from about 50 km to about 30 km. Thus, the geologic inhomogeneities of dimensions within and close to this range will influence the observed wave amplitudes. Furthermore, since the strong shaking is typically destructive only at distances less than 50-100 km from the source (Trifunac and Brady, 1975), it is seen that the entire transmission path will contribute to the changes in wave amplitudes. It follows that the extent of "local" site conditions must be measured in terms of the wavelengths associated with the periods of motion which are most important for a particular analysis. For a tall building, a dam, or a bridge, for example, these "local" site dimensions might be of the order of 10 km. For a stiff, small building, these dimensions may be from 10 m to several hundred meters.

How the "local" site conditions change the incident wave motions depends also on the direction of wave arrival. In a realistic three-dimensional setting the wave focusing and amplification may become very complex and difficult to predict deterministically. If one knew (1) where the next earthquake will occur, and (2) if one had a realistic three-dimensional model of "local" conditions, it would be possible to compute detailed transfer functions for a site. Unfortunately, at present, neither of these two conditions can be met. The candidate sites for future earthquake loci can be speculated on only through some type of model of local seismicity. The three-dimensional geologic mapping up to the depths of say 10 km is not available for many parts of the world and when something is available, the spatial resolution and detail may not always be adequate for the purpose of deterministic computations. Even when must of the required information is available, it still will be necessary to describe the result in terms of a distribution function because: (1) earthquake sources are distributed in space and time and their future occurrence can be described only in a probabilistic manner; and (2) the deterministic calculations of waves propagating in three dimensions through an inhomogeneous medium will, for some time, be able to provide credible results only for periods of ground motion longer than say 1 second (Anderson and Trifunac, 1977). Thus, it is seen that some type of random approach for representation of higher frequencies may be required.

At present, many investigators continue to study the effects of local conditions by employing simplified site classification in which the overall depth of near surface soil layers is typically of the order of tens of meters. From the linear wave propagation viewpoint, it can be seen that this approach is capable of portraying the effects in the high frequency range only (say, $f > 5$ Hz). For these high frequencies (short wavelengths), inhomogeneities in the top 10 km of the earth's crust lead to significant "random" scattering so that it appears optimistic to expect that deterministic calculations for the top hundred meters near the ground surface may have any significant additional impact on the overall picture of the motion there.

Significant trends in the duration of strong shaking (Westermo and Trifunac, 1978; 1979) and in the Fourier spectrum amplitudes (Trifunac and Lee, 1978) at intermediate and at long period motion require that local effects be measured on the scale of kilometers. This suggests description of local conditions in terms of the overall geologic structure there. By using the geologic site classification of Trifunac and Brady (1975), it has been possible to develop a family of empirical scaling laws for different spectral amplitudes (Trifunac and Anderson, 1977; 1978a,b) and for the duration of strong shaking (Trifunac and Westermo, 1976; 1977). While these models will remain useful for the estimation of amplitudes and of duration of strong shaking when only limited near-surface geology is known at the site, analyses show that a more refined site classification should incorporate some measure of the "size" of the local inhomogeneities (Westermo and Trifunac, 1978; 1979; Trifunac and Lee, 1978).

The aim of this report is to show that the scaling of the Pseudo Relative Velocity (PSV) spectra can be analyzed by introducing the depth of sediments beneath the site as a scaling parameter. In general, wave velocities and rigidities increase with depth. While these increases may be irregular functions of depth, significant increases in velocity and in rigidity should be experienced at the transition from sediments into sound igneous rock. Therefore, the impedance jumps and the depth of these discontinuities may then play an important role in governing the wave amplitudes and the number of consecutive reflections (duration) of strong motion between the ground surface and this "strongest" discontinuity. While the depth of sediments alone is far from sufficient to describe all important properties of the local site conditions, other analyses show that the depth as a parameter does contribute to the changes of Fourier amplitudes and of duration.

The estimates of the depths of sedimentary and alluvial deposits beneath recording stations considered in this analysis range from 0 km to about 6 km, with most sites having depth less than about 4 km. Computation of these depths and other characteristics of the data base is described elsewhere and need not be repeated here (Westermo and Trifunac, 1978).

SCALING OF PSV SPECTRA IN TERMS OF M, R, h AND v

In following the direction of the preceeding analyses (Trifunac and Lee, 1978), the dependence of the spectral amplitudes of strong motion is presented here in terms of the functional form of the definition of the local magnitude scale, M, and with a "correction" function which includes the effects of geologic site conditions (h), horizontal versus vertical motions (v=0 for horizontal and v=1 for vertical), frequency dependent attenuation and the distribution of observed amplitudes with respect to the assumed model amplitudes. In contrast with the earlier model for scaling of PSV spectrum amplitudes (Trifunac and Anderson, 1977) which was based on rough site classification (s=0 for alluvium, s=2 for igneous basement rock sites, and s=1 for intermediate sites), in this paper, we introduce a more continuous dependence on the "size" of local geologic conditions in terms of h (measured in km) and representing the depth of sediments beneath the station. The scaling equation is then

$$\log_{10}[PSV(T)] = M + \log_{10}A_0(R) - b(T)M - c(T) - d(T)h - e(T)v - f(T)M^2 - g(T)R \quad . \tag{1}$$

In (1), PSV(T) is the amplitude of PSV spectra at period T and $\log_{10}A_0(R)$ represents the empirically determined function describing the overall attenuation of amplitudes with epicentral distance, R (Richter, 1958).

The scaling functions b(T) through g(T) are determined through the regression analysis at 91 periods. This analysis is performed in such a way as to minimize the possible bias in the result that may come from uneven distribution of data among magnitude, site conditions and from the abundance of data for some earthquakes. All procedures in data preparation and selection, and the form of the regression analysis employed here are the same as in Trifunac and Lee (1978), and in Trifunac and Anderson (1977), and thus will not be repeated here.

After smoothing along $\log_{10}T$ axis, the functions a(T) through g(T) (Figure 1) can be described by their amplitudes at 11 periods between $T = 0.04$ sec and $T = 7.5$ sec (Table I). The 11 periods appear to be sufficient for most practical computations since the smoothness of b(T) through g(T) is such that almost any interpolation scheme will yield adequate estimates of their amplitudes at intermediate periods.

The functional form of the dependence of $\log_{10}[PSV(T)]$ on h was examined in some detail since there is no obvious physical reason why it should be linear in h. Several regression analyses have shown that only d(T)h is a significant contributor to (1) with coefficients of h^2, h^3 and higher powers of h leading to the values which were undistinguishable from zero at 95% confidence level.

If $\hat{b}(T)$ through $\hat{g}(T)$ represent the best estimates of the functions b(T) through g(T), the $\log_{10}[\hat{PSV}(T)]$ represents the best estimate of $\log_{10}[PSV(T)]$ at some period T. The residuals

$$\varepsilon(T) = \log_{10}[PSV(T)] - \log_{10}[\hat{PSV}(T)] \qquad (2)$$

where in $\log_{10}[PSV(T)]$ the PSV spectrum is computed from recorded accelerograms then describe the distribution of the observed PSV(T) about the estimated $\hat{PSV}(T)$. In this work, we assume that $\varepsilon(T)$ can be described by a distribution of the form (Trifunac and Anderson, 1977; 1978a)

$$p(\varepsilon,T) = [1 - \exp(-\exp(\alpha(T)\varepsilon(T) + \beta(T)))]^{N(T)} \qquad (3)$$

where $p(\varepsilon,T)$ represents the probability that $\log_{10}[PSV(T)] - \log_{10}[\hat{PSV}(T)] \le \varepsilon(T)$. From (3), it follows that $\varepsilon(T) = 1/\alpha(T)\ [\ell n(-\ell n(1 - p^{1/N})) - \beta(T)]$

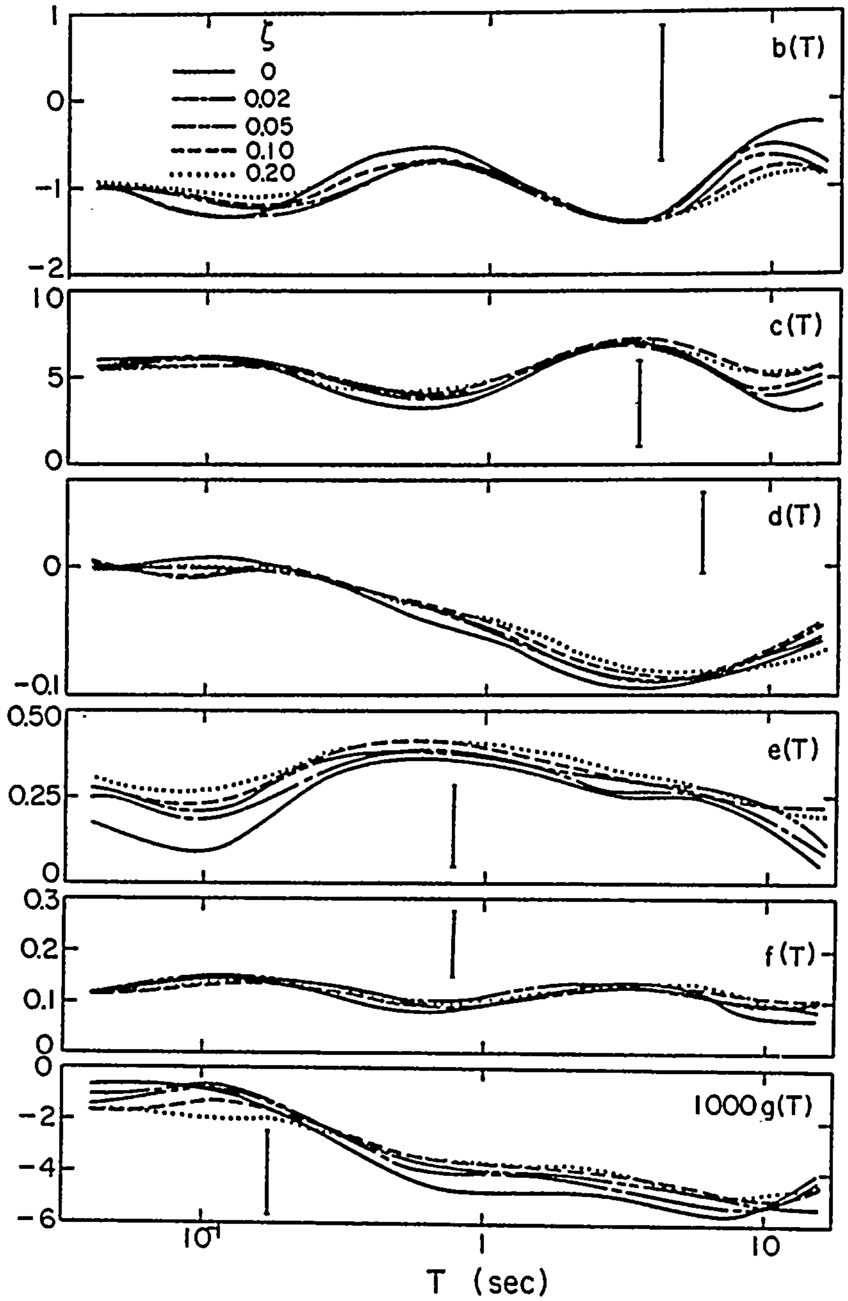

Figure 1

TABLE I

Regression Parameters for Equation (1) and α(T), β(T), N(T) at Eleven Selected Periods

Period,T(sec)	.040	.065	0.11	0.19	0.34	0.50	0.90	1.60	2.80	4.40	7.50
ζ = 0.0											
b(T)	-1.020	-1.140	-1.320	-1.150	-0.748	-0.577	-0.717	-1.110	-1.380	-1.250	-0.600
c(T)	5.950	6.090	6.150	5.240	3.850	3.350	4.030	5.670	6.810	6.420	4.260
10*d(T)	0.011	0.023	0.046	-0.039	-0.217	-0.344	-0.524	-0.747	-0.929	-0.932	-0.806
e(T)	0.168	0.120	0.109	0.227	0.329	0.344	0.342	0.311	0.260	0.250	0.217
f(T)	0.125	0.133	0.146	0.132	0.101	0.087	0.094	0.117	0.136	0.130	0.087
1000*g(T)	-0.757	-0.795	-0.972	-1.850	-3.140	-3.970	-4.590	-4.540	-4.680	-5.150	-5.530
α(T)	1.280	1.190	1.150	1.240	1.340	1.350	1.410	1.420	1.400	1.780	2.710
β(T)	1.000	0.988	0.977	0.985	0.992	0.995	0.912	0.760	0.491	-0.021	-0.691
N(T)	10	10	10	10	10	10	8	6	4	2	1
ζ = 0.02											
b(T)	-0.978	-1.080	-1.280	-1.270	-0.980	-0.784	-0.803	-1.120	-1.410	-1.300	-0.675
c(T)	5.750	5.890	6.060	5.660	4.620	4.090	4.420	5.790	7.030	6.660	4.570
10*d(T)	0.006	-0.003	0.004	-0.035	-0.135	-0.246	-0.457	-0.680	-0.846	-0.875	-0.783
e(T)	0.254	0.213	0.191	0.271	0.353	0.367	0.364	0.326	0.275	0.266	0.229
f(T)	0.125	0.132	0.148	0.148	0.124	0.106	0.101	0.119	0.140	0.134	0.092
1000*g(T)	-1.090	-0.868	-0.709	-1.600	-2.950	-3.670	-4.100	-4.160	-4.410	-4.900	-5.460
α(T)	1.630	1.490	1.380	1.410	1.490	1.490	1.530	1.510	1.440	1.800	2.720
β(T)	1.010	0.997	0.990	0.997	1.000	1.000	0.910	0.742	0.473	-0.300	-0.683
N(T)	10	10	10	10	10	10	8	6	4	2	1
ζ = 0.05											
b(T)	-0.928	-1.010	-1.180	-1.200	-0.945	-0.771	-0.821	-1.130	-1.400	-1.320	-0.761
c(T)	5.260	5.710	5.810	5.490	4.590	4.120	4.550	5.870	7.050	6.800	4.940
10*d(T)	-0.009	-0.040	-0.042	-0.025	-0.101	-0.220	-0.421	-0.636	-0.812	-0.855	-0.781
e(T)	0.270	0.240	0.229	0.294	0.365	0.381	0.381	0.351	0.304	0.292	0.254
f(T)	0.121	0.127	0.141	0.143	0.122	0.105	0.103	0.120	0.138	0.134	0.097
1000*g(T)	-1.220	-1.050	-0.835	-1.560	-2.790	-3.420	-3.850	-3.990	-4.130	-4.350	-4.870
α(T)	1.670	1.560	1.470	1.490	1.560	1.560	1.600	1.570	1.480	1.820	2.710
β(T)	1.010	1.000	0.995	1.000	1.000	1.000	0.908	0.740	0.471	-0.039	-0.715
N(T)	10	10	10	10	10	10	8	6	4	2	1

TABLE I -- Continued

ζ = 0.10											
b(T)	-0.871	-0.953	-1.110	-1.130	-0.897	-0.755	-0.861	-1.130	-1.360	-1.360	-0.938
c(T)	5.450	5.540	5.630	5.360	4.540	4.170	4.750	5.930	6.950	6.990	5.570
10*d(T)	-0.015	-0.043	-0.019	-0.002	-0.115	-0.224	-0.397	-0.612	-0.777	-0.831	-0.785
e(T)	0.270	0.256	0.256	0.310	0.370	0.387	0.390	0.366	0.317	0.279	0.234
f(T)	0.116	0.123	0.136	0.137	0.118	0.104	0.107	0.121	0.136	0.138	0.111
1000*g(T)	-1.650	-1.560	-1.350	-1.700	-2.630	-3.220	-3.620	-3.730	-4.050	-4.520	-5.000
α(T)	1.680	1.590	1.530	1.560	1.620	1.600	1.650	1.620	1.530	1.860	2.750
β(T)	1.010	1.000	1.000	1.000	0.999	0.999	0.906	0.737	0.466	-0.036	-0.696
N(T)	10	10	10	10	10	10	8	6	4	2	1
ζ = 0.20											
b(T)	-0.873	-0.940	-1.050	-1.040	-0.891	-0.795	-0.837	-1.060	-1.310	-1.340	-1.030
c(T)	5.460	5.520	5.520	5.210	4.660	4.430	4.770	5.780	6.830	6.980	5.940
10*d(T)	-0.0004	-0.021	0.002	-0.018	-0.150	-0.238	-0.364	-0.564	-0.748	-0.806	-0.775
e(T)	0.290	0.279	0.283	0.330	0.383	0.400	0.400	0.378	0.337	0.292	0.237
f(T)	0.116	0.122	0.131	0.130	0.117	0.107	0.105	0.116	0.133	0.138	0.118
1000*g(T)	-1.550	-1.790	-1.900	-2.030	-2.800	-3.380	-3.620	-3.590	-3.900	-4.320	-4.640
α(T)	1.700	1.620	1.580	1.620	1.660	1.630	1.690	1.680	1.600	1.940	2.820
β(T)	1.010	1.010	1.000	1.000	1.010	1.010	0.909	0.732	0.465	-0.032	-0.688
N(T)	10	10	10	10	10	10	8	6	4	2	1

and this result can then be employed to calculate from (1) the spectral amplitudes which have a probability p of not being exceeded.

The probability $p^*(\varepsilon,T)$ that $\varepsilon(T)$ will not be exceeded can be calculated at different periods T from amplitudes of PSV(T) spectra computed from recorded accelerograms and from $\hat{PSV}(T)$ estimated from (1). After finding the fraction of the residuals $\varepsilon(T)$ which are smaller than a chosen value, for $P^*(\varepsilon,T) = 0.1, 0.2, \ldots, 0.8$ and 0.9, $\varepsilon(T)$ smoothed along the $\log_{10}T$ axis then appears as in Figure 2 for five fractions of critical damping, $\zeta = 0.0$, 0.02, 0.05, 0.10 and 0.20. The smoothed surface $p^*(\varepsilon,T)$ thus represents the distribution of data ($\log_{10}[PSV(T)]$, computed from recorded accelerograms) with respect to the estimate $\log_{10}[\hat{PSV}(T)]$ in equation (1).

By means of a regression of equation (3) on the data presented in Figure 2, it is possible to compute the estimates of $\alpha(T)$, $\beta(T)$ and N(T) at 91 periods between 0.04 sec and 15 sec. Figures 3 and 4 show smoothed $\alpha(T)$, N(T) and $\beta(T)$. $\alpha(T)$ and $\beta(T)$ are shown for five damping values between 0.0 and 0.20. Dependence of N(T) has been neglected. Figure 5 presents the largest differences in the Kolmogorov-Smirnov test and the χ^2 amplitudes plotted versus T and assuming that the model in equation (3) with coefficients $\alpha(T)$, $\beta(T)$ and N(T) as in Figures 3 and 4 describe the observed distribution. The theoretical limits on the K-S and χ^2 amplitudes for 95% confidence level are also plotted in Figure 5 and show that except for high frequencies and the χ^2 test, the model in equation (3) appears to be adequate for describing $p(\varepsilon,T)$ in Figure 2. Figure 6 then presents the average, $\mu(T)$, and the standard deviation, $\sigma(T)$, for $\varepsilon(T)$ in Figure 2 and for five dampings, ζ.

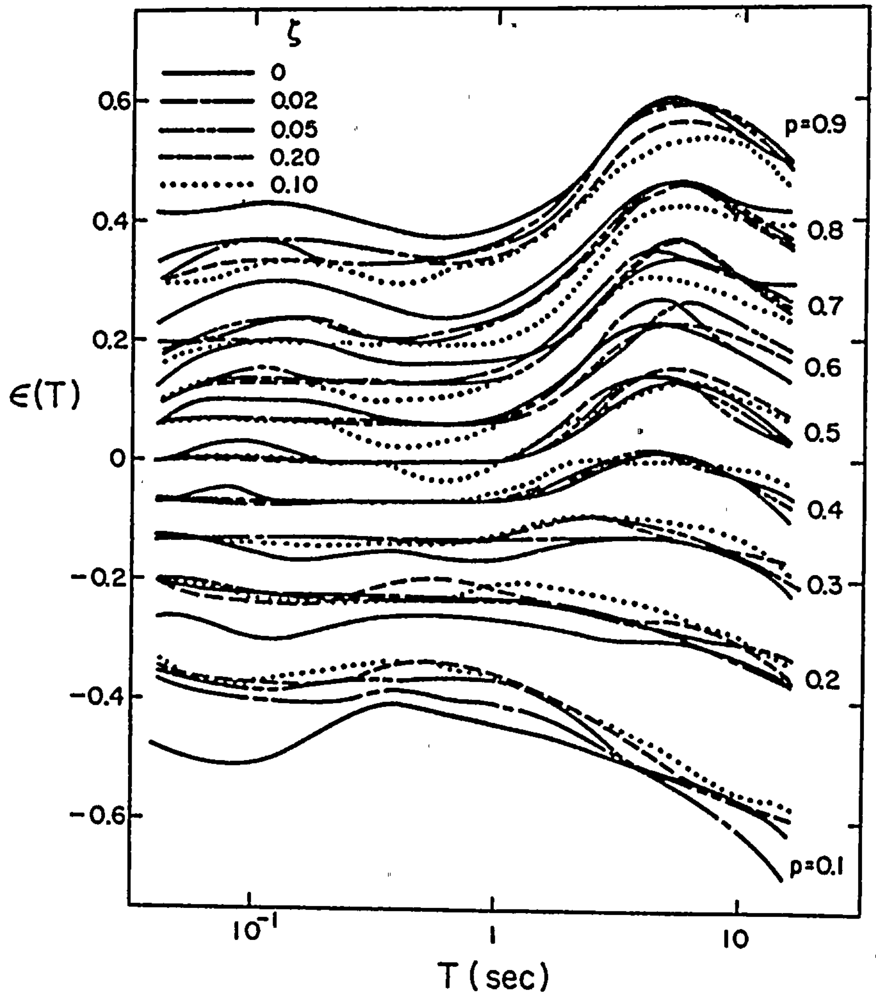
ζ
0
0.02
0.05
0.20
0.10
0.6
0.4
0.2
0
−0.2
−0.4
−0.6
∈(T)
p=0.9
0.8
0.7
0.6
0.5
0.4
0.3
0.2
p=0.1
10^{-1}
1
10
T (sec)

Figure 2

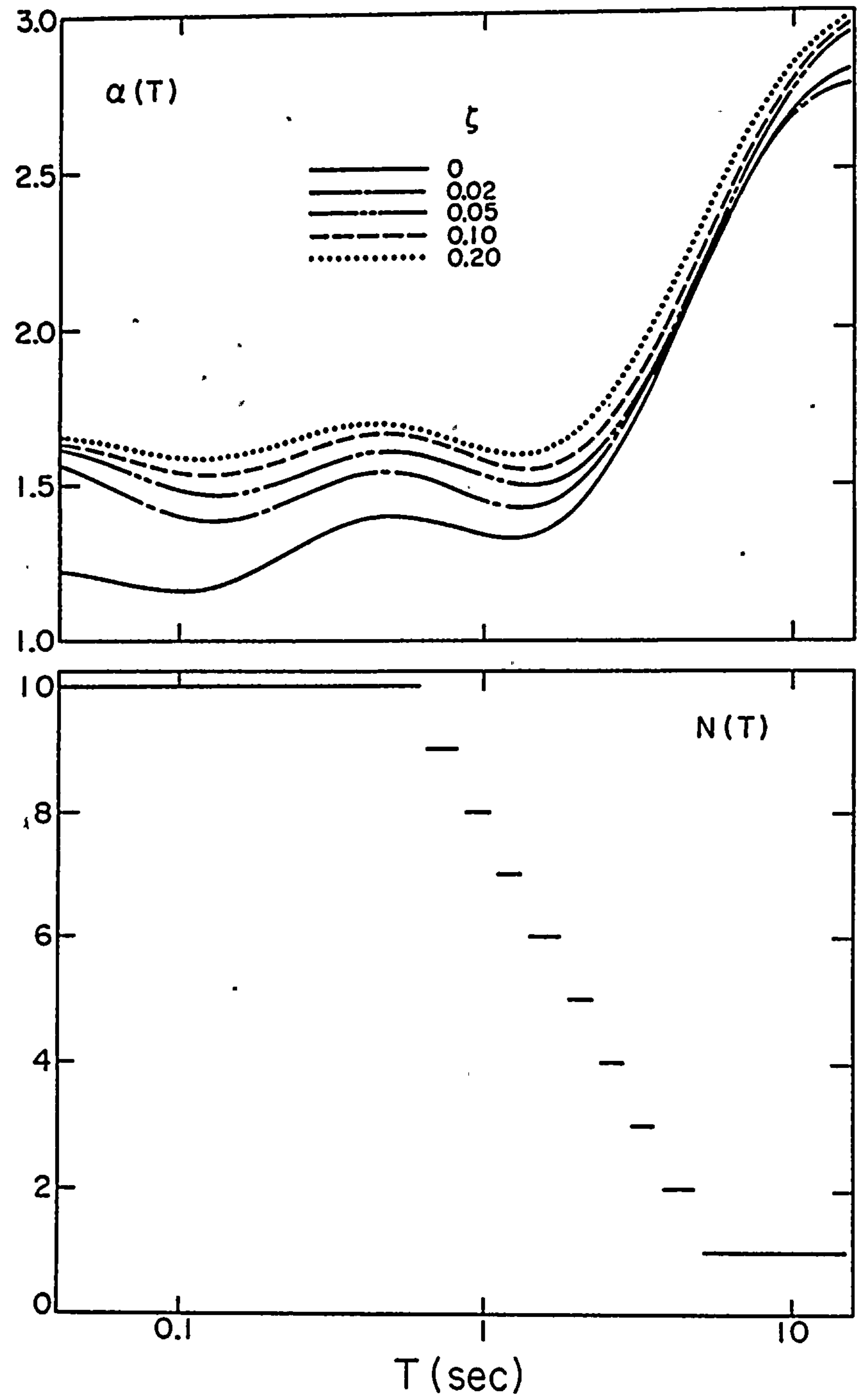

Figure 3

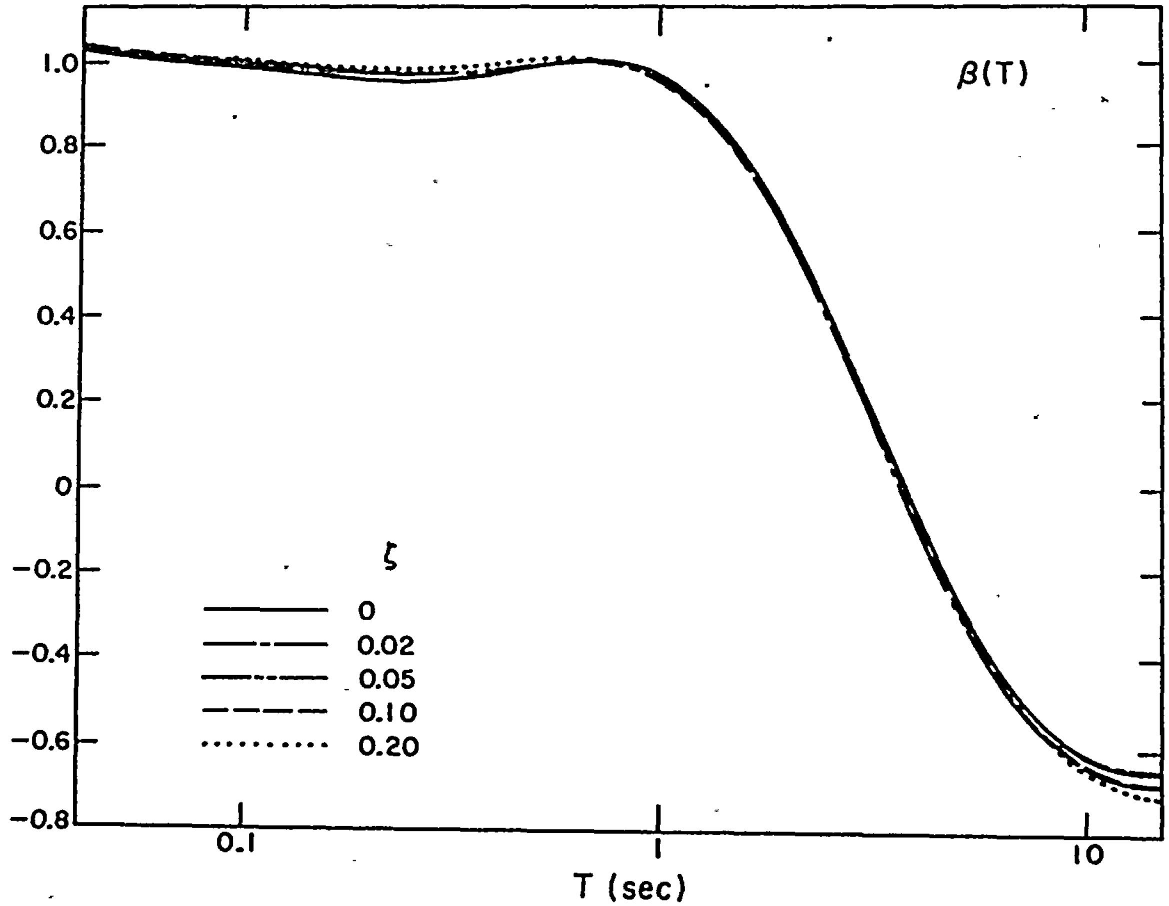

Figure 4

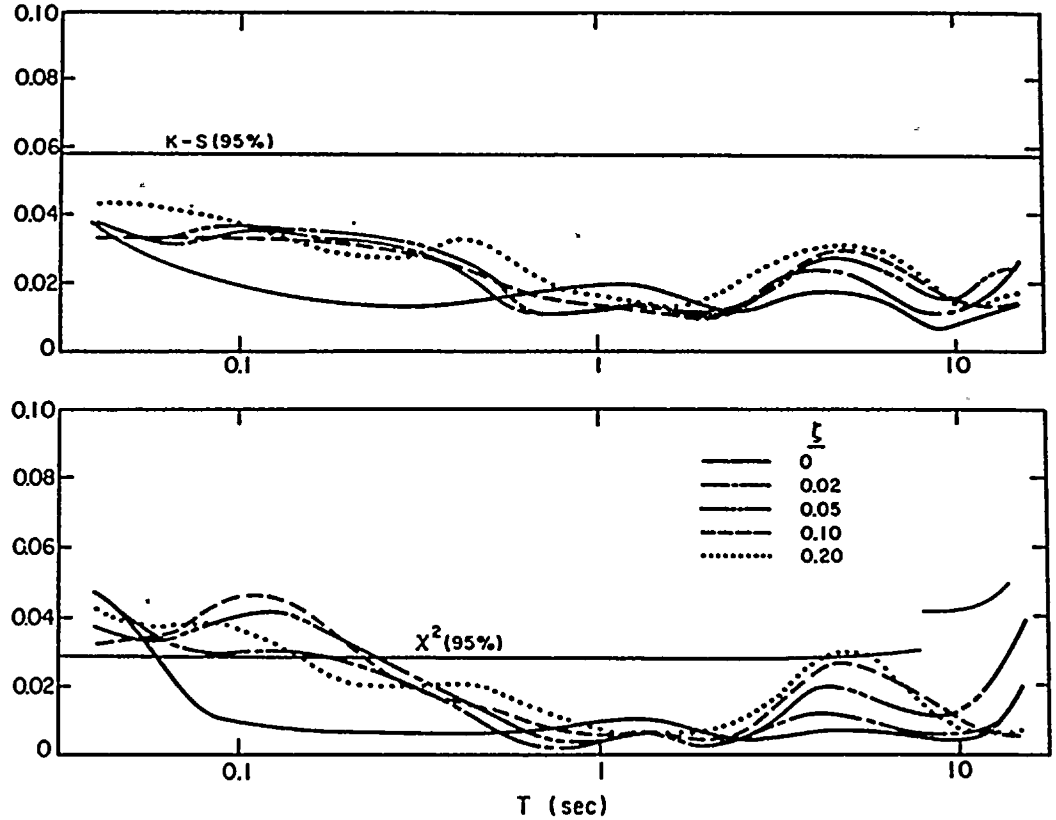
0.10
0.08
0.06
0.04
0.02
0
K-S (95%)
0.1
1
10
0.10
0.08
0.06
0.04
0.02
0
ζ
0
0.02
0.05
0.10
0.20
X² (95%)
0.1
1
10
T (sec)

Figure 5

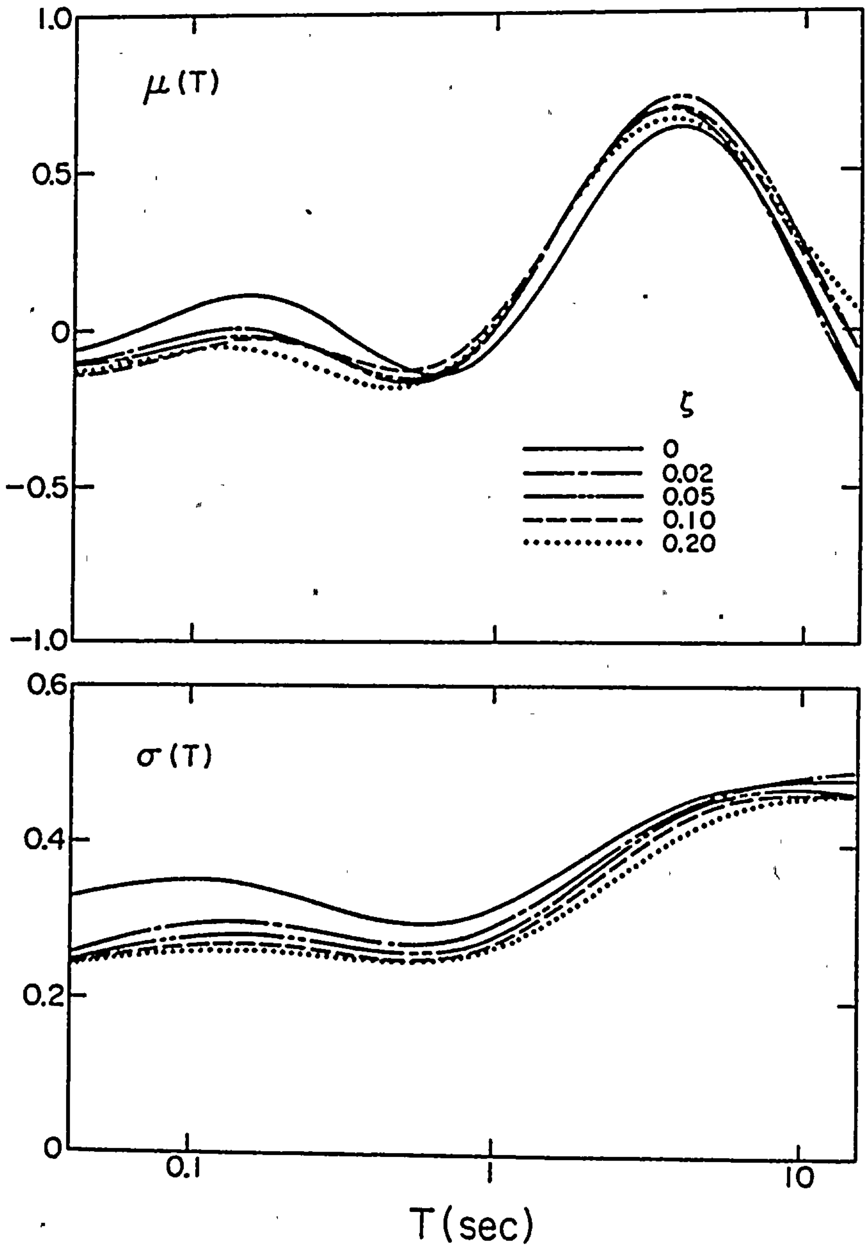

Figure 6

Table I presents the estimates of b(T) through g(T), α(T), β(T) and N(T) at eleven selected periods and for five percentages of critical damping $\zeta = 0.0$, 0.02, 0.05, 0.10 and 0.20. Approximate significance tests (Westermo and Trifunac, 1978) of the coefficient functions b(T) through g(T) (vertical bars in Figure 1 correspond to the 95% confidence interval) show that all these functions are significantly different from zero in large subregions of the entire interval $T \varepsilon$ [0.04 sec, 15 sec]. The function d(T), for example, is significantly different from zero for periods longer than about 0.3 sec. Table II presents $\log_{10}A_0(R)$ which has been empirically determined for southern California (Richter, 1958).

Equation (1) applies in the interval $M_{min} \leq M \leq M_{max}$, where $M_{min} = -b(T)/(2f(T))$ and $M_{max} = (1 - b(T))/(2f(T))$. For $M \leq M_{min}$, M is used only in the first term M in equation (1), while in the terms b(T)M and $f(T)M^2$, M_{min} is used. For $M \geq M_{max}$, $M = M_{max}$ is used in all terms of (1). The reasons for this are described in Trifunac (1976) and in Trifunac and Anderson (1977), and reflect the observations that the local Richter magnitude scale, which is representative of most data employed in this analysis, appears to become saturated as M grows beyond 7 to 7.5.

Figures 7 through 16 present examples of PSV(T) spectra computed from equation (1) and for $M = 4.5$, 5.5, 6.5 and 7.5, for $h = 0$ and 4 km, for $p = 0.5$ and for $\zeta = 0.0$, 0.02, 0.05, 0.10 and 0.20. The shaded regions in these and many subsequent figures represent the range between average and average plus one standard deviation of minimum recording and digitization noise amplitudes. These noise amplitudes have been computed by digitization of a fine straight line (Trifunac, 1976) which is 2 to 3 times narrower than the 4 x enlargements of typical acceleration

TABLE II

$\log_{10}A_o(R)$ Versus Epicentral Distance R*

R(km)	$-\log_{10}A_o(R)$	R(km)	$-\log_{10}A_o(R)$	R(km)	$-\log_{10}A_o(R)$
0	1.400	70	2.805	190	3.480
5	1.500	80	2.920	200	3.530
10	1.605	85	2.958	210	3.581
15	1.716	90	2.989	220	3.631
20	1.833	95	3.020	230	3.680
25	1.955	100	3.044	240	3.729
30	2.078	110	3.089	250	3.779
35	2.199	120	3.135	260	3.828
40	2.314	130	3.182	270	3.877
45	2.421	140	3.230	280	3.926
50	2.517	150	3.279	290	3.975
55	2.603	160	3.328	300	4.024
60	2.679	170	3.378	310	4.072
65	2.746	180	3.429	320	4.119

R(km)	$-\log_{10}A_o(R)$	R(km)	$-\log_{10}A_o(R)$
330	4.164	470	4.660
340	4.209	480	4.685
350	4.253	490	4.709
360	4.295	500	4.732
370	4.336	510	4.755
380	4.376	520	4.776
390	4.414	530	4.797
400	4.451	540	4.817
410	4.485	550	4.835
420	4.518	560	4.853
430	4.549	570	4.869
440	4.579	580	4.885
450	4.607	590	4.900
460	4.634		

*Only the first two digits may be assumed to be significant.

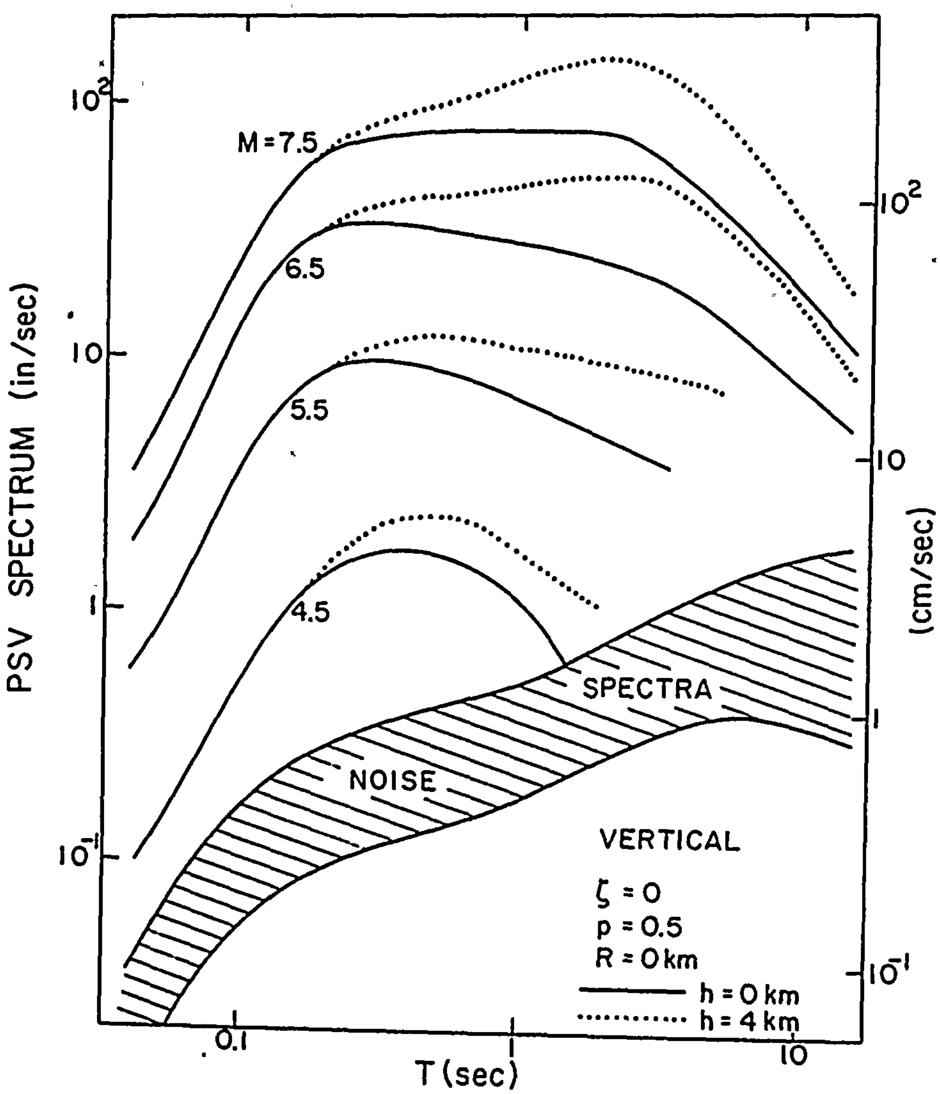
PSV SPECTRUM (in/sec)
(cm/sec)
T(sec)
M=7.5
6.5
5.5
4.5
NOISE
SPECTRA
VERTICAL
ζ = 0
p = 0.5
R = 0 km
h = 0 km
h = 4 km
10^2
10
1
10^{-1}
0.1
1
10

Figure 7

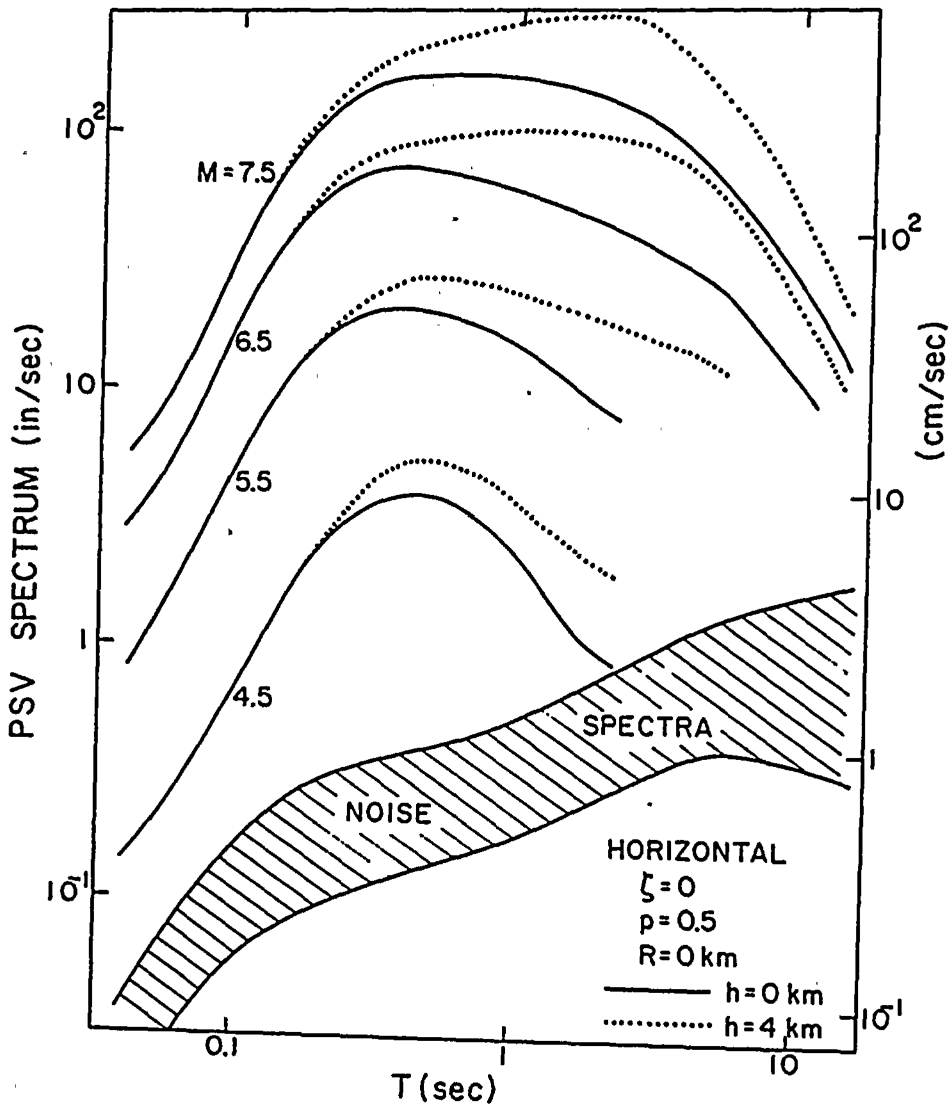
PSV SPECTRUM (in/sec)
(cm/sec)
T (sec)
M=7.5
6.5
5.5
4.5
NOISE
SPECTRA
HORIZONTAL
ζ=0
p=0.5
R=0 km
h=0 km
h=4 km
10²
10
1
10⁻¹
0.1
1
10

Figure 8

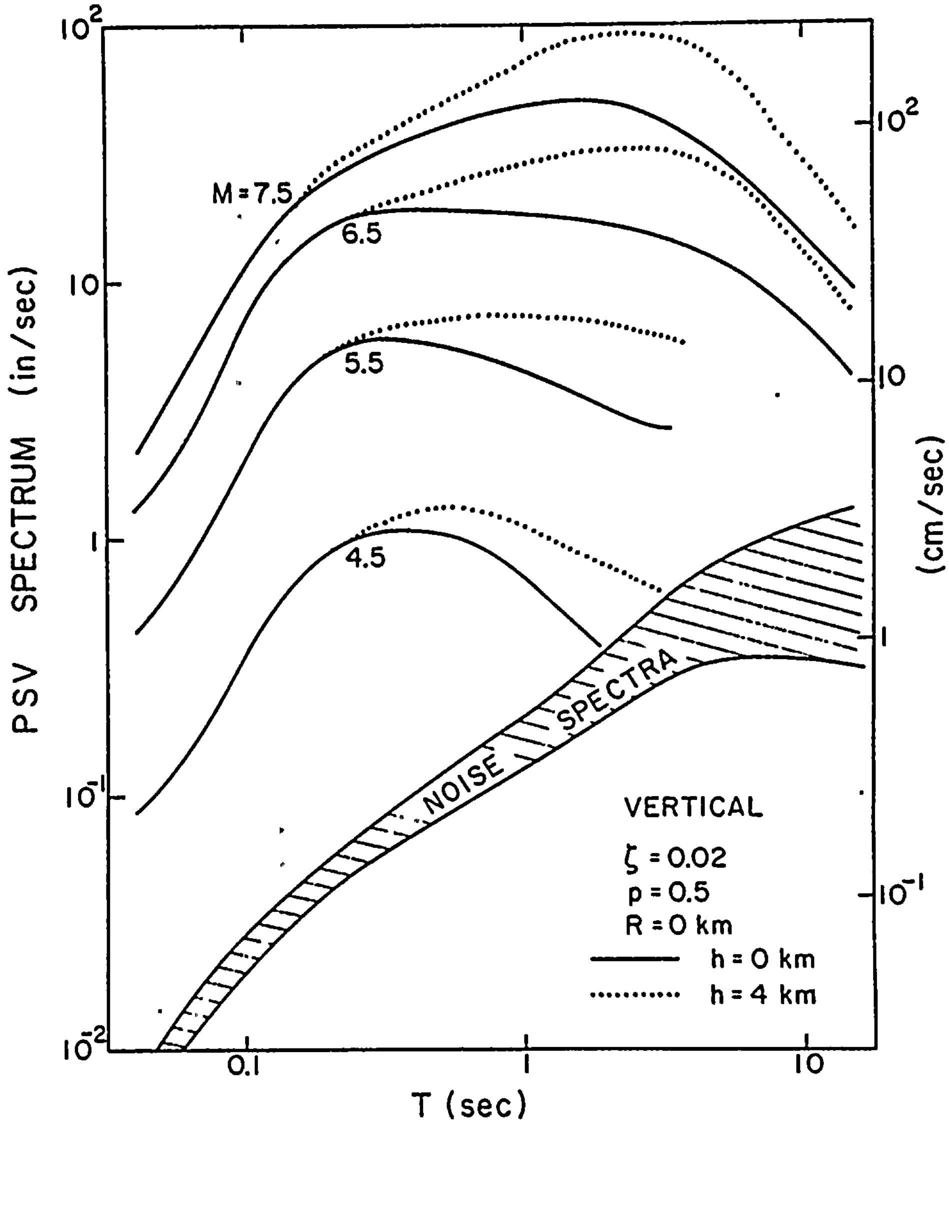

10^2
10
1
10^{-1}
10^{-2}
PSV SPECTRUM (in/sec)
(cm/sec)
10^2
10
1
10^{-1}
M = 7.5
6.5
5.5
4.5
NOISE SPECTRA
VERTICAL
ζ = 0.02
p = 0.5
R = 0 km
h = 0 km
h = 4 km
0.1
1
10
T (sec)

Figure 9

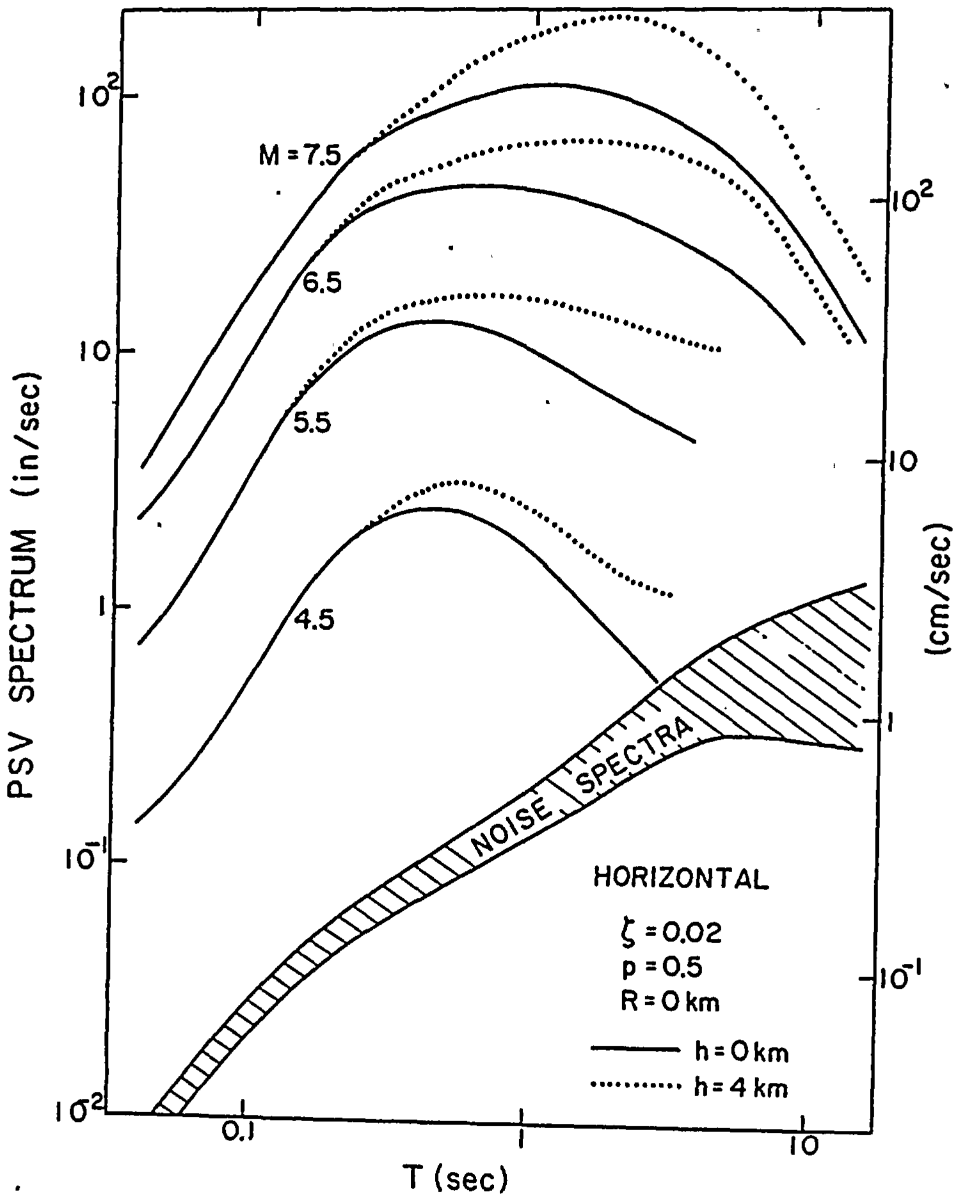
PSV SPECTRUM (in/sec)
(cm/sec)
T (sec)
M = 7.5
6.5
5.5
4.5
NOISE SPECTRA
HORIZONTAL
ζ = 0.02
p = 0.5
R = 0 km
h = 0 km
h = 4 km

Figure 10

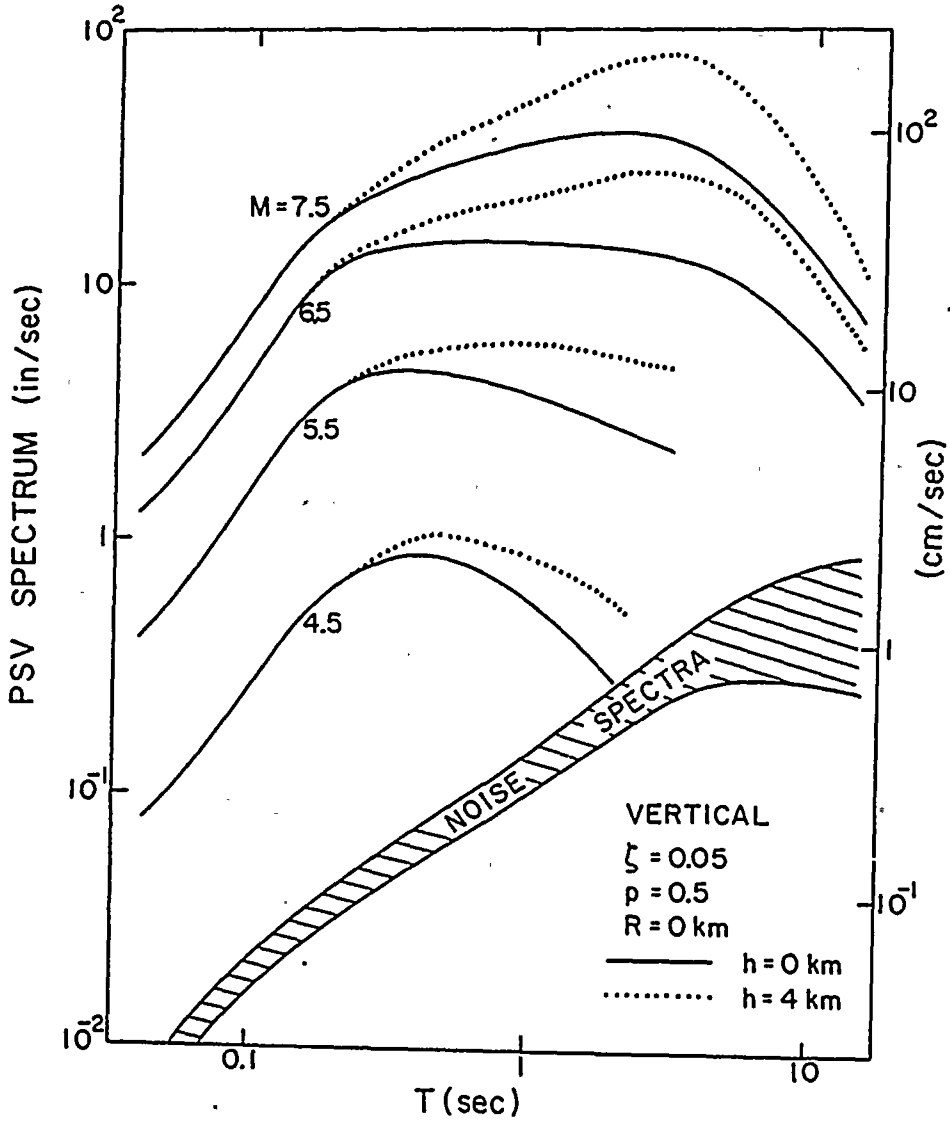

PSV SPECTRUM (in/sec)
(cm/sec)
T (sec)
M = 7.5
6.5
5.5
4.5
NOISE SPECTRA
VERTICAL
ζ = 0.05
p = 0.5
R = 0 km
h = 0 km
h = 4 km

Figure 11

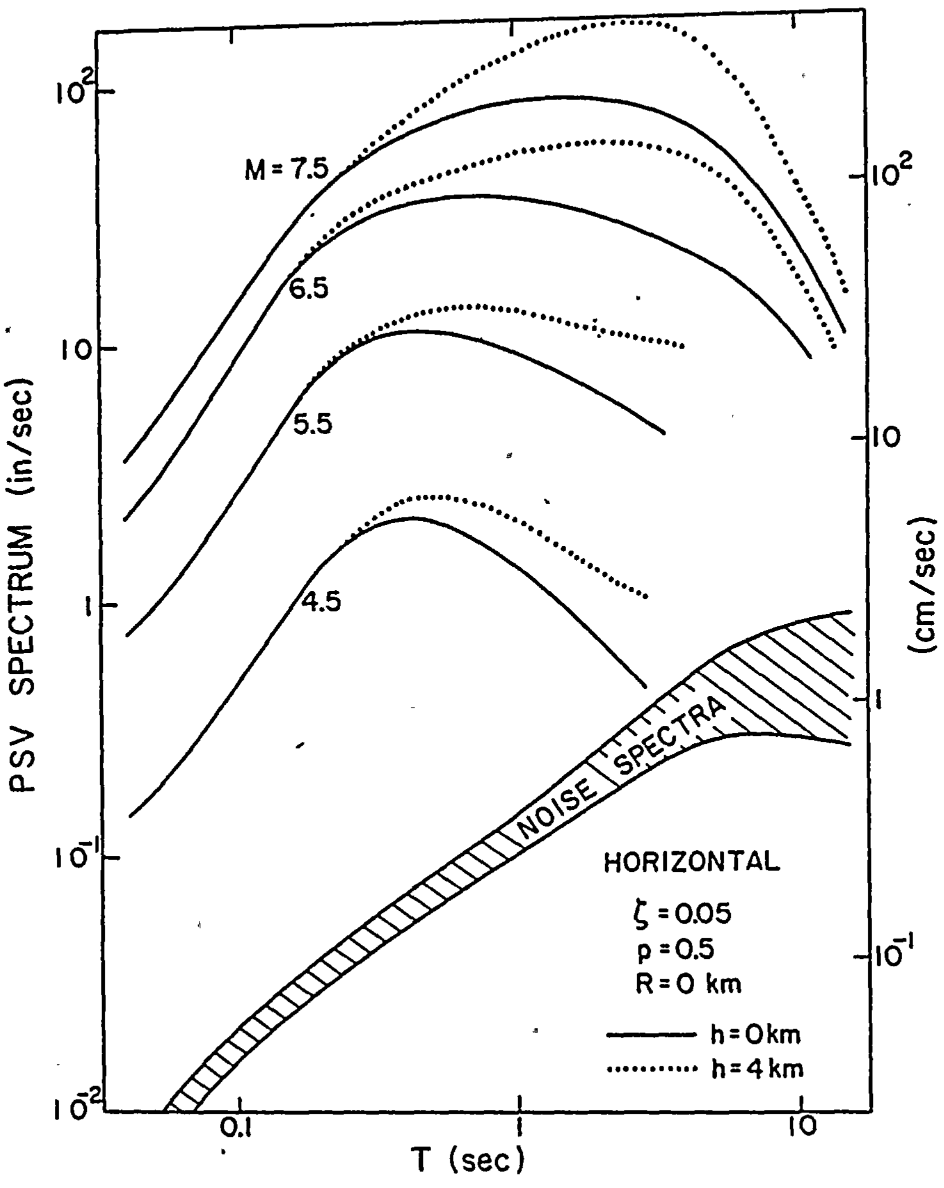
PSV SPECTRUM (in/sec)
(cm/sec)
T (sec)
M = 7.5
6.5
5.5
4.5
NOISE SPECTRA
HORIZONTAL
ζ = 0.05
p = 0.5
R = 0 km
h = 0km
h = 4 km

Figure 12

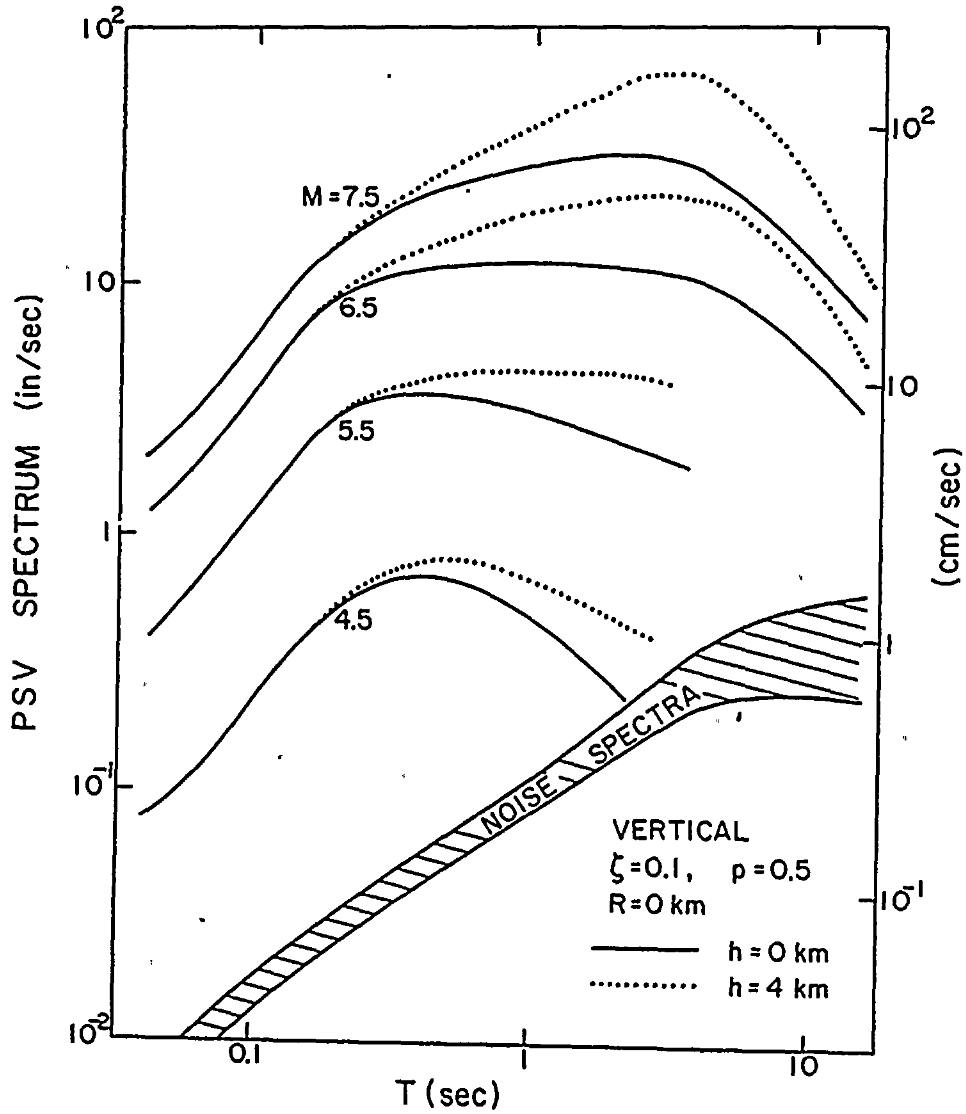

10^2
10
1
10^{-1}
10^{-2}
10^2
10
1
10^{-1}
M = 7.5
6.5
5.5
4.5
NOISE SPECTRA
VERTICAL
ζ = 0.1, p = 0.5
R = 0 km
h = 0 km
h = 4 km
PSV SPECTRUM (in/sec)
(cm/sec)
0.1
1
10
T (sec)

Figure 13

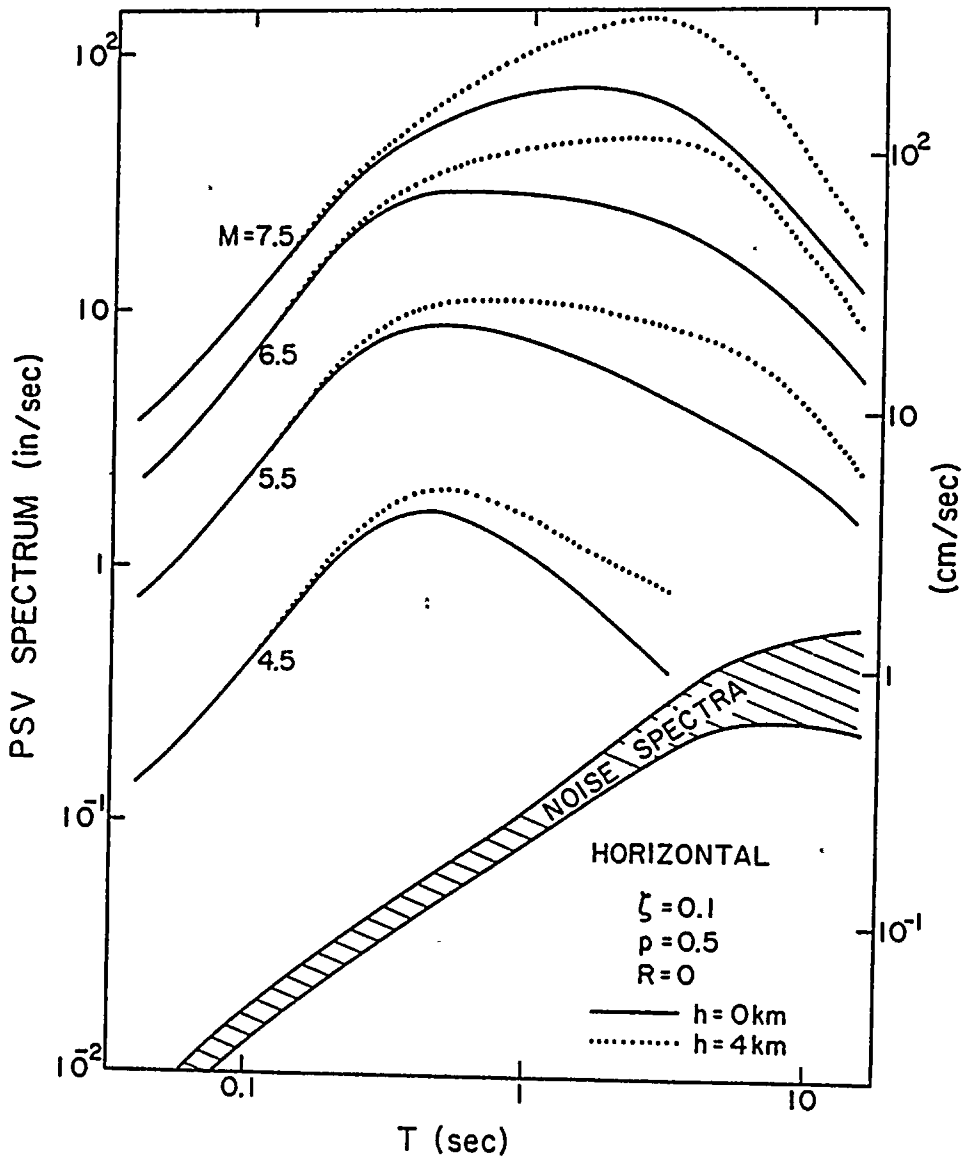

PSV SPECTRUM (in/sec)
(cm/sec)
T (sec)
M=7.5
6.5
5.5
4.5
NOISE SPECTRA
HORIZONTAL
ζ =0.1
p =0.5
R=0
h=0km
h=4km

Figure 14

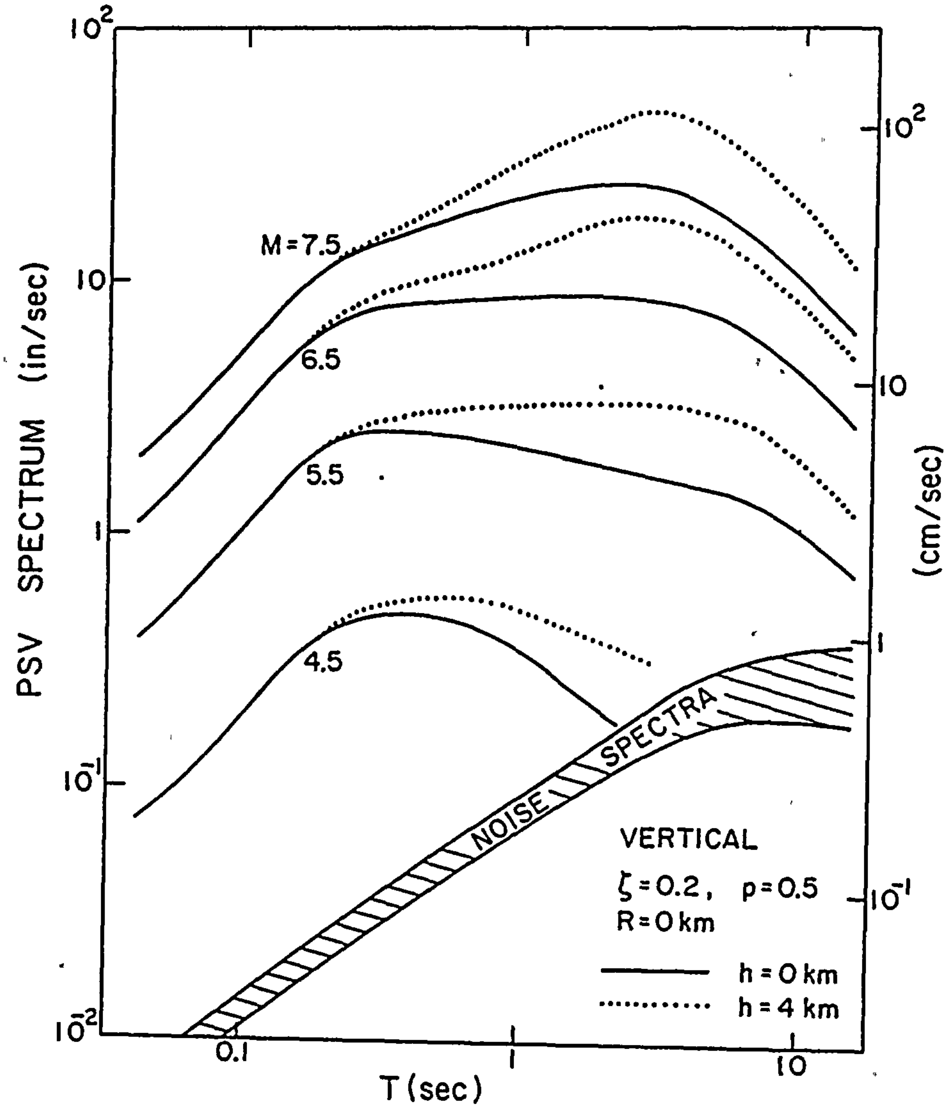
PSV SPECTRUM (in/sec)
(cm/sec)
T (sec)
M=7.5
6.5
5.5
4.5
NOISE SPECTRA
VERTICAL
ζ=0.2, p=0.5
R=0 km
h = 0 km
h = 4 km

Figure 15

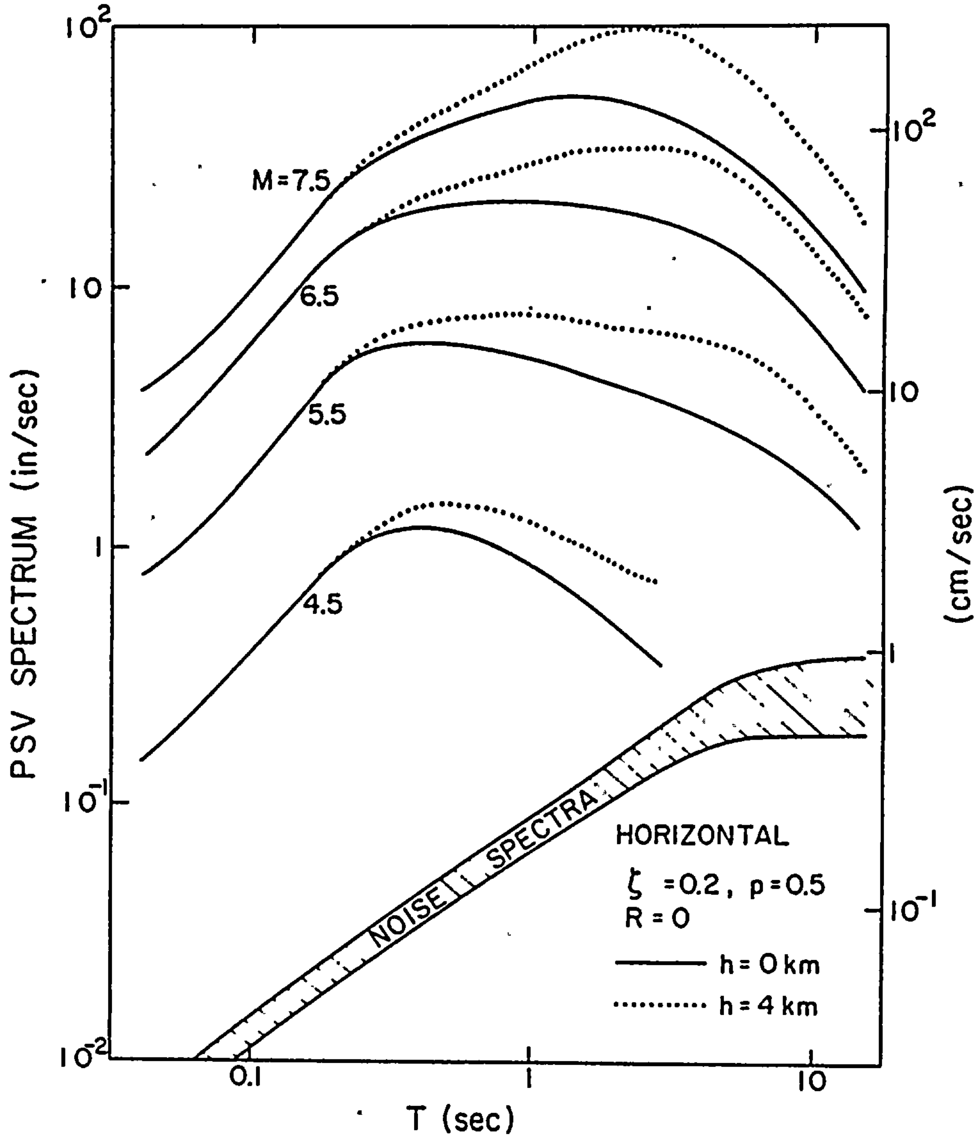

10^2
10
1
10^{-1}
10^{-2}
PSV SPECTRUM (in/sec)
(cm/sec)
10^2
10
1
10^{-1}
M=7.5
6.5
5.5
4.5
NOISE SPECTRA
HORIZONTAL
ζ =0.2, p=0.5
R = 0
h = 0 km
h = 4 km
0.1
1
10
T (sec)

Figure 16

traces. Comparison of these noise amplitudes with the results of recent studies presented by Trifunac and Lee (1979) shows that for high frequencies ($f > 5$ Hz) spectrum amplitudes resulting from hand-digitization noise are slightly larger or comparable to the noise amplitudes resulting from well-controlled automatic digitization. At long periods, the noise amplitudes shown in figures 7 through 16 are 2 to 3 times smaller than the estimates of noise amplitudes presented by Trifunac and Lee (1979). While it appears now that the most reliable estimates of digitization and processing noise are those presented by Trifunac and Lee (1979), in all previous calculations we used the wave amplitudes as presented in Trifunac (1976). For consistency with all earlier analyses and without any significant effects on the results which are presented here, we employ the same noise amplitudes in this work.

The trends of computed PSV(T) spectrum amplitudes in Figures 7 through 16 are in many ways similar to those discussed by Trifunac and Anderson (1978a). The rate of growth of amplitudes with M clearly decreases as M approaches $M = 7.5$. The effect of local geologic conditions is important for intermediate and long periods and small for high frequencies. This is illustrated by full and dotted lines in Figures 7 through 16 which represent spectra for $h = 0$ and $h = 4$ km. The vertical spectrum amplitudes are nearly as large as the horizontal amplitudes for high frequencies.

Figures 17 through 21 illustrate the effects of epicentral distance R and damping ζ, on the changes of spectral amplitudes for $p = 0.5$, $M = 6.5$, $h = 2$ and for horizontal (full lines) and vertical (dotted lines)

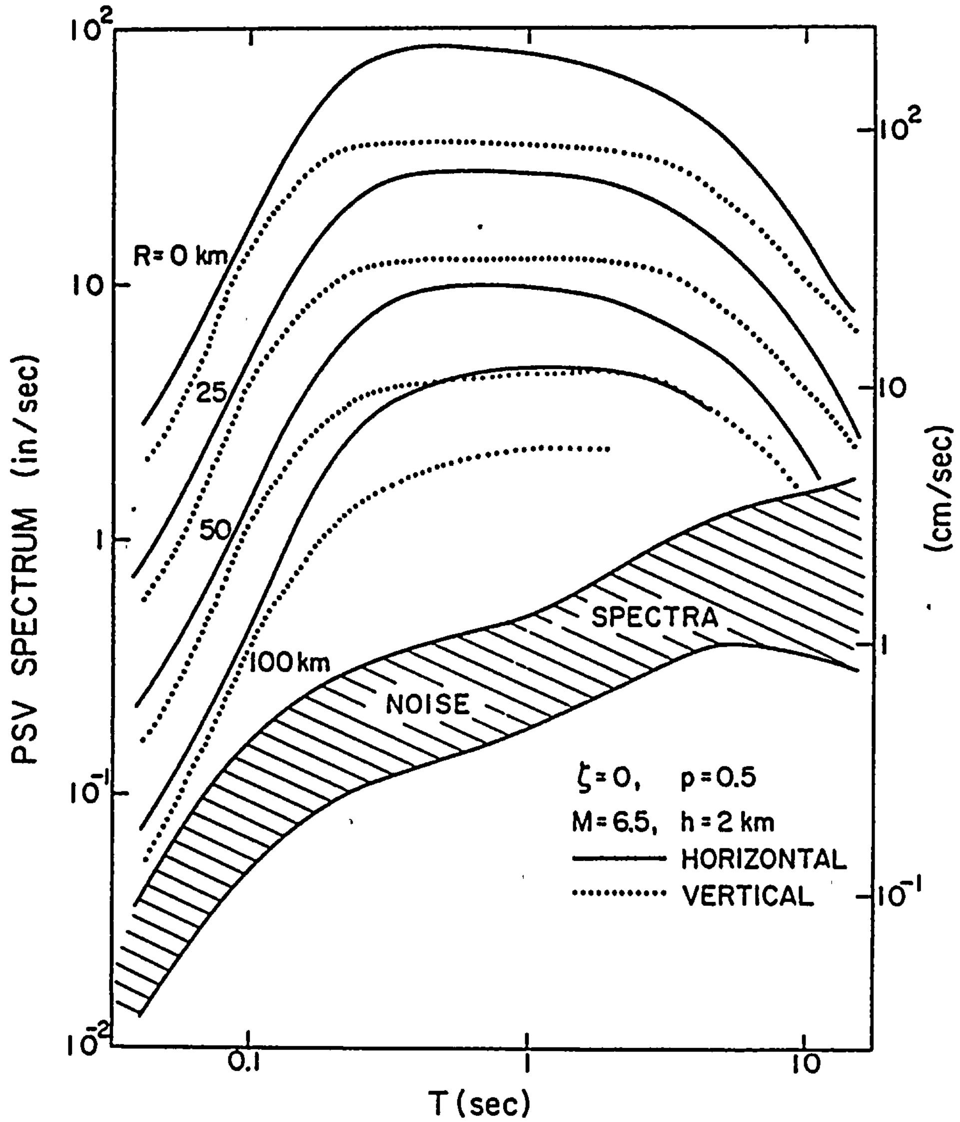

PSV SPECTRUM (in/sec)
(cm/sec)
T (sec)
R= 0 km
25
50
100 km
NOISE
SPECTRA
ζ= 0, p = 0.5
M= 6.5, h = 2 km
HORIZONTAL
VERTICAL

Figure 17

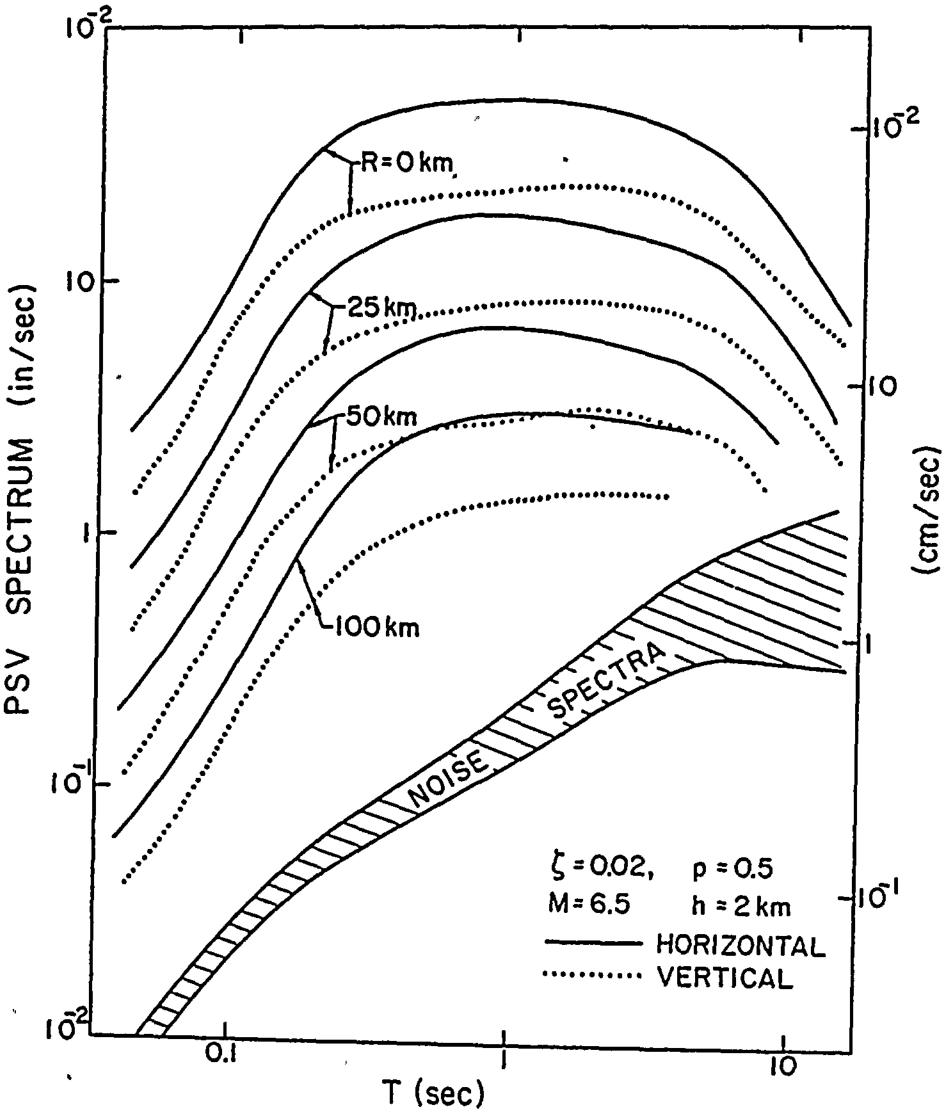
PSV SPECTRUM (in/sec)
(cm/sec)
T (sec)
R = 0 km
25 km
50 km
100 km
NOISE SPECTRA
ζ = 0.02, p = 0.5
M = 6.5 h = 2 km
HORIZONTAL
VERTICAL

Figure 18

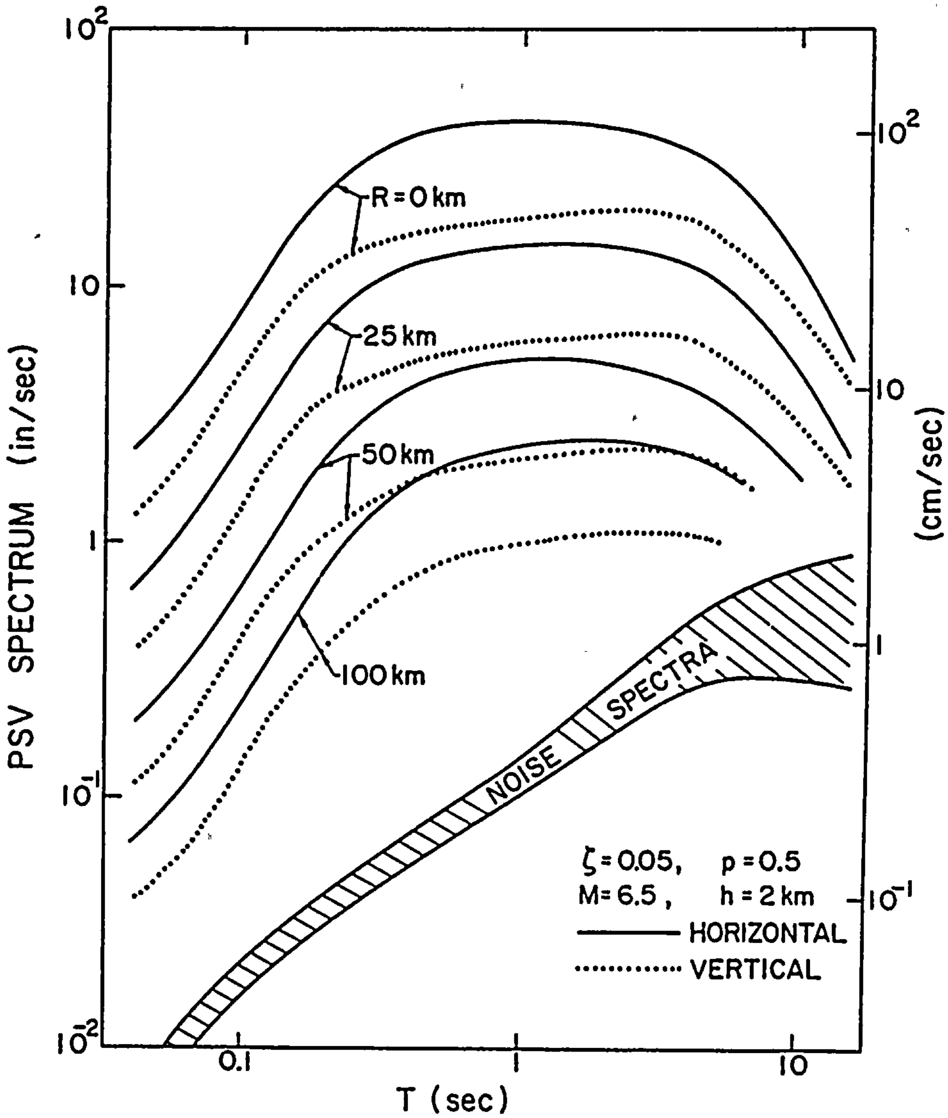

10^2
10
1
10^{-1}
10^{-2}
PSV SPECTRUM (in/sec)
10^2
10
1
10^{-1}
(cm/sec)
0.1
1
10
T (sec)
R = 0 km
25 km
50 km
100 km
NOISE SPECTRA
ζ = 0.05, p = 0.5
M = 6.5, h = 2 km
HORIZONTAL
VERTICAL

Figure 19

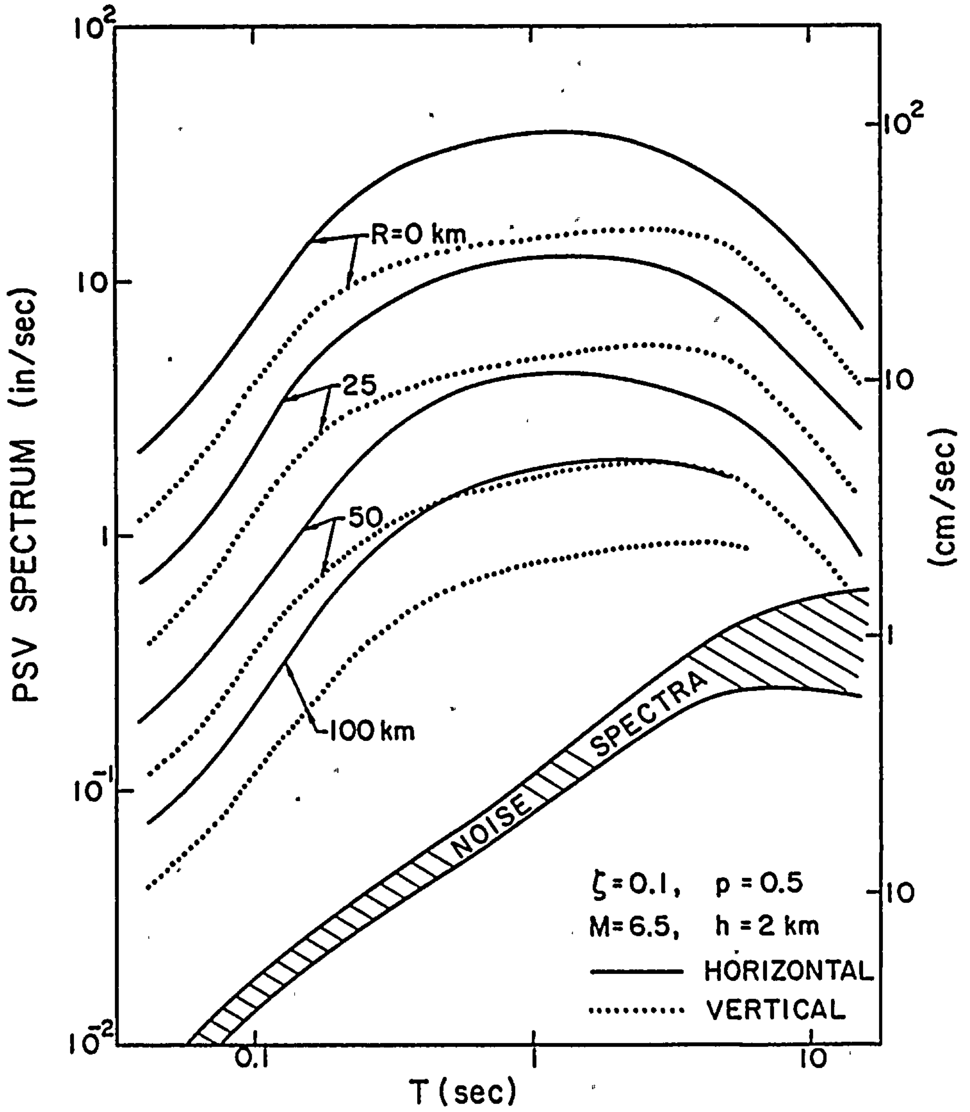
PSV SPECTRUM (in/sec)
(cm/sec)
T (sec)
R=0 km
25
50
100 km
NOISE SPECTRA
ζ=0.1, p = 0.5
M=6.5, h = 2 km
HORIZONTAL
VERTICAL

Figure 20

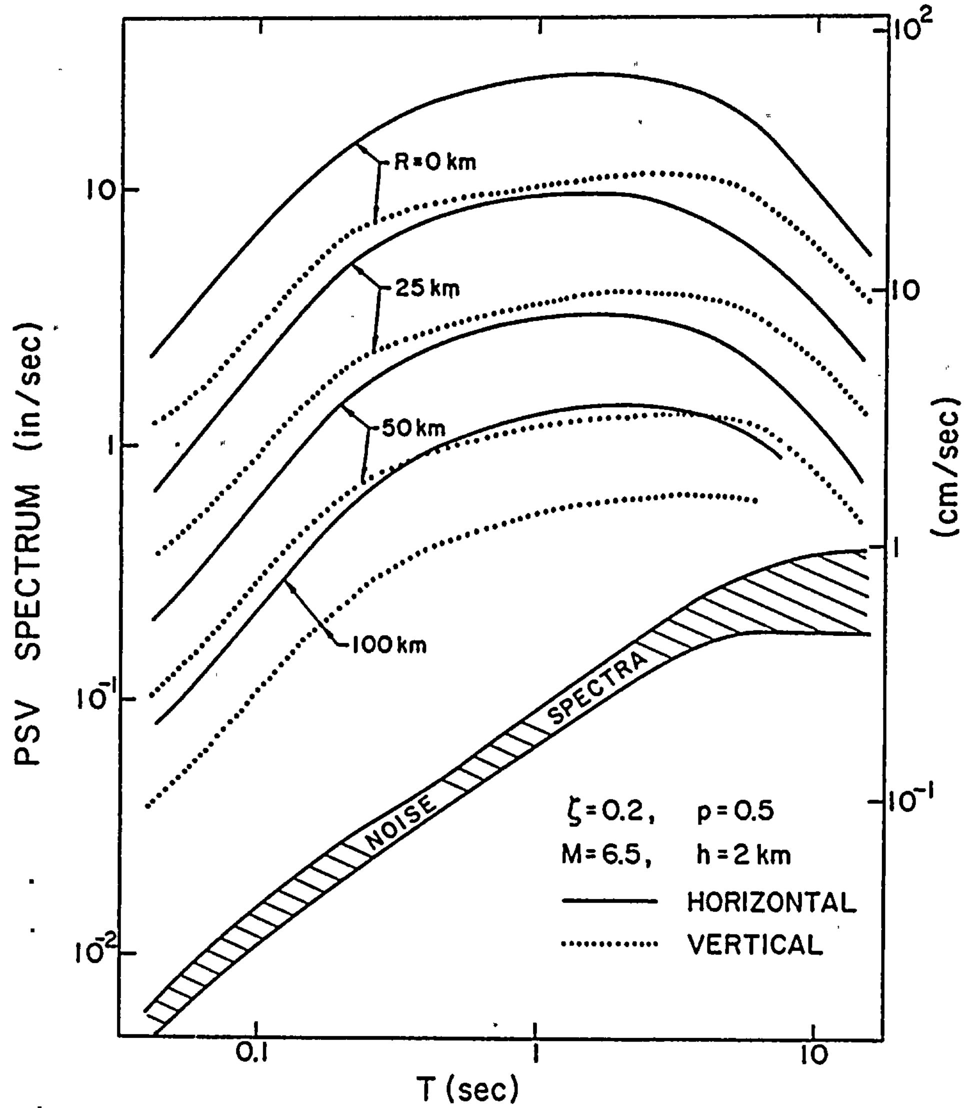
PSV SPECTRUM (in/sec)
(cm/sec)
T (sec)
R=0 km
25 km
50 km
100 km
NOISE SPECTRA
ζ=0.2, p=0.5
M=6.5, h=2 km
HORIZONTAL
VERTICAL
10
1
10^{-1}
10^{-2}
10^2
10
1
10^{-1}
0.1
1
10

Figure 21

motions. It is seen that for small ζ vertical and horizontal spectrum amplitudes are nearly the same. With increasing damping the high frequency spectrum amplitudes of vertical motions become progressively smaller and for $\zeta = 0.20$ the shapes of horizontal and vertical spectra become similar and not too dependent on epicentral distance R.

Figures 22, 23 and 24 compare the amplitudes of PSV spectra computed from acceleration recorded during the Imperial Valley, California earthquake of 1940, in El Centro, with spectrum amplitudes from equation (1) for $p = 0.1$ and 0.9, $M = 6.4$, $h = 19500$ ft, $R = 15$ km, $\zeta = 0.0$, 0.02, 0.05, 0.10 and 0.20, and for vertical and two horizontal components. The agreement between computed and observed amplitudes is fair for vertical motions and good for horizontal motions.

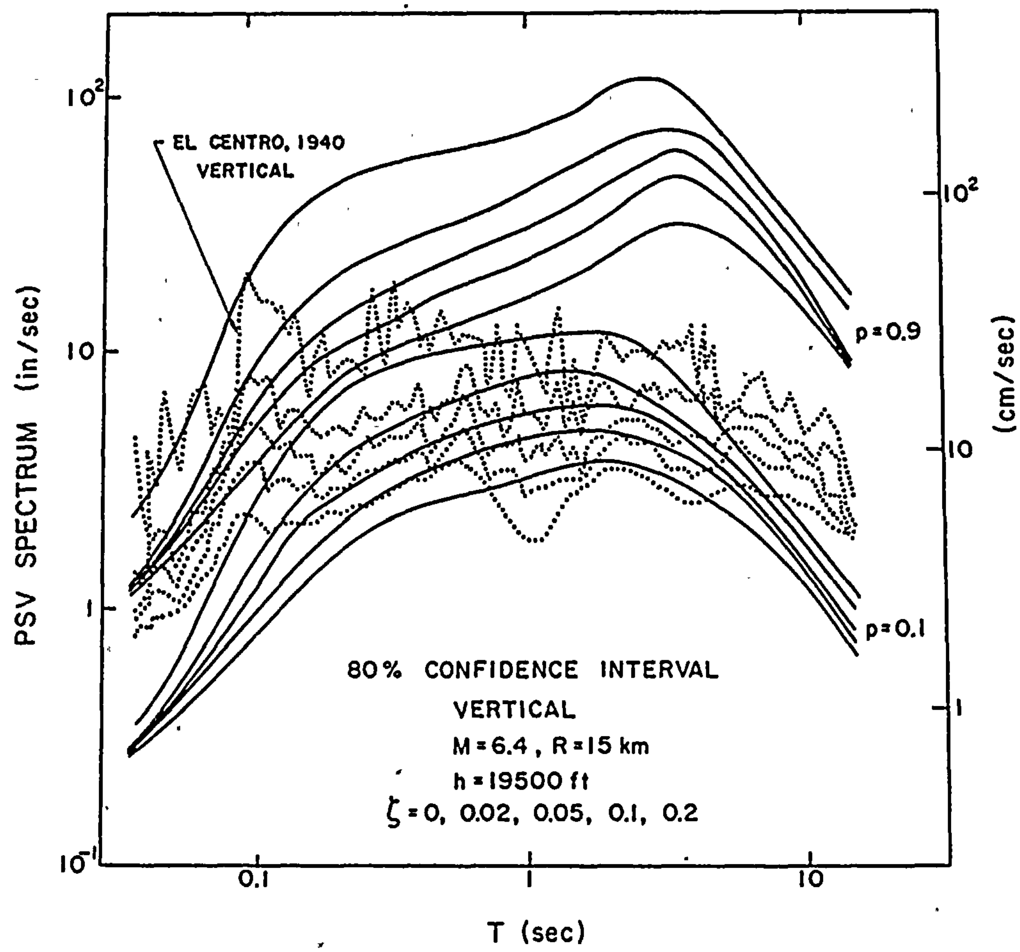
EL CENTRO, 1940
VERTICAL
PSV SPECTRUM (in/sec)
(cm/sec)
p=0.9
p=0.1
80% CONFIDENCE INTERVAL
VERTICAL
M=6.4, R=15 km
h=19500 ft
ζ=0, 0.02, 0.05, 0.1, 0.2
T (sec)

Figure 22

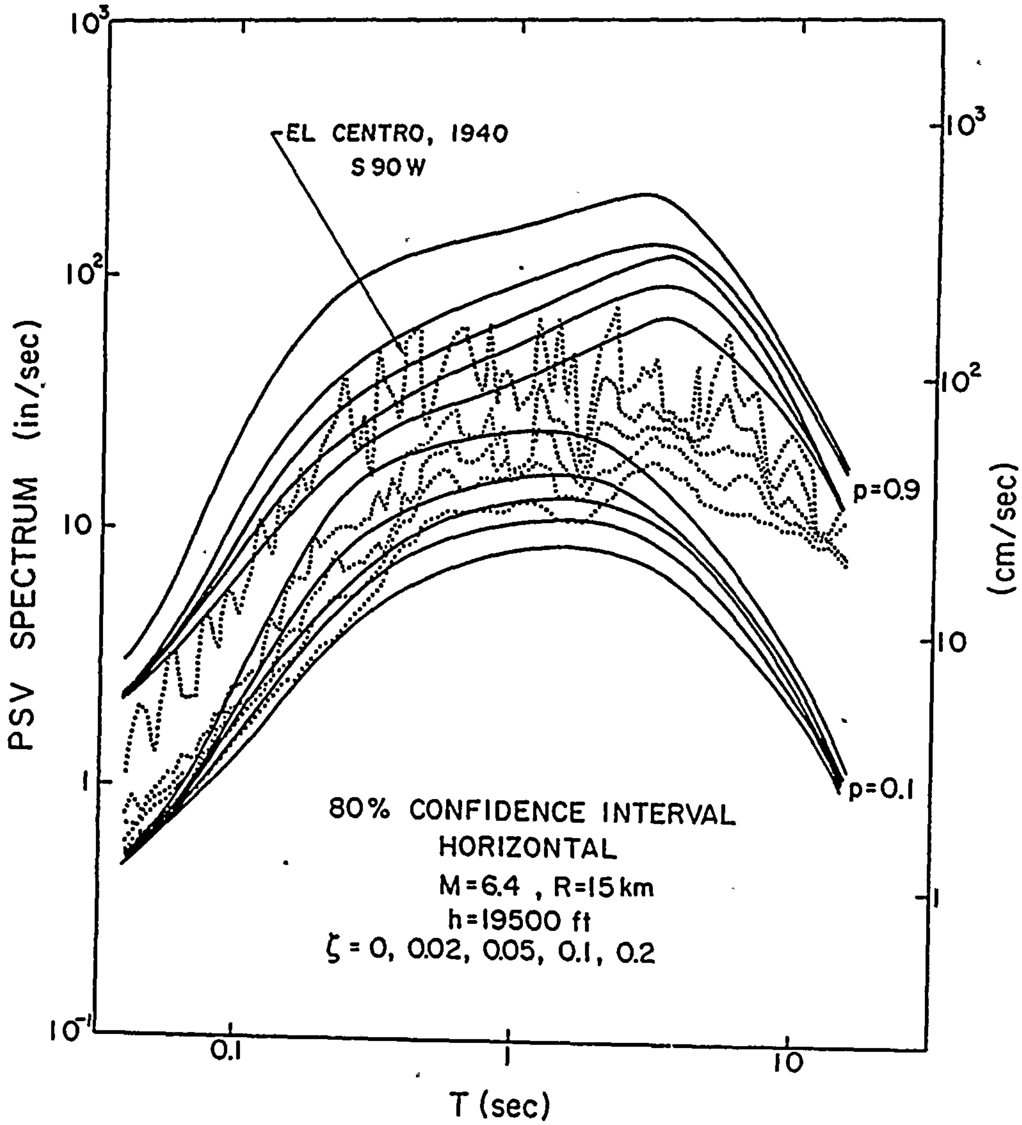

EL CENTRO, 1940
S 90 W
PSV SPECTRUM (in/sec)
(cm/sec)
T (sec)
p=0.9
p=0.1
80% CONFIDENCE INTERVAL
HORIZONTAL
M=6.4 , R=15 km
h=19500 ft
ζ = 0, 0.02, 0.05, 0.1, 0.2

Figure 23

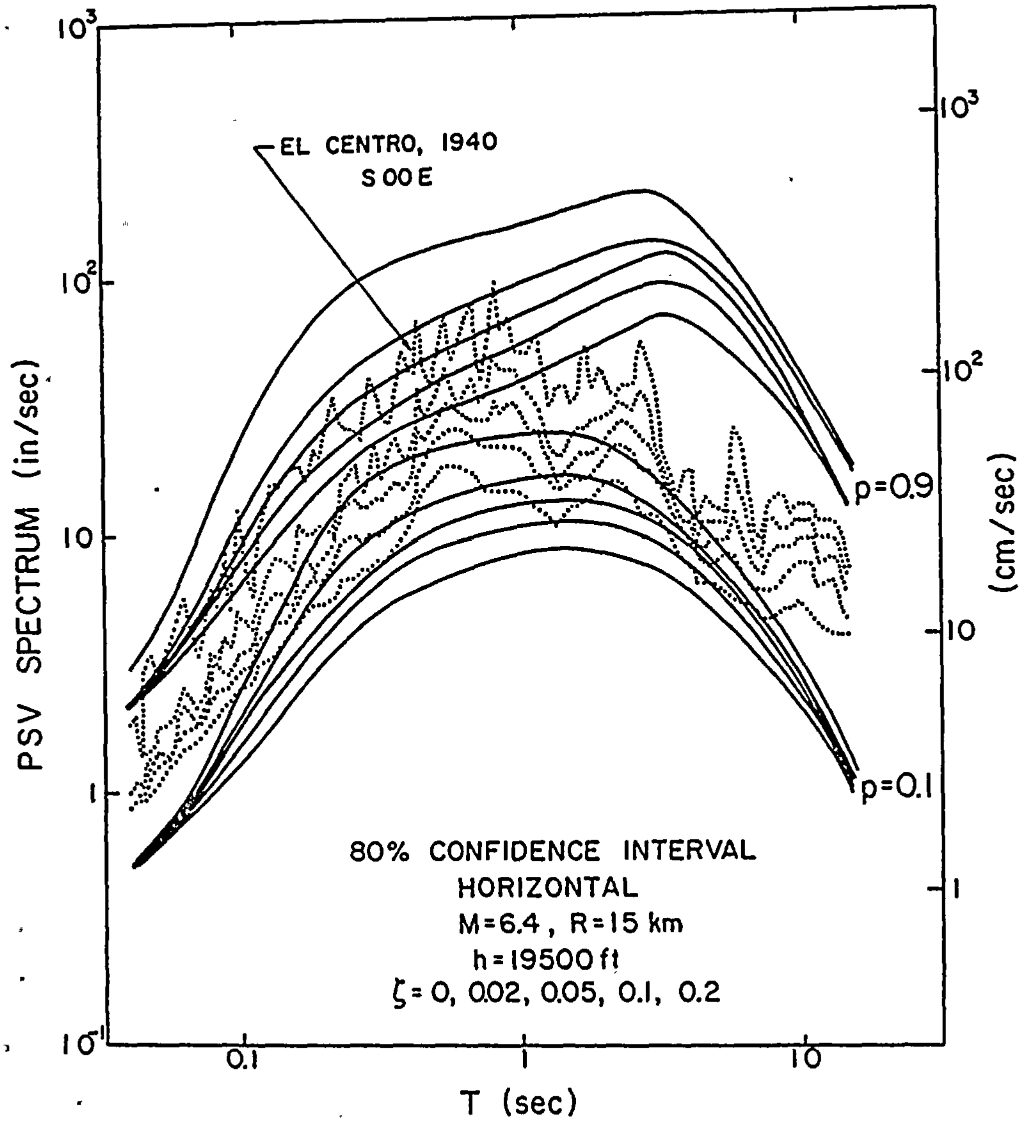

EL CENTRO, 1940
S 00 E
PSV SPECTRUM (in/sec)
(cm/sec)
p=0.9
p=0.1
80% CONFIDENCE INTERVAL
HORIZONTAL
M=6.4, R=15 km
h=19500 ft
ζ= 0, 0.02, 0.05, 0.1, 0.2
T (sec)

Figure 24

SCALING OF PSV SPECTRA IN TERMS OF MMI, h AND v

Following our previous work (Trifunac, 1979; Trifunac and Lee, 1978), we write

$$\log_{10}[PSV(T)] = b(T)I_{MM} + c(T) + d(T)h + e(T)v \qquad (4)$$

where I_{MM} represents a numerical value (1,2,3,...,11 and 12) assigned to the corresponding level on the Modified Mercalli Intensity (MMI) at the site (I,II,..., XI and XII) (Trifunac, 1979), and h and v have the same meaning as in (1). The explicit dependence of PSV(T) on epicentral distance is omitted here. Such dependence would decrease the uncertainties associated with the estimation of PSV(T) in (4), but would render the expression applicable only to those regions which have similar intensity attenuation with distance as southern California, the source of most records in the present data base. Though a particular intensity of shaking can be assigned for a small nearby earthquake as for a distant large earthquake, formally equation (4) depends only on the MMI at the site and thus is more general. A recent study (Anderson, 1979) has confirmed the usefulness of this approach by showing that the end result in earthquake risk mapping based on equation (4) leads to equal or smaller uncertainties than the scaling based on equation (1) which includes explicit dependence on R.

The estimates of b(T) through e(T), denoted by $\hat{b}(T)$ through $\hat{e}(T)$, have been computed for the regression analysis at 91 periods between 0.04 sec and 15 sec, and smoothed along $\log_{10}T$ axis (Figure 25). Table III presents these amplitudes at eleven selected periods. Figure 26 presents the residuals $\varepsilon(T)$ as defined in equation (2) by the difference between $\log_{10}PSV(T)$ and $\log_{10}\hat{PSV}(T)$ for $\zeta = 0.0$, 0.02, 0.05, 0.10 and 0.20.

TABLE III

Regression Parameters for Equation (4) and α(T), β(T), N(T) at Eleven Selected Periods

Period, T(sec)	.040	.065	0.11	0.19	0.34	0.505	0.90	1.60	2.80	4.40	7.50
ζ = 0.0											
b(T)	0.349	0.332	0.300	0.276	0.266	0.267	0.291	0.325	0.328	0.292	0.235
c(T)	-2.730	-2.355	-1.605	-1.061	-0.833	-0.809	-1.006	-1.380	-1.560	-1.421	-1.240
10*d(T)	-0.253	-0.276	-0.283	-0.092	0.149	0.287	0.523	0.801	1.054	1.097	0.908
e(T)	-0.134	-0.099	-0.109	-0.233	-0.329	-0.347	-0.346	-0.286	-0.208	-0.212	-0.234
α(T)	1.940	1.808	1.751	2.012	2.393	2.506	3.634	3.196	2.666	2.500	2.636
β(T)	0.230	0.211	0.184	0.175	0.176	0.181	-0.457	-0.502	-0.531	-0.533	-0.492
N(T)	2	2	2	2	2	2	1	1	1	1	1
ζ = 0.02											
b(T)	0.310	0.307	0.298	0.286	0.279	0.282	0.307	0.341	0.348	0.307	0.241
c(T)	-2.600	-2.360	-1.846	-1.368	-1.119	-1.106	-1.296	-1.630	-1.793	-1.608	-1.340
10*d(T)	-0.096	-0.134	-0.211	-0.173	-0.007	0.161	0.435	0.714	0.963	1.020	0.877
e(T)	-0.238	-0.202	-0.188	-0.267	-0.341	-0.358	-0.353	-0.302	-0.235	-0.235	-0.246
α(T)	2.310	2.144	2.030	2.209	2.523	2.610	3.804	3.356	2.729	2.487	2.606
β(T)	0.230	0.218	0.198	0.182	0.176	0.182	-0.453	-0.503	-0.540	-0.541	-0.494
N(T)	2	2	2	2	2	2	1	1	1	1	1
ζ = 0.05											
b(T)	0.304	0.299	0.291	0.283	0.281	0.287	0.313	0.347	0.354	0.316	0.250
c(T)	-2.560	-2.340	-1.887	-1.471	-1.249	-1.240	-1.436	-1.757	-1.910	-1.748	-1.477
10*d(T)	-0.084	-0.130	-0.211	-0.158	-0.011	0.128	0.376	0.664	0.963	1.060	0.925
e(T)	-0.257	-0.230	-0.222	-0.288	-0.352	-0.366	-0.363	-0.319	-0.262	-0.258	-0.263
α(T)	2.410	2.256	2.150	2.309	2.602	2.670	3.869	3.423	2.779	2.494	2.559
β(T)	0.231	0.222	0.203	0.188	0.181	0.185	-0.450	-0.496	-0.530	-0.528	-0.484
N(T)	2	2	2	2	2	2	1	1	1	1	1

TABLE III -- Continued

ζ = 0.10											
b(T)	0.301	0.296	0.288	0.283	0.283	0.290	0.315	0.347	0.355	0.324	0.264
c(T)	-2.560	-2.352	-1.927	-1.561	-1.369	-1.366	-1.556	-1.847	-2.000	-1.861	-1.624
10*d(T)	-0.041	-0.084	-0.179	-0.161	-0.039	0.101	0.375	0.647	0.892	0.982	0.874
e(T)	-0.273	-0.254	-0.250	-0.305	-0.361	-0.372	-0.365	-0.328	-0.274	-0.257	-0.258
α(T)	2.440	2.328	2.260	2.409	2.652	2.710	3.924	3.493	2.859	2.567	2.596
β(T)	0.230	0.223	0.208	0.192	0.184	0.186	-0.450	-0.495	-0.532	-0.530	-0.487
N(T)	2	2	2	2	2	2	1	1	1	1	1
ζ = 0.20											
b(T)	0.292	0.289	0.285	0.283	0.287	0.295	0.318	0.346	0.354	0.329	0.278
c(T)	-2.500	-2.334	-1.987	-1.681	-1.529	-1.536	-1.686	-1.937	-2.090	-2.001	-1.817
10*d(T)	-0.046	-0.059	-0.128	-0.120	-0.007	0.112	0.316	0.567	0.834	0.937	0.881
e(T)	-0.277	-0.270	-0.280	-0.325	-0.369	-0.379	-0.372	-0.339	-0.287	-0.265	-0.262
α(T)	2.480	2.418	2.411	2.533	2.681	2.710	3.934	3.538	2.966	2.677	2.663
β(T)	0.227	0.222	0.210	0.196	0.190	0.194	-0.434	-0.480	-0.525	-0.526	-0.483
N(T)	2	2	2	2	2	2	1	1	1	1	1

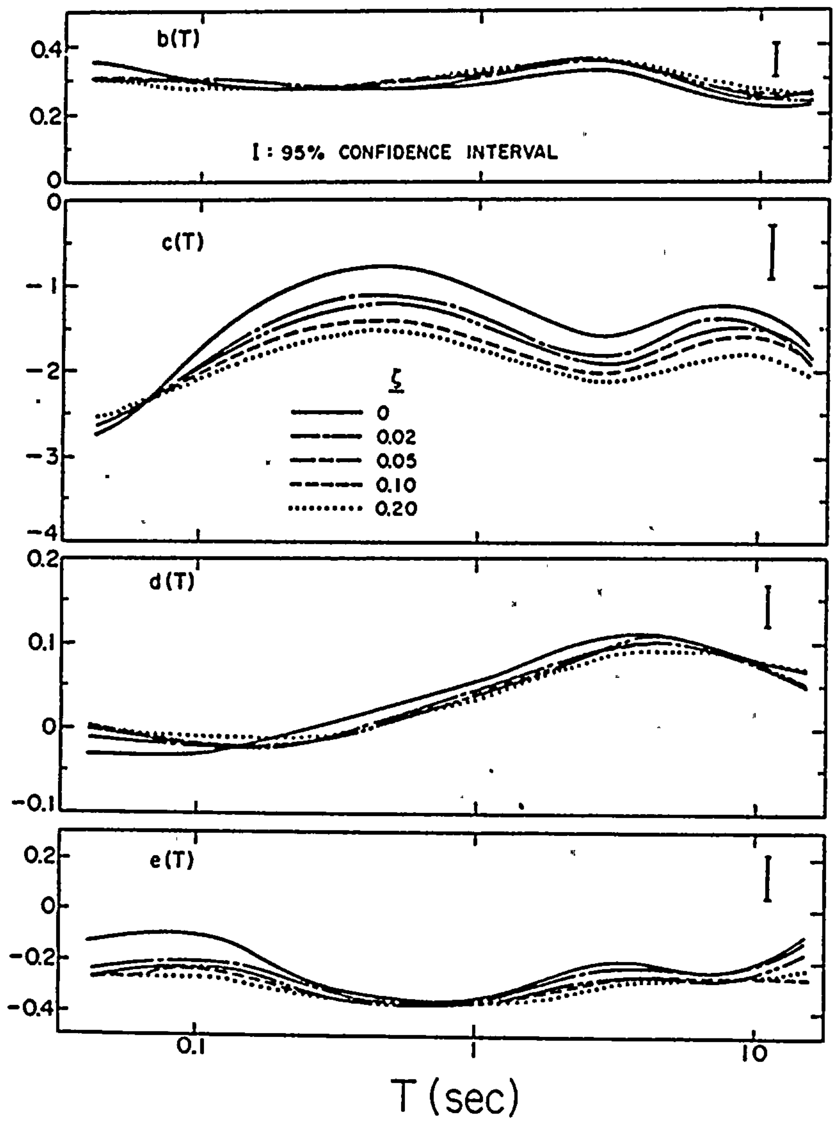

b(T)
0.4
0.2
0
I : 95% CONFIDENCE INTERVAL
c(T)
0
-1
-2
-3
-4
ζ
0
0.02
0.05
0.10
0.20
d(T)
0.2
0.1
0
-0.1
e(T)
0.2
0
-0.2
-0.4
0.1
1
10
T (sec)

Figure 25

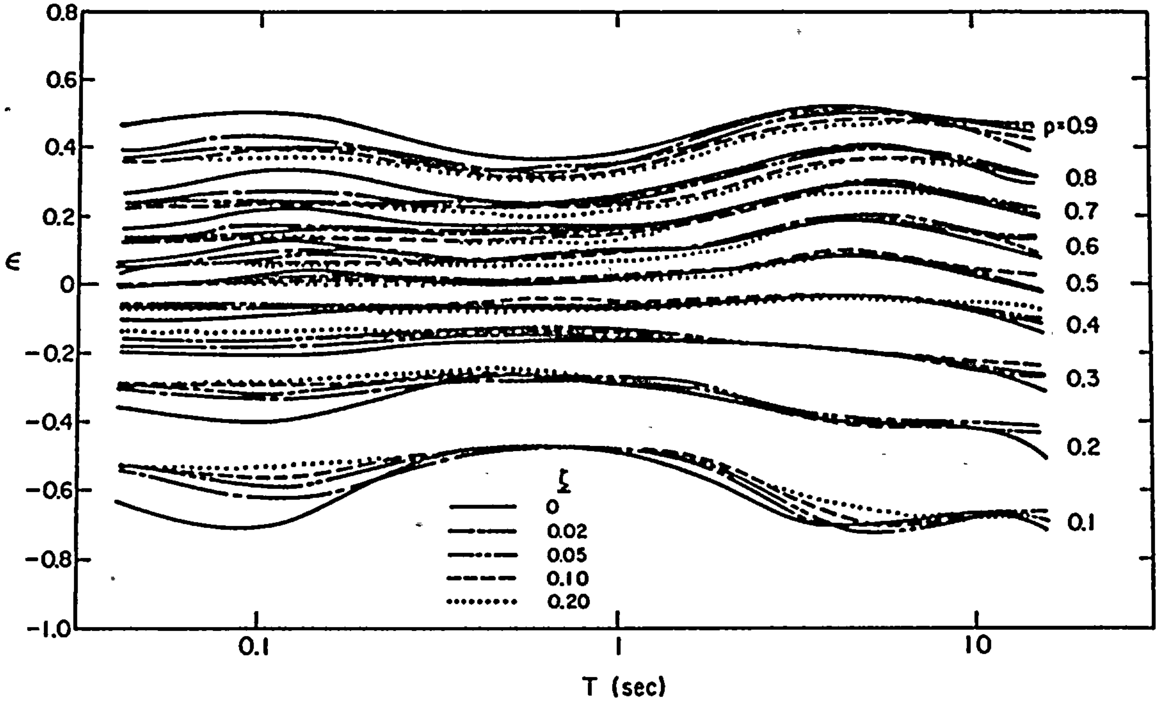

0.8
0.6
0.4
0.2
0
−0.2
−0.4
−0.6
−0.8
−1.0
ε
0.1
1
10
T (sec)
p=0.9
0.8
0.7
0.6
0.5
0.4
0.3
0.2
0.1
ζ
0
0.02
0.05
0.10
0.20

Figure 26

The coefficients $\alpha(T)$, $\beta(T)$ and $N(T)$ in equation (3), which also applies here, are also given in Table III. By choosing the probability that $\log_{10}PSV(T)$ will not be exceeded, computing the corresponding $\varepsilon(T)$ and adding this to $PSV(T)$ amplitudes in equation (4) will yield a distribution of spectral amplitudes for given I_{MM}, h and v.

Figure 27 shows the plot of $\alpha(T)$, $\beta(T)$ and $N(T)$ versus T computed from regression analysis of the data on $\varepsilon(T)$ (Figure 26) and in terms of the assumed distribution function given by equation (3). The expected value $\mu(T)$ and the standard deviation $\sigma(T)$ of this distribution are also shown in Figure 27. Figure 28 shows the smoothed largest differences (Kolmogorov-Smirnov test) between the distribution of $\varepsilon(T)$ as modeled by equation (3) and the data (Figure 26) as well as the amplitudes of χ^2 test versus period T. Comparisons with theoretical limits corresponding to the 95% confidence level show that the distribution function, defined in equation (3), together with the scaling functions $\alpha(T)$, $\beta(T)$ and $N(T)$, is an acceptable candidate for analytic approximation of the distribution of $\log_{10}[PSV(T)]$ with respect to the estimate $\log_{10}[\hat{PSV}(T)]$.

Figures 29 through 38 present examples of PSV(T) spectral amplitudes computed from equation (4) and for MMI = IV, VI, VIII, X and XII, h = 0, 4 km, $\zeta = 0.0$, 0.02, 0.05, 0.10 and 0.20, and for vertical and horizontal motions. The plotted amplitudes for MMI levels X and XII are outside the range where data is now available and thus cannot be tested. Those amplitudes should be considered here only as an illustration of what results from extrapolating on the basis of equation (4). Figures 39, 40 and 41 show comparison of spectra based on equation (4) (MMI = VIII, h = 19,500 ft), and the corresponding spectra from recorded accelerograms.

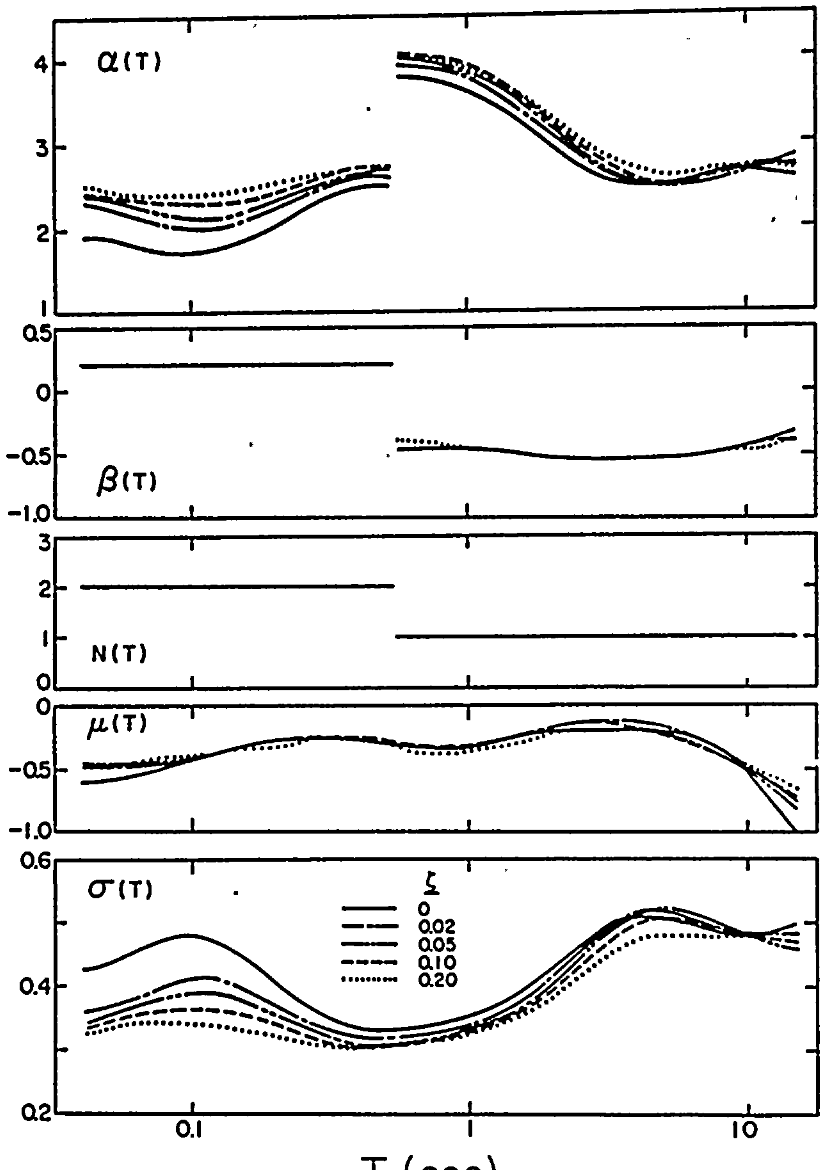
α(T)
4
3
2
1
0.5
0
-0.5
β(T)
-1.0
3
2
1
N(T)
0
0
μ(T)
-0.5
-1.0
0.6
σ(T)
ζ
0
0.02
0.05
0.10
0.20
0.4
0.2
0.1
1
10
T (sec)

Figure 27

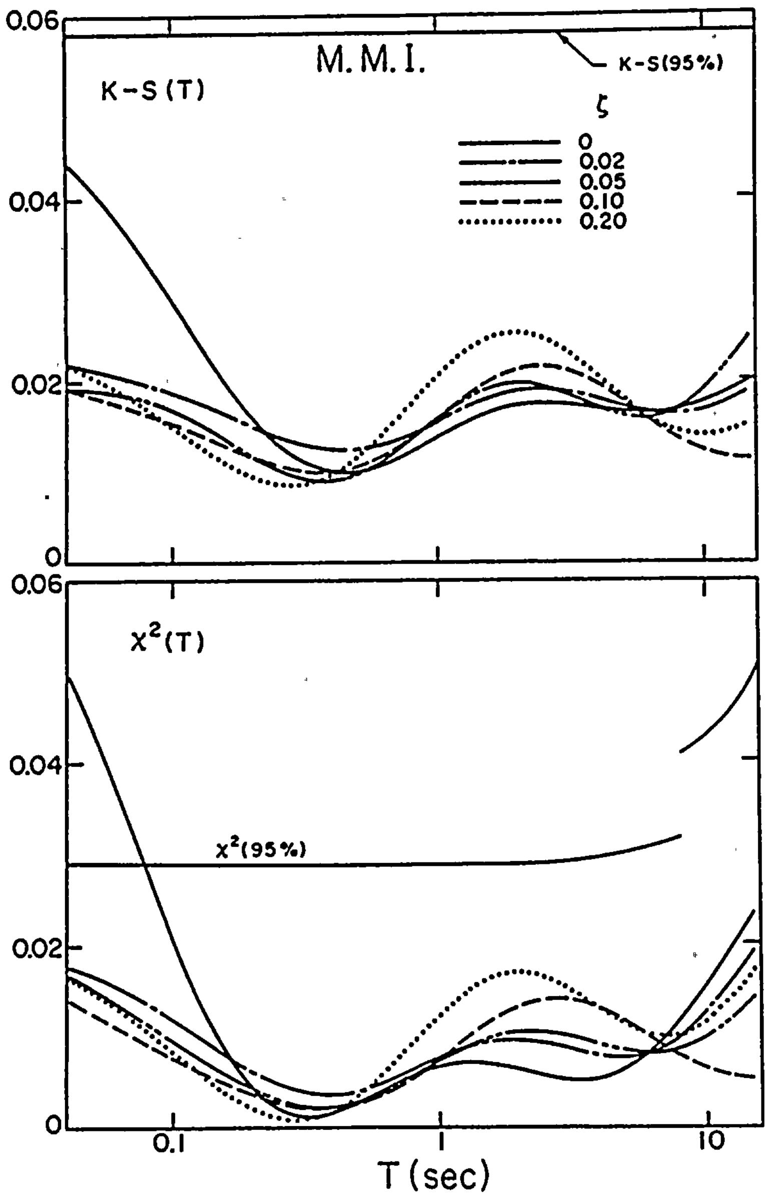

0.06
M.M.I.
K-S(95%)
K-S(T)
ζ
0
0.02
0.05
0.10
0.20
0.04
0.02
0
0.06
X²(T)
0.04
X²(95%)
0.02
0
0.1
1
10
T (sec)

Figure 28

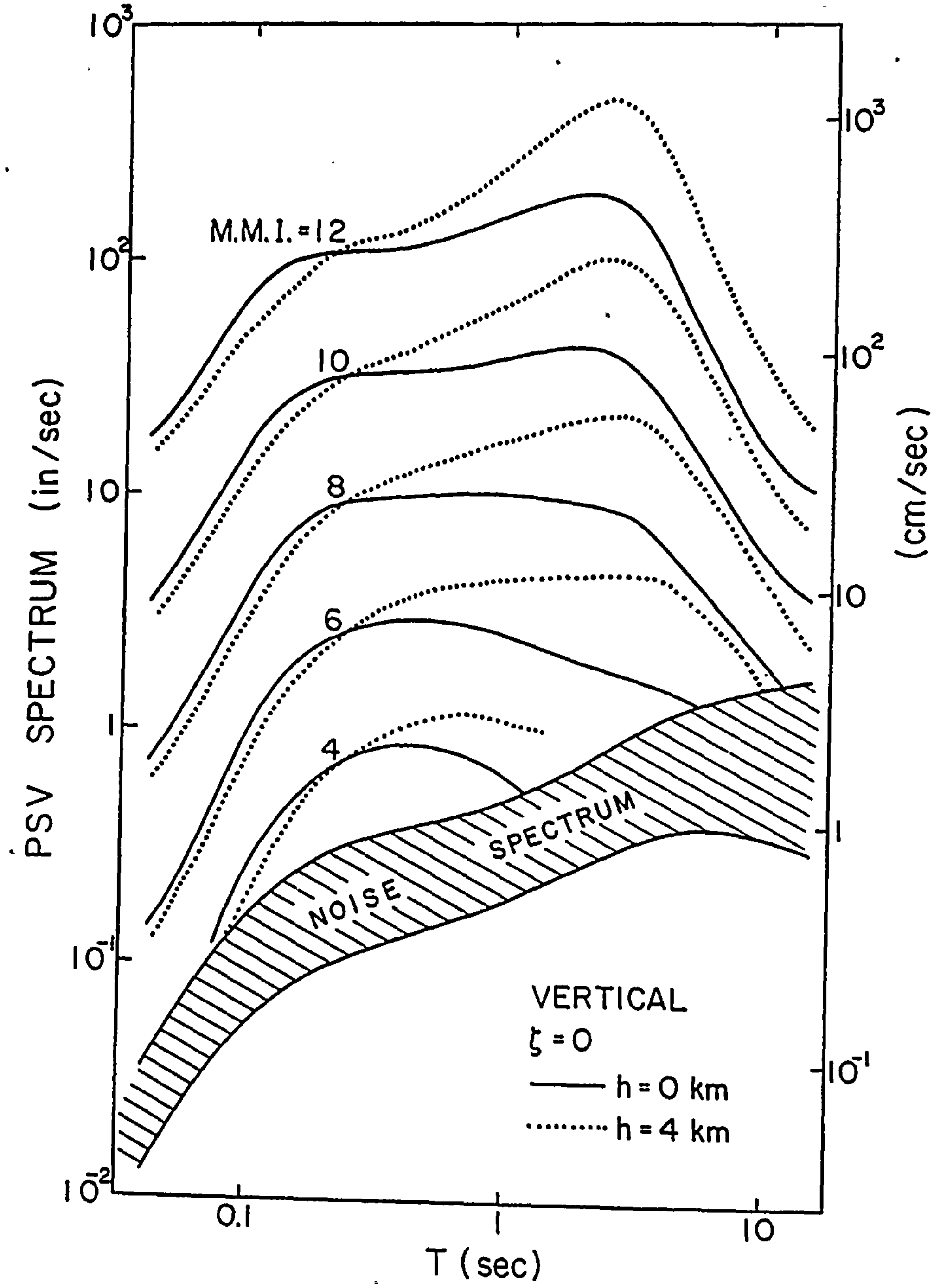

PSV SPECTRUM (in/sec)
(cm/sec)
T (sec)
M.M.I.=12
10
8
6
4
NOISE SPECTRUM
VERTICAL
ζ=0
h=0 km
h=4 km
10^3
10^2
10
1
10^{-1}
10^{-2}
0.1
1
10

Figure 29

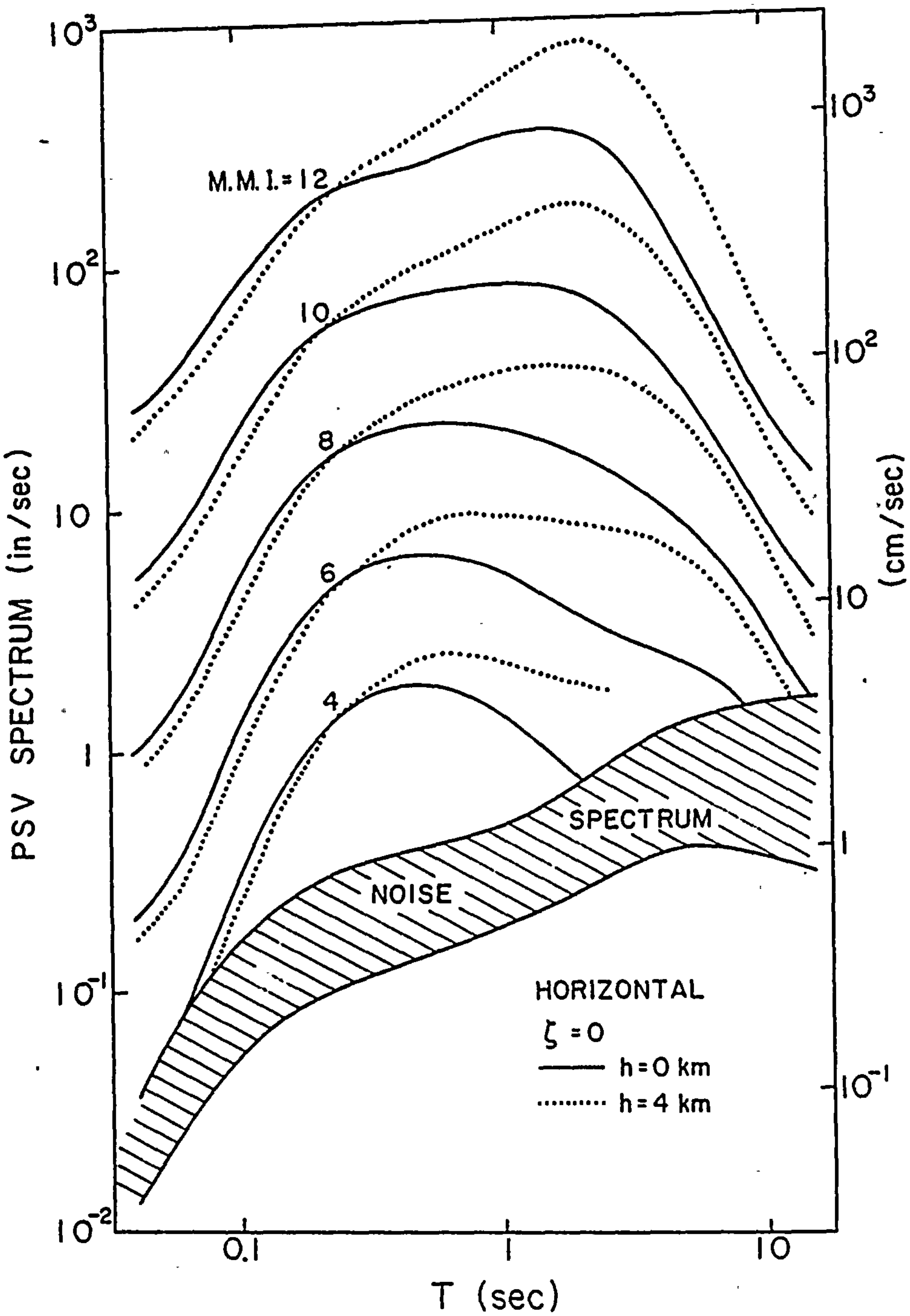

10^3
10^2
10
1
10^{-1}
10^{-2}
10^3
10^2
10
1
10^{-1}
PSV SPECTRUM (in/sec)
(cm/sec)
M.M.I.=12
10
8
6
4
SPECTRUM
NOISE
HORIZONTAL
ζ =0
h=0 km
h=4 km
0.1
1
10
T (sec)

Figure 30

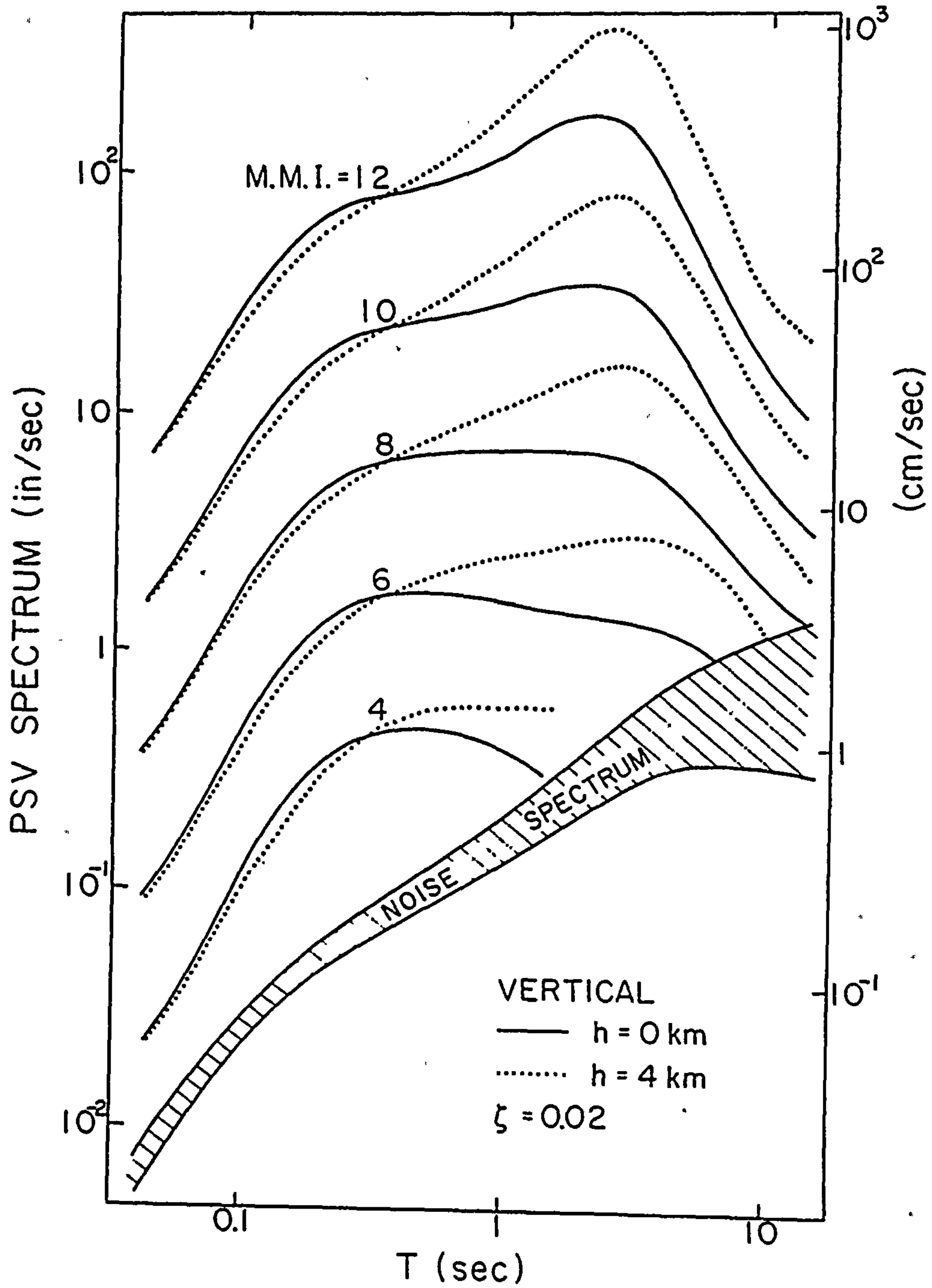
M.M.I. = 12
10
8
6
4
NOISE SPECTRUM
VERTICAL
h = 0 km
h = 4 km
ζ = 0.02
PSV SPECTRUM (in/sec)
(cm/sec)
T (sec)
10^2
10
1
10^{-1}
10^{-2}
10^3
10^2
10
1
10^{-1}
0.1
1
10

Figure 31

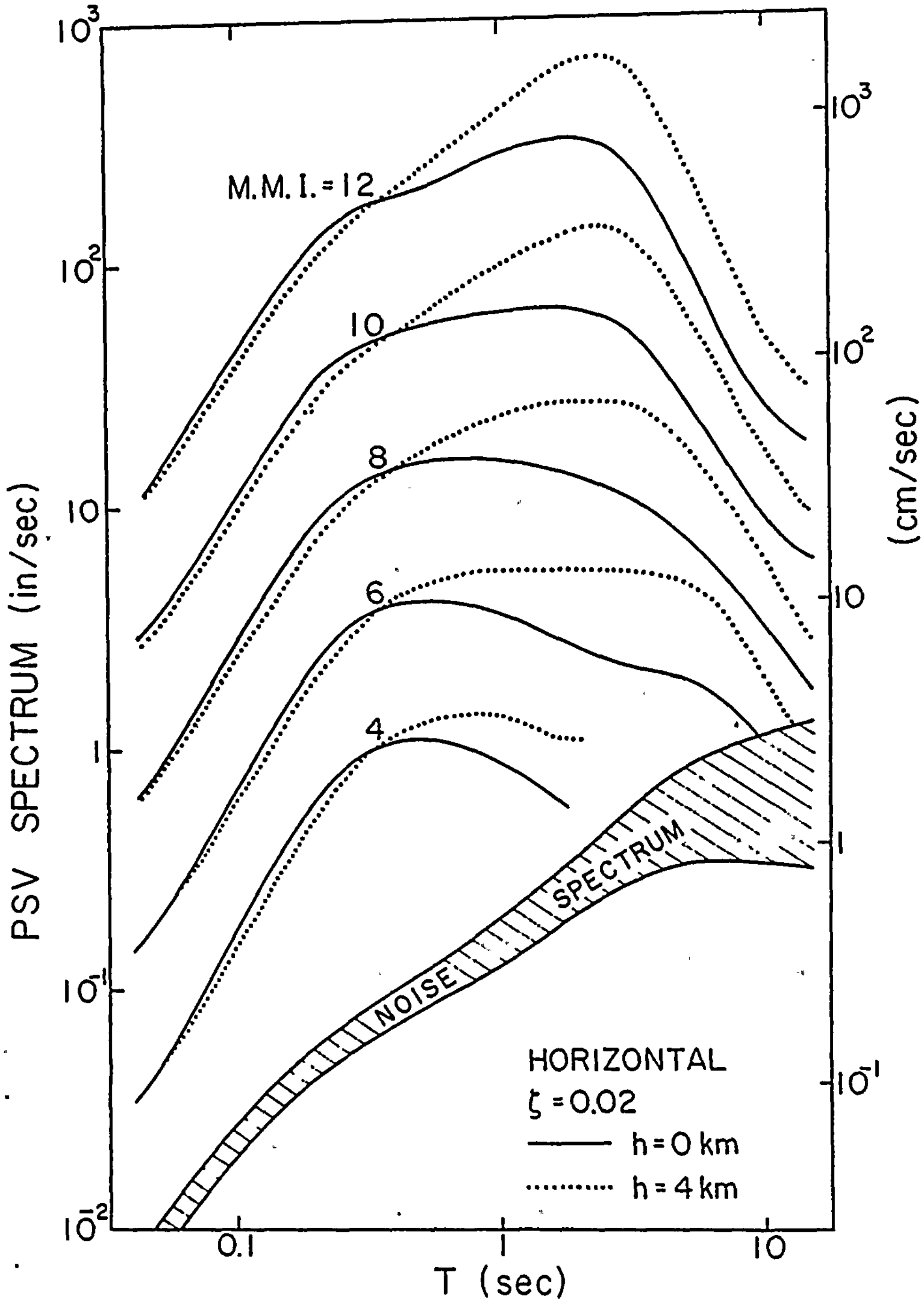

10^3
10^2
10
1
10^{-1}
10^{-2}
PSV SPECTRUM (in/sec)
10^3
10^2
10
1
10^{-1}
(cm/sec)
M.M.I.=12
10
8
6
4
NOISE SPECTRUM
HORIZONTAL
ζ = 0.02
h = 0 km
h = 4 km
0.1
1
10
T (sec)

Figure 32

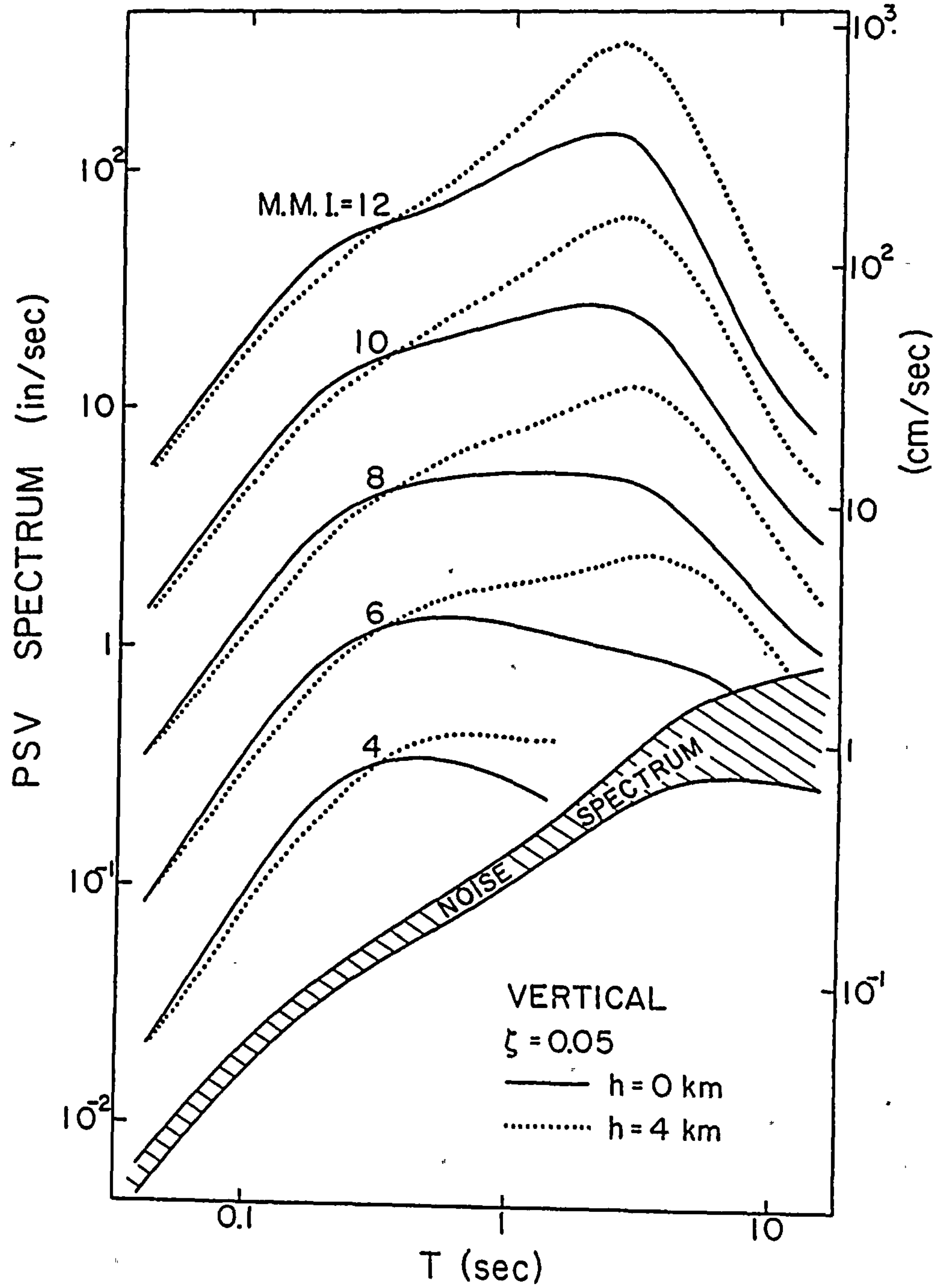

PSV SPECTRUM (in/sec)
(cm/sec)
T (sec)
10^2
10
1
10^{-1}
10^{-2}
10^3
10^2
10
1
10^{-1}
0.1
1
10
M.M.I.=12
10
8
6
4
NOISE SPECTRUM
VERTICAL
ζ = 0.05
h = 0 km
h = 4 km

Figure 33

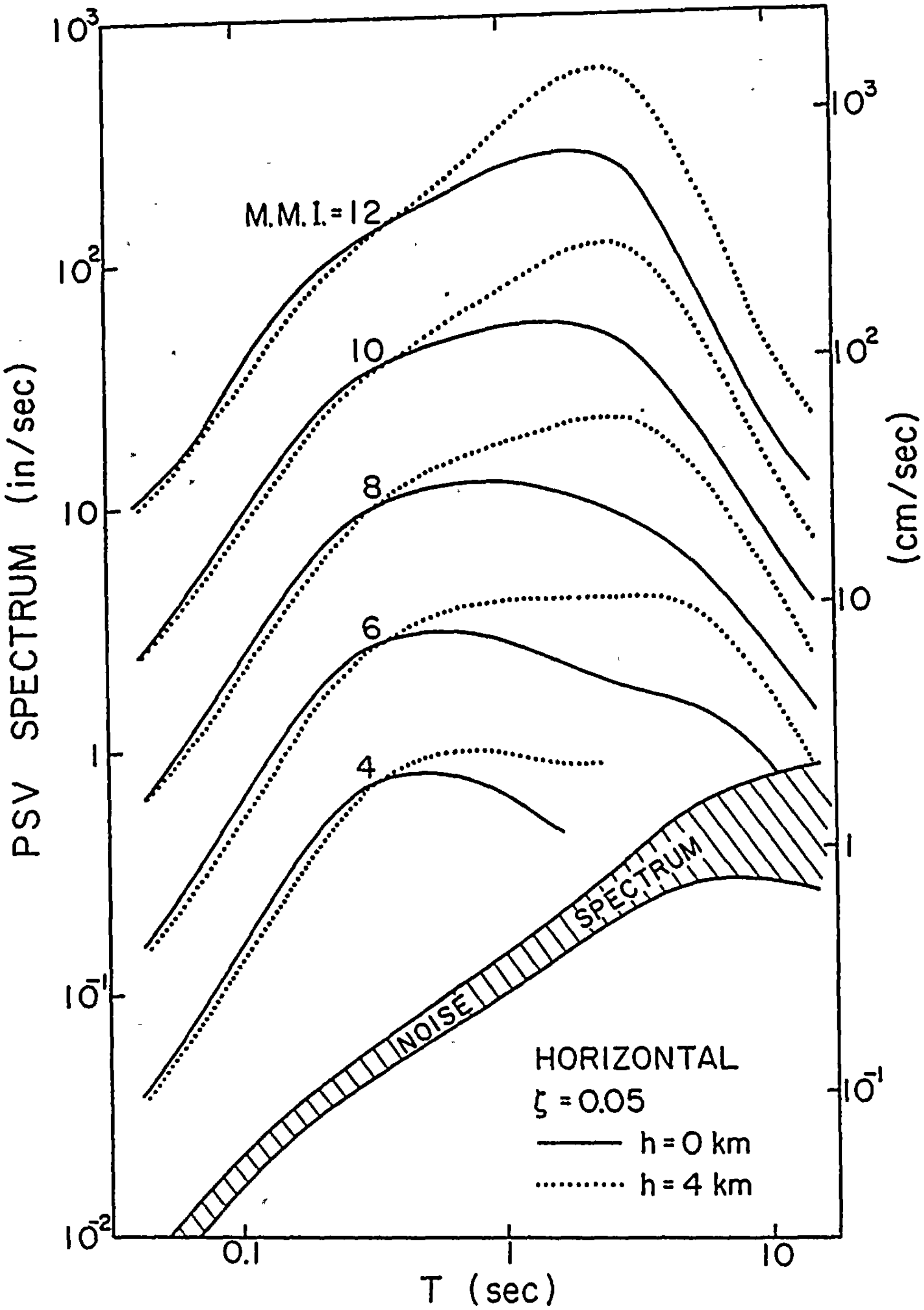

PSV SPECTRUM (in/sec)
(cm/sec)
T (sec)
M.M.I.=12
10
8
6
4
NOISE
SPECTRUM
HORIZONTAL
ζ = 0.05
h = 0 km
h = 4 km

Figure 34

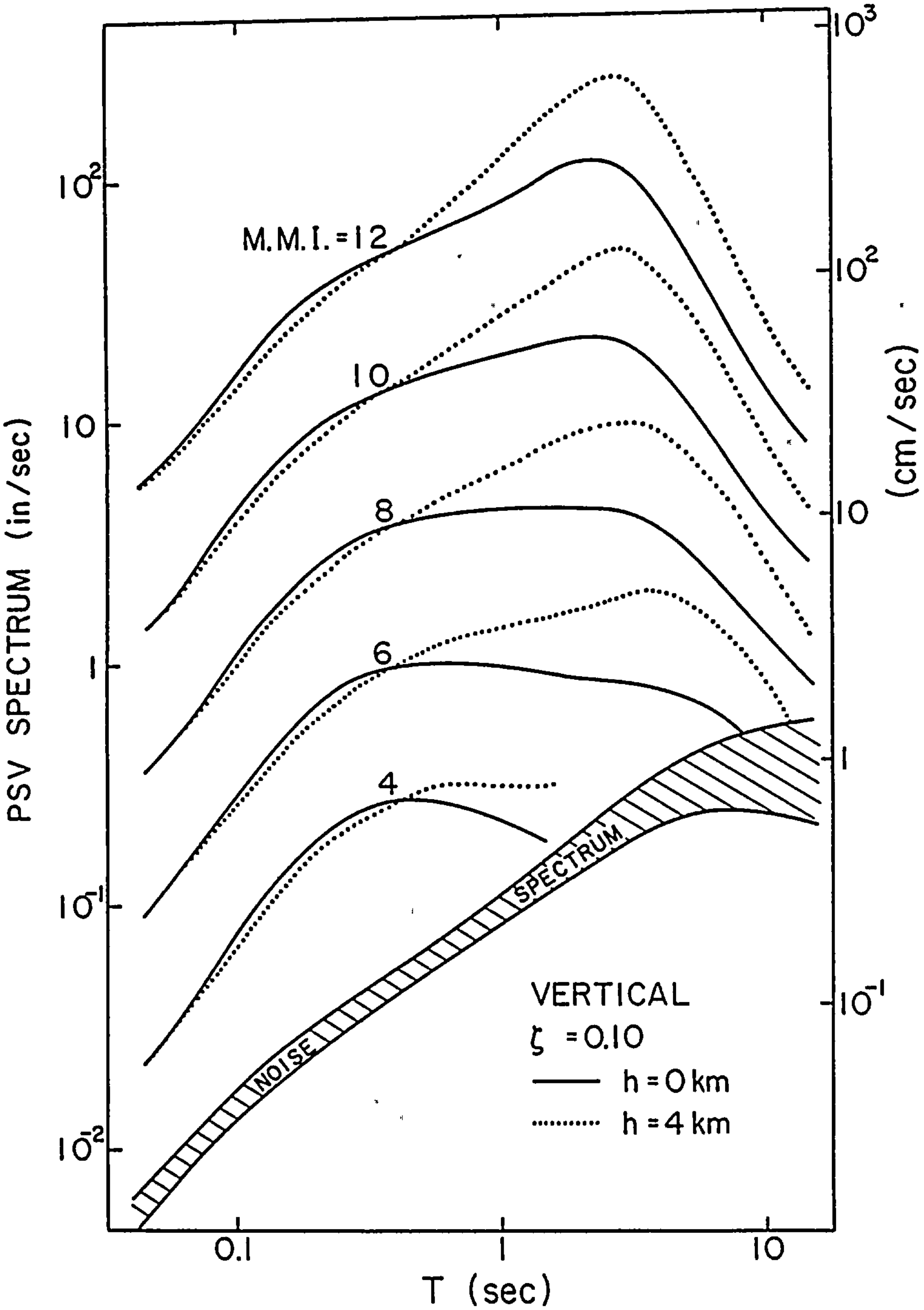
PSV SPECTRUM (in/sec)
(cm/sec)
T (sec)
M.M.I.=12
10
8
6
4
NOISE
SPECTRUM
VERTICAL
ζ =0.10
h=0 km
h=4 km
10^2
10
1
10^{-1}
10^{-2}
10^3
10^2
10
1
10^{-1}
0.1
1
10

Figure 35

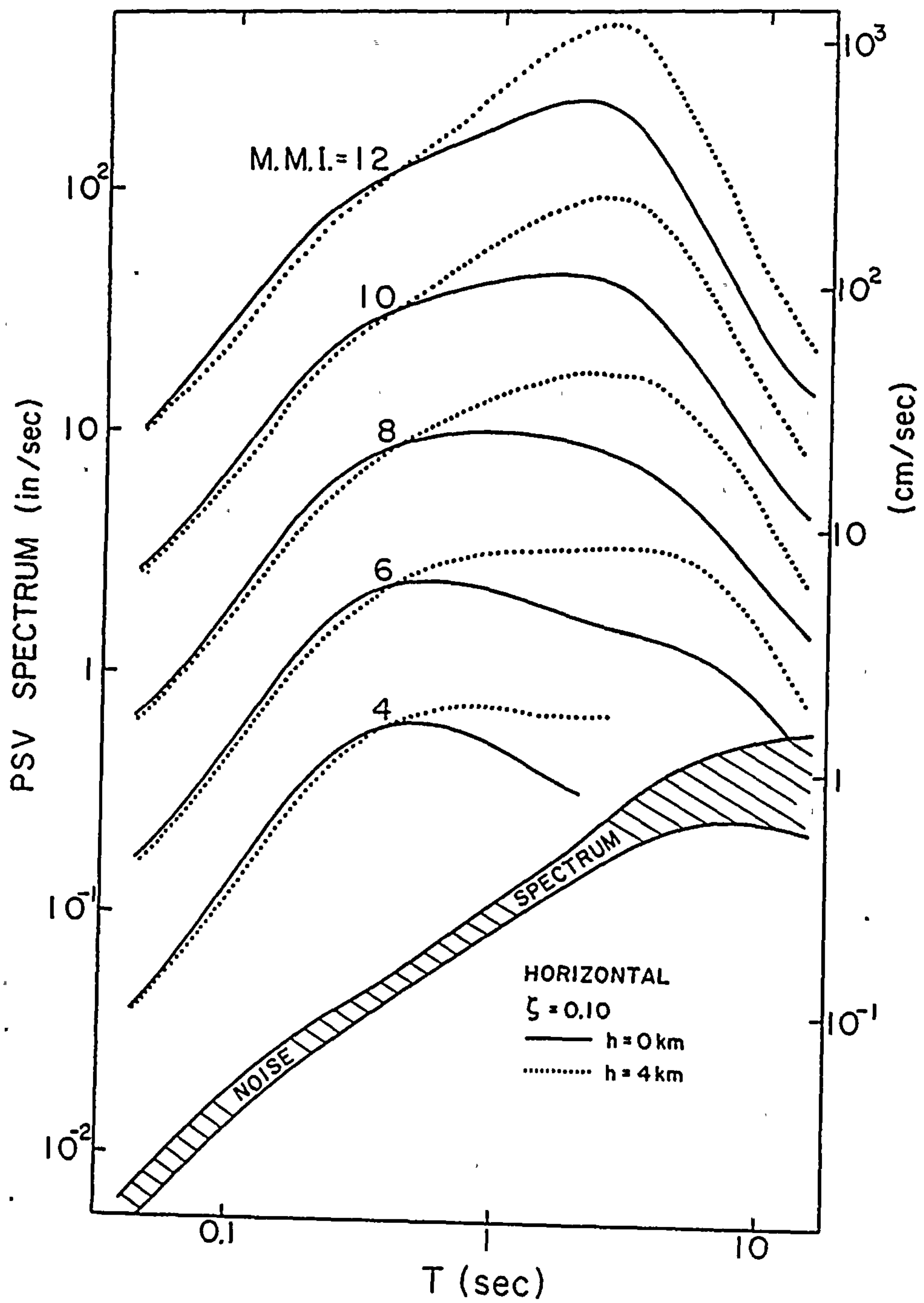

M.M.I.=12
10
8
6
4
NOISE
SPECTRUM
HORIZONTAL
ζ = 0.10
h = 0 km
h = 4 km
PSV SPECTRUM (in/sec)
(cm/sec)
T (sec)
0.1
1
10

Figure 36

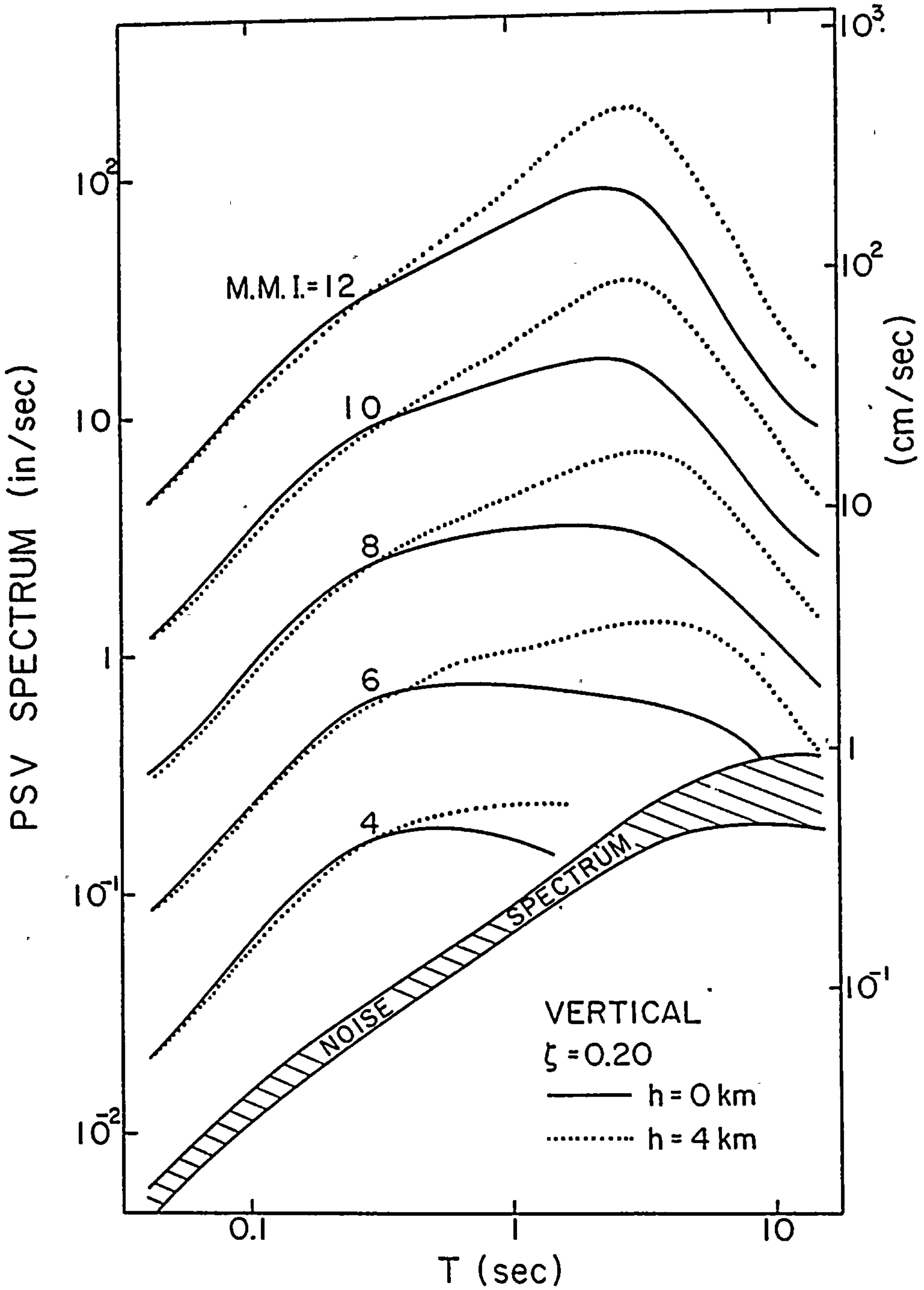
PSV SPECTRUM (in/sec)
(cm/sec)
T (sec)
M.M.I.=12
10
8
6
4
NOISE SPECTRUM
VERTICAL
ζ=0.20
h=0 km
h=4 km
0.1
1
10
10^2
10
1
10^{-1}
10^{-2}
10^3
10^2
10
1
10^{-1}

Figure 37

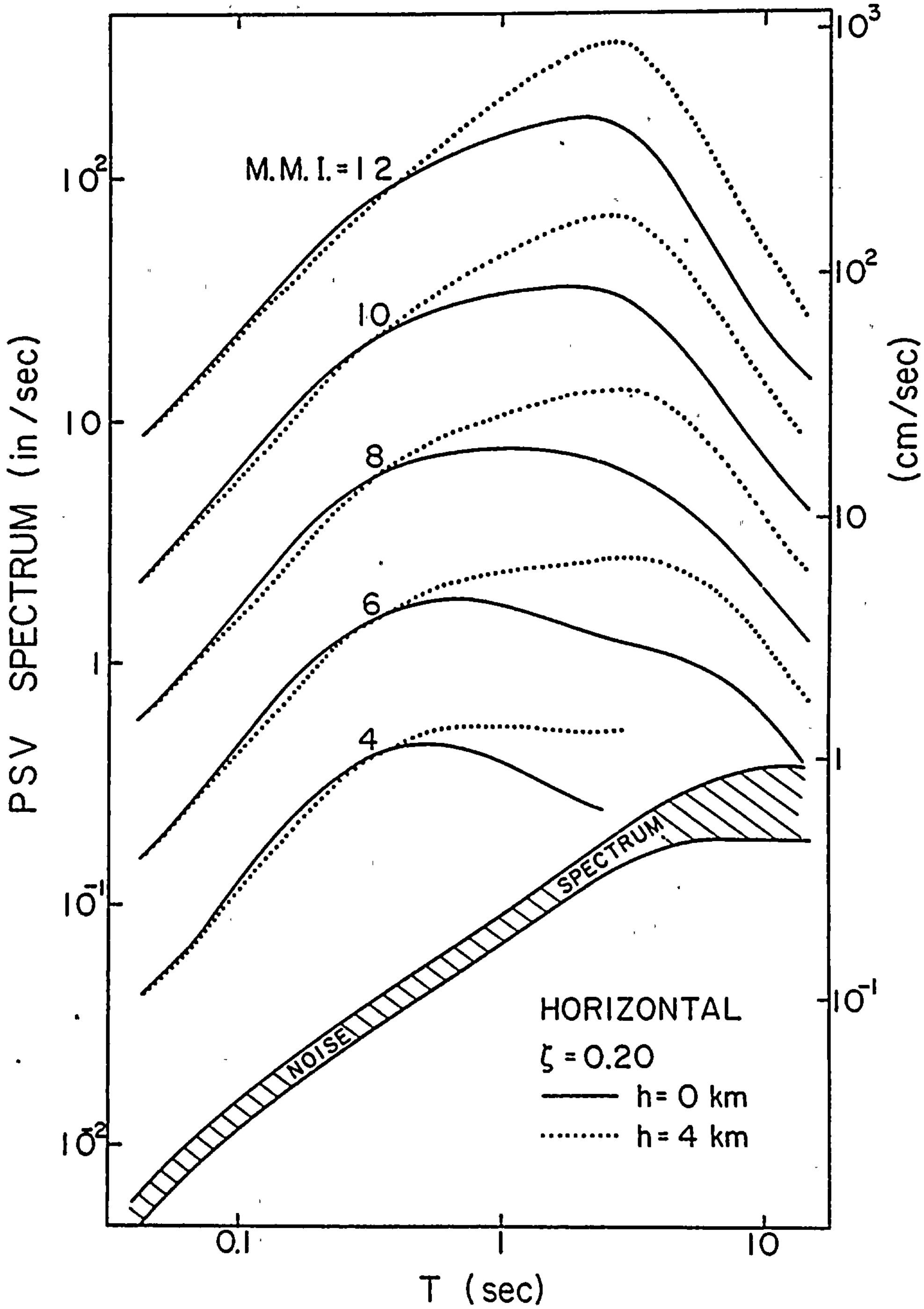

M.M.I.=12
10
8
6
4
10^2
10
1
10^{-1}
10^{-2}
10^3
10^2
10
1
10^{-1}
PSV SPECTRUM (in/sec)
(cm/sec)
0.1
1
10
T (sec)
NOISE
SPECTRUM
HORIZONTAL
ζ = 0.20
h= 0 km
h= 4 km

Figure 38

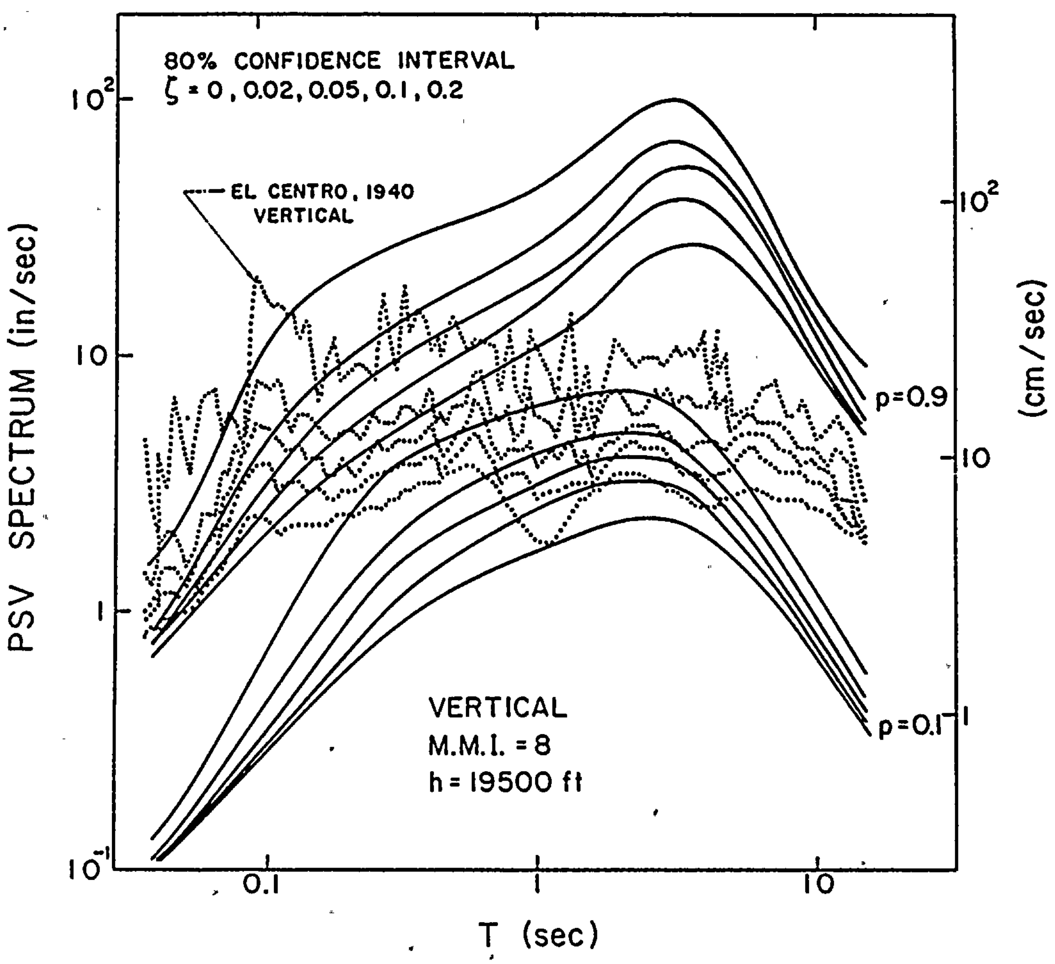
80% CONFIDENCE INTERVAL
ζ = 0, 0.02, 0.05, 0.1, 0.2
EL CENTRO, 1940 VERTICAL
PSV SPECTRUM (in/sec)
(cm/sec)
p=0.9
p=0.1
VERTICAL
M.M.I. = 8
h = 19500 ft
T (sec)
10²
10
1
10⁻¹
0.1
1
10

Figure 39

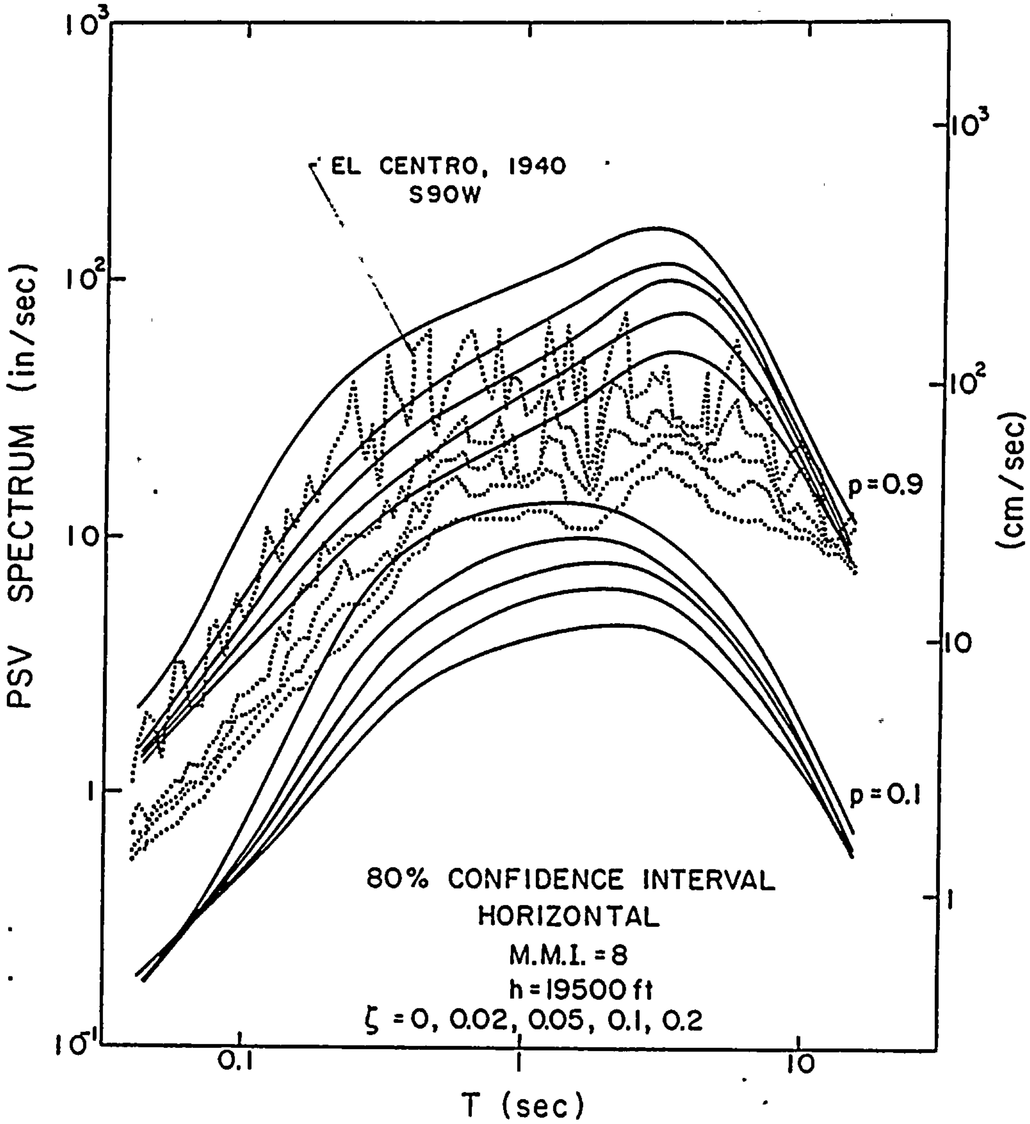

PSV SPECTRUM (in/sec)
(cm/sec)
EL CENTRO, 1940
S90W
p=0.9
p=0.1
80% CONFIDENCE INTERVAL
HORIZONTAL
M.M.I. = 8
h = 19500 ft
ζ = 0, 0.02, 0.05, 0.1, 0.2
T (sec)

Figure 40

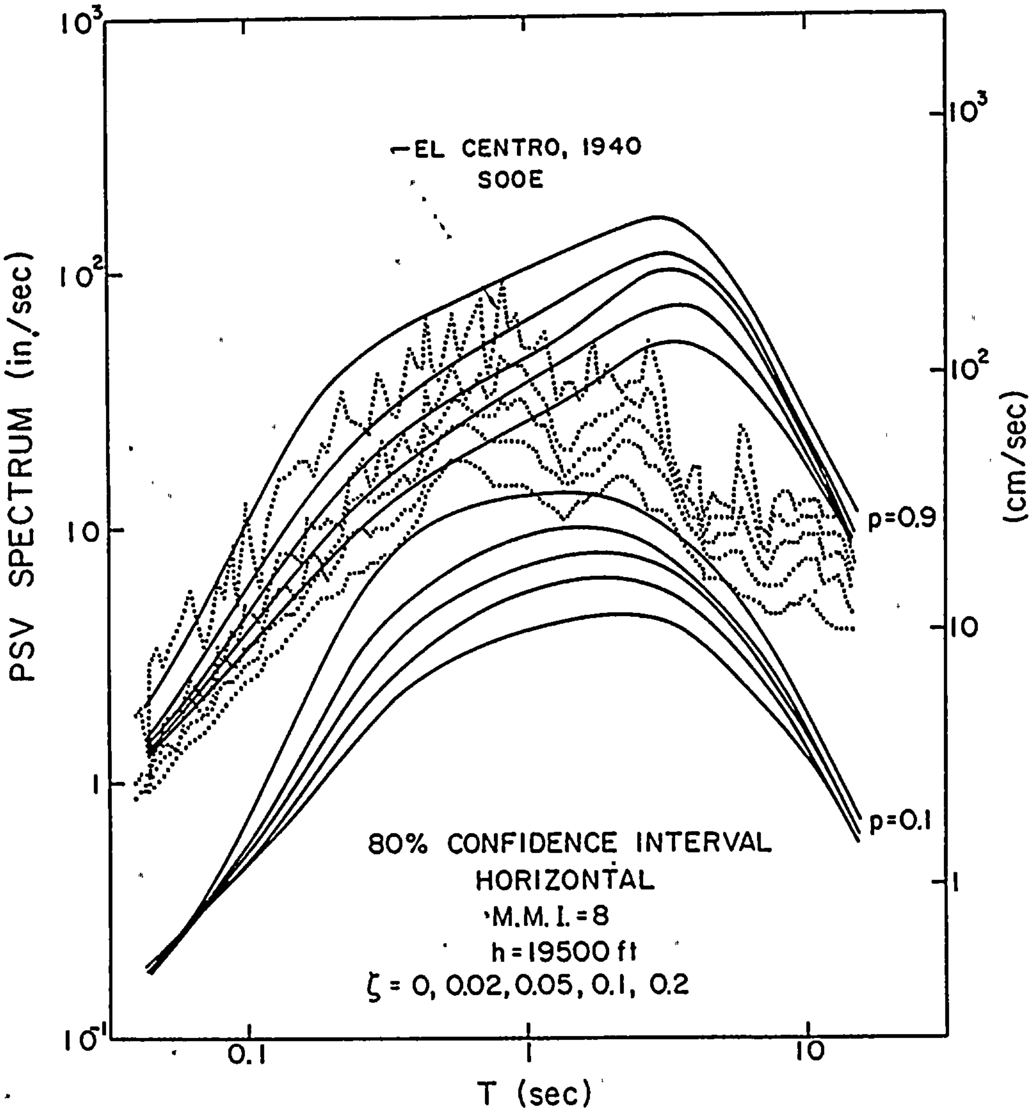
—EL CENTRO, 1940
SOOE
PSV SPECTRUM (in./sec)
(cm/sec)
10^3
10^2
10
1
10^{-1}
0.1
1
10
T (sec)
p=0.9
p=0.1
80% CONFIDENCE INTERVAL
HORIZONTAL
M.M.I.=8
h=19500 ft
ζ = 0, 0.02, 0.05, 0.1, 0.2

Figure 41

As suggested by Trifunac and Anderson (1977; 1978a,b) and Trifunac and Lee (1978), it is useful to check the internal consistency between equations (1) and (4). Considering the distribution of the available data among different epicentral distances, magnitudes and site intensities (Trifunac and Anderson, 1977), it is seen that the "degree of extrapolation" into the range of "largest amplitude of motion" is smaller for equation (1) than for equation (4). The bulk of the available data is now distributed between $M = 4.0$ and $M = 7.5$ and between MMI = IV and MMI = VII through VIII. If the "largest amplitudes of strong shaking" correspond to $M = 7.5$ to 8 with $R = 0$ km and MMI = XII, it will be seen that because of the saturation of the magnitude scale near $M = 7.5$ to 8 (Trifunac, 1976; Trifunac and Anderson, 1977) equation (1) formally does not require much extrapolation before $M = M_{max}$ is reached. On the other hand, extrapolation to MMI = XII on the basis of a regression model based on the data between MMI = IV to VIII is considerable, since there are four intensity levels between MMI = VIII and MMI = XII as there are between MMI = IV and MMI = VIII. Figures 42 and 43 show the largest amplitudes of PSV spectra for $M = 8.5$ and $R = 0$ and for MMI = XII. Both sets of spectra are plotted for $h = 2$ km, $\zeta = 0.0$, 0.02, 0.05, 0.10 and 0.20, and for vertical and horizontal motions. It is concluded from these figures that the slope Of equation (4) with respect to I_{MM} is not contradicted by comparison with extrapolation based on equation (1).

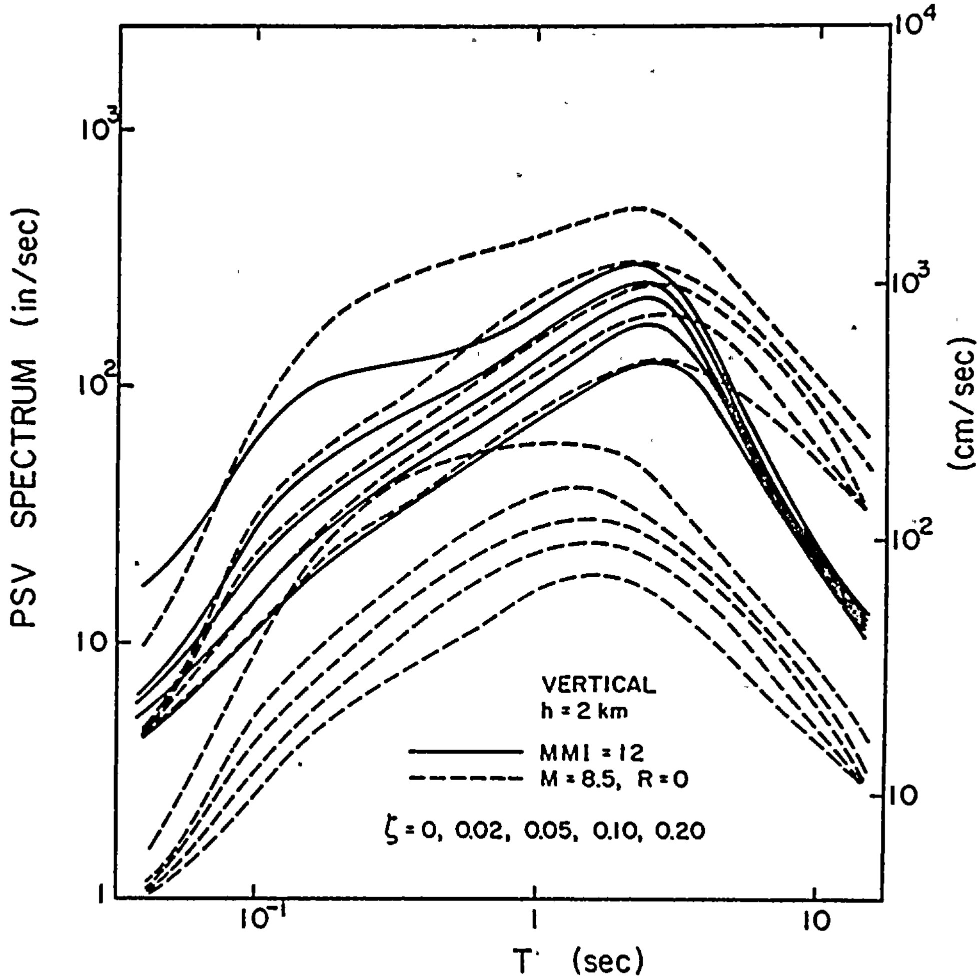
PSV SPECTRUM (in/sec)
(cm/sec)
T (sec)
VERTICAL
h = 2 km
MMI = 12
M = 8.5, R = 0
ζ = 0, 0.02, 0.05, 0.10, 0.20

Figure 42

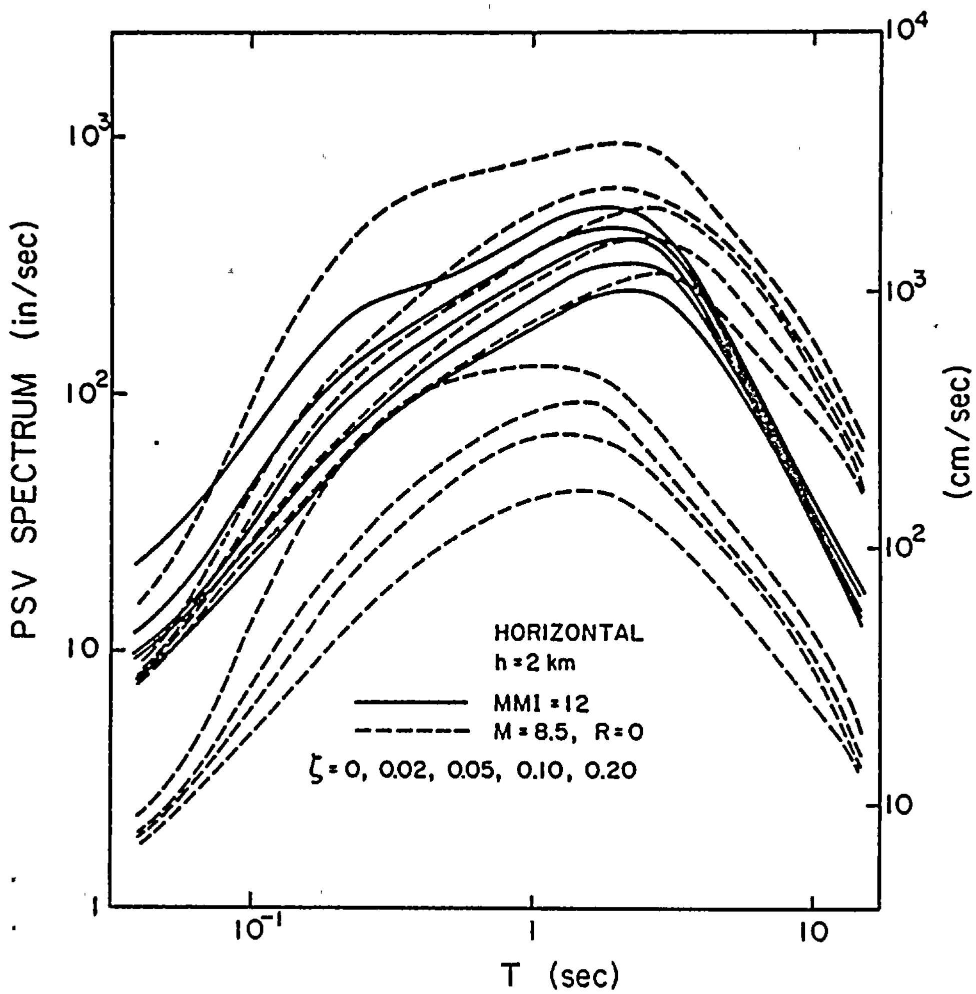
PSV SPECTRUM (in/sec)
(cm/sec)
T (sec)
1
10
10^2
10^3
10^4
10^{-1}
HORIZONTAL
h = 2 km
MMI = 12
M = 8.5, R = 0
ζ = 0, 0.02, 0.05, 0.10, 0.20

Figure 43

CONCLUSIONS

The empirical scaling equations for PSV spectrum amplitudes presented in this paper display a number of trends in the amplitudes of strong earthquake shaking which should be useful for their estimation. Inasmuch as so-far available data has been employed in this work, together with detailed scaling relationships which were tested previously in similar (Trifunac and Lee, 1978) and related analyses (Trifunac and Anderson, 1977; 1978a,b), it is noted here that the nature of these models must be considered as preliminary only. These models will have to evolve continuously through introduction of additional significant scaling parameters and through the improvement in the existing functional form of equations like (1) and (4). These improvements must be based on the physical nature of the phenomenon and various present and future new terms in the empirical scaling function should be based on the functional form predicted by theory and experiment.

Numerous recent analyses with objectives similar to those in this paper, have addressed the problem of empirical scaling of strong motion characteristics through the formalism of a regression analysis only and on the basis of often arbitrary functional forms which are convenient for the fitting routines but cannot be judged by known physical features of the problem. An attenuation often chosen in many regression analyses of the amplitudes of strong shaking is of the form $(a+R)^{-n}$, for example, where a and n are constants determined through some fitting routine. While this functional form of attenuation can model <u>one</u> type of wave in <u>one</u> distance range, it is not capable of describing the near-field terms ($\sim R^{-4}$, $\sim R^{-2}$), body waves ($\sim R^{-1}$) and surface waves ($\sim R^{\frac{1}{2}}$) simultaneously in one scaling relation. By using $\log_{10}A_0(R)$ determined empirically in southern California, we have, through experimental means, approached the attenuation description in a physically proper way. In this sense, as many terms as possible in the empirical regression analysis should be based on, or be directly motivated by, the functional forms known to us from the earthquake fracture mechanics and the wave propagation theory. Formal regression analyses may eventually suggest the proper scaling forms but sound theoretical basis or at least consideration of the known laws of wave propagation coupled with detailed regression analysis of recorded motions will provide much faster and more direct avenues towards the improved scaling relationships. Though such principles have governed our choice of terms in equations (1) and (4), much remains to be improved. For example, it is clear that the attenuation of amplitudes with distance must depend on the size of the fault relative to R and thus, on M or MMI at the epicenter. It also must depend on the geologic features of the propagation path in the sense analogous to the effects of local geologic conditions. Inasmuch as it is possible to develop theoretical models for such dependence, the present data base seems inadequate to justify detailed analyses of this type because the small number of recordings is just not sufficient to test and discriminate among many specific theoretical assumptions.

At present, the simple rough models in equations (1) and (4) show that there is significant effect of geologic site conditions in intermediate and long period waves. The average values of response amplitudes increase with depth, h, of local sediments, if the period of ground motion is longer than about 0.3 sec. The scatter in particular recordings with respect to these average trends, however, increases with the size and complexity of the geologic conditions. For periods shorter than about 0.3 sec amplitude changes with h are small. Though the systematic trends appear and lead to larger amplitudes on igneous basement rocks there, the data and the scaling models considered do not lead to d(T) which is significantly different from zero at high frequencies.

The changes of PSV spectrum amplitudes and of its overall shape depend simultaneously on magnitude, local intensity, epicentral distance, horizontal versus vertical motions, local geologic conditions and the probability that certain amplitudes of a chosen T will be exceeded. In practical terms, this means that the common procedure(s) for prediction of response spectrum amplitudes in terms of some peak of ground motion (typically peak acceleration) and a "standard spectrum shape(s)" cannot provide a scaling method which is capable of producing spectral amplitudes which are consistent with recordings at all levels of shaking, under different local conditions and uniformly for all periods of motion. The direct method of estimating spectral amplitudes as presented here offers all these advantages simultaneously and eliminates the uncertainties which result from using the scaling in terms of peak acceleration.

REFERENCES

Anderson, J.G. (1979). Uniform Risk Fourier Amplitude Spectra Derived from Intensity Data on Earthquake Occurrence, NUREG/CR=0689, E1-E27.

Anderson, J.G., and M.D. Trifunac (1977). Current Computational Methods in Studies of Earthquake Source Mechanisms and Strong Ground Motion, Proc. Symp. Appl. Comp. Methods in Engr., USC, Los Angeles, Vol. II, 929-939.

Richter, C.F. (1958). Elementary Seismology, Freeman and Co., San Francisco.

Trifunac, M.D. (1971). Response Envelope Spectrum and Interpretation of Strong Earthquake Ground Motion, Bull. Seism. Soc. Amer., 61, 343-356.

Trifunac, M.D. (1973). Analysis of Strong Earthquake Ground Motion for Prediction of Response Spectra, Int. J. Earthquake Eng., and Struc. Dyn., Vol. 2, 59-69.

Trifunac, M.D., and A.G. Brady (1975). On the Correlation of Seismic Intensity Scales with the Peaks of Recorded Strong Ground Motion, Bull. Seis. Soc. Amer., 65, 139-162.

Trifunac, M.D. (1976). Preliminary Empirical Model for Scaling Fourier Amplitude Spectra of Strong Ground Acceleration in Terms of Earthquake Magnitude, Source to Station Distance and Recording Site Conditions, Bull. Seis. Soc. Amer., 66, 1343-1373.

Trifunac, M.D. (1979). Preliminary Empirical Model for Scaling Fourier Amplitude Spectra of Strong Motion Acceleration in Terms of Modified Mercalli Intensity and Geologic Site Conditions, Int. J. Earthquake Engr. and Struc. Dyn., 7, 63-79.

Trifunac, M.D., and J.G. Anderson (1977). Preliminary Empirical Models for Scaling Absolute Acceleration Spectra, Dept. of Civil Engr., Report No. 77-03, Univ. of Southern Calif., Los Angeles.

Trifunac, M.D., and J.G. Anderson (1978a). Preliminary Empirical Models for Scaling Pseudo Relative Velocity Spectra, Dept. of Civil Engr., Report No. 78-04, Univ. of Southern Calif., Los Angeles.

Trifunac, M.D., and J.G. Anderson (1978b). Preliminary Models for Scaling Relative Velocity Spectra, Dept. of Civil Engr., Report No. 78-05, Univ. of Southern Calif., Los Angeles.

Trifunac, M.D., and V.W. Lee (1978). Dependence of the Fourier Amplitude Spectra of Strong Motion Acceleration on the Depth of Sedimentary Deposits, Dept. of Civil Engr., Report No. 78-14, Univ. of Southern Calif., Los Angeles.

Trifunac, M.D., and V.W. Lee (1979). Automatic Digitization and Processing of Strong Motion Accelerograms, Dept. of Civil Engr., Report No. 79-15 I, II, Univ. of Southern California, Los Angeles.

Trifunac, M.D., and B.D. Westermo (1976). Dependence of Duration of Strong Earthquake Ground Motion on Magnitude, Epicentral Distance, Geologic Conditions at the Recording Station and Frequency of Motion, Dept. of Civil Engr., Report No. 76-02, Univ. of Southern Calif., Los Angeles.

Trifunac, M.D., and B.D. Westermo (1977). A Note on the Correlation of Frequency Dependent Duration of Strong Ground Motion with the Modified Mercalli Intensity and the Geologic Conditions at the Recording Station, Bull. Seism. Soc. Amer., 67, 917-927.

Westermo, B.D., and M.D. Trifunac (1978). Correlation of the Frequency Dependent Duration of Strong Earthquake Ground Motion with the Magnitude, Epicentral Distance and the Depth of Sediments at the Recording Site, Dept. of Civil Engr., Report No. 78-12, Univ. of Southern Calif., Los Angeles.

Westermo, B.D., and M.D. Trifunac (1979). Correlations of the Frequency Dependent Duration of Strong Ground Motion with the Modified Mercalli Intensity and the Depth of Sediments at the Recording Site, Dept. of Civil Engr., Report No. 79-01, Univ. of Southern Calif., Los Angeles.

ACKNOWLEDGEMENTS

We thank J.G. Anderson for critical reading of the text and for many useful comments and suggestions.

This work was supported by a contract from the U.S. Nuclear Regulatory Commission.

1

App. III-A

ON THE CORRELATION OF SEISMIC INTENSITY SCALES WITH THE PEAKS OF RECORDED STRONG GROUND MOTION

By M. D. Trifunac and A. G. Brady

ABSTRACT

Correlations of the recorded peak acceleration, velocity and displacement, and

Bulletin of the Seismological Society of America. Vol. 65, No. 1, pp. 139–162. February 1975

ON THE CORRELATION OF SEISMIC INTENSITY SCALES WITH THE PEAKS OF RECORDED STRONG GROUND MOTION

BY M. D. TRIFUNAC AND A. G. BRADY

ABSTRACT

Correlations of the recorded peak acceleration, velocity and displacement, and the Modified Mercalli intensity have been carried out for 57 earthquakes and 187 strong-motion accelerograms recorded in the Western United States. Correlations of peak acceleration with intensity, characterized by the data scatter exceeding one order of magnitude, have lead to average peak accelerations which are higher than those reported by a majority of previous investigators. New correlations, also characterized by scatter of data of about one order of magnitude, have been presented for peak velocities and displacements of strong ground motion versus Modified Mercalli intensity.

Grouping of all recorded data according to the geology underlying the strong-motion accelerograph stations was carried out and permitted a study of the possible effects that local geology might have on the peaks of strong-motion acceleration, velocity, and displacement. Results of this analysis are as follows: (1) For ground shaking of a particular Modified Mercalli intensity, average peak acceleration recorded on hard rock is higher by a factor less than about two than the average peak acceleration recorded on alluvium; (2) the effect of local geology on the average peak velocity leads to marginally higher peak values on alluvium; and (3) the peak ground displacements are larger, by a factor less than two, when recorded on alluvium rather than on hard rock.

INTRODUCTION

Since the mid-sixteenth century when the first known attempts were made to classify earthquakes according to some scale, well over 50 earthquake intensity scales have been proposed in different countries all over the world. A summary and the bibliography on these scales may be found in the papers by Gorshkov and Shenkareva (1958) and by Barosh (1969).

Earthquake intensity scales are designed to describe the effects of earthquakes on man, structures, and their surroundings. Although certain instruments have been occasionally employed in determination of the severity of shaking (e.g., Medvedev, 1953), a majority of intensity scales used today still represent subjective description of human response to shaking and the description of associated building damage. Therefore, numerous factors related to the density of population, type of construction, and the social, economic, and cultural environment may significantly affect the final quantitative description of the intensity of shaking at a particular site.

It is important to consider, also, the fact that modern architectural and engineering concepts include tall buildings and other structures whose natural periods of vibration are well above the range of periods of those structures which were considered in the original descriptions of the intensity of shaking. The existing intensity scales therefore may not be applicable when considering the damage to these and other special structures and care has to be exercised in these cases.

In the United States, the Modified Mercalli intensity scale is used (Wood and Neumann, 1931). Since 1949, the JMA (Japan Meteorological Agency) intensity scale has become the standard seismic intensity scale in Japan (Kawasumi, 1951). In Russia, the GEOFIAN (Geophysics Institute of the Academy of Sciences) scale was employed until recently (Medvedev, 1953). Figure 1 shows the correlation of these three major intensity scales made possible by a comparison of the detailed description of the intensity at each level. During the last several years some effort has been devoted toward correlation and unifying various scales used in different countries. An example of such an attempt is the MKS intensity scale proposed by Medvedev, Sponheuer, and Karnik (1963). It is now in use in Russia and is being tried in several other countries. For most practical purposes the MKS and the Modified Mercalli intensities are essentially the same.

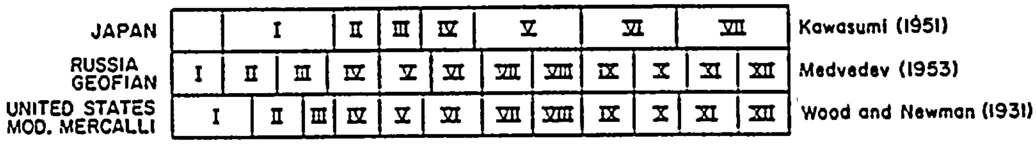

FIG. 1. Correlation of three major intensity scales.

During the last 40 years, with the rapid development of strong-motion seismology and earthquake engineering, a significant number of excellent records have been obtained from strong-motion accelerographs and can now be used for analysis. The magnitudes of the earthquakes which were recorded range from 3.0 to 7.7, with epicentral distances ranging from a few tens to several hundred kilometers. It should be noted, however, that although the number of recorded accelerograms is now just becoming adequate for some preliminary statistical evaluation of ground motion parameters and their correlation with the results of corresponding source mechanism studies, these data are still too sparse to characterize the nature of seismic risk and the statistics of expected levels of strong ground motion over a longer time frame. Consequently, in most seismic risk evaluations for important structures, like nuclear power plants, tall buildings, schools, dams, etc., use is made of data on recorded earthquake magnitudes and/or available reported earthquake intensities. An incomplete record of earthquake intensities can be extended as far back as written documents and reports can be found in newspapers, old books, and old scripts. The difficulty associated with characterization of earthquake risk by an intensity scale is that, as will be shown in this paper, the subjective and qualitative nature of intensity scales allows only a first-order correlation with the measured parameters of strong ground motions.

Statistical characterization of the expected levels of ground motion at a given site in terms of earthquake intensity for a respective area will likely remain a common engineering practice for some years to come. For this reason, it seems worthwhile now to re-evaluate the nature of correlations that may exist between earthquake intensity and the amplitudes of recorded strong ground motion and to re-examine the meaning of such correlations irrespective of how ill-defined they may be. Our present effort is further motivated by the fact that the ongoing massive program of strong-motion data processing at the Earthquake Engineering Research Laboratory of the California Institute of Technology has provided abundant data of excellent quality particularly suited for such analysis.

A Note on Human Response to Vibrations

The intricate nature of the subjective human response to and the description of the general state of shaking induced by an earthquake plays an important role in the process of evaluation and assigning of a level on the earthquake intensity scale for a given site.

It seems appropriate, therefore, to summarize here some of the characteristic amplitudes and frequency bands that characterize the human response to shocks and vibrations.

Numerous tests reviewed by Goldman and Gierke (1961) have shown that the frequencies to which the human body responds with anxiety, discomfort, and pain range from several to about 500 Hz. Thus, for example, the natural frequency of the thorax-abdomen system for an average human subject is between 3 and 4 Hz. For the sitting man, the fundamental frequency of the whole body is between 4 and 6 Hz. For the standing man, this frequency is between 5 and 12 Hz. Resonance of the head relative to the shoulders has been observed in the frequency band between about 20 and 30 Hz. In this frequency range the amplitudes of head displacement may exceed the amplitudes of the shoulder

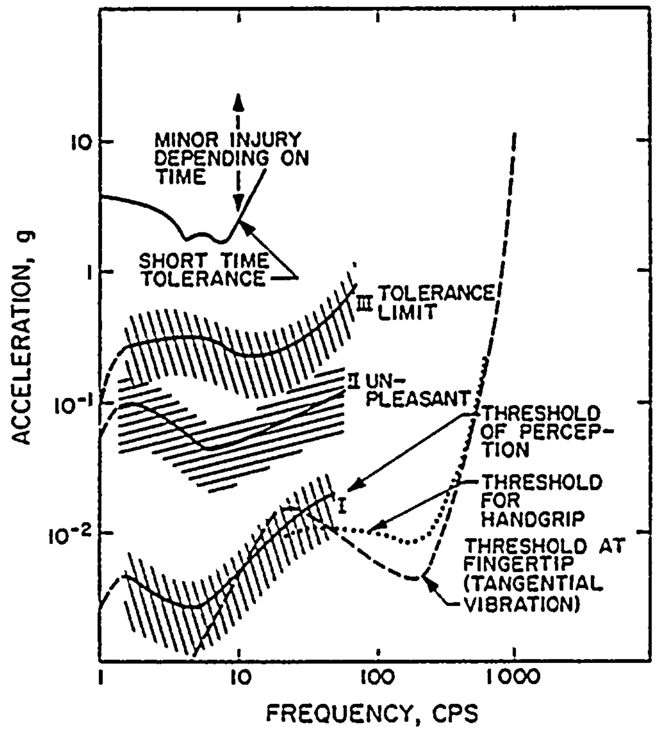

FIG. 2. Threshold of perception, unpleasantness limit, and tolerance limit of steady-state vibrations as a function of frequency.

displacement by a factor of about 3. One important effect of this resonance is that visual acuity deteriorates during vibration. The resonant vibration of an eyeball may take place between 60 and 90 Hz. The fundamental frequency of the skull is between 300 and 400 Hz, while the resonant vibration of the lower jaw relative to the skull takes place between 100 and 200 Hz. It appears, therefore, that from the earthquake excitation viewpoint, which is in the frequency band between 0 and about 30 Hz, one of the most important resonant vibrations of the human body, which is excited in the standing, sitting, or lying position, is that of the thorax-abdomen system.

Figure 2, redrawn from Goldman and Gierke (1961), summarizes frequency-dependent amplitudes of steady-state vibrations that are associated with the threshold of perception, unpleasantness, and the tolerance limits of human response. These results have been derived from subjects exposed to vibration for 5 min or longer and thus represent a lower bound of the vibration tolerance criteria that would apply directly to the transient excitation whose duration and character would correspond to that of earthquakes. The top curve in Figure 2 summarizes the tolerance criteria for short exposure, less than 5 min, to vertical vibration. No single prominent criterion of tolerance can be found, although the experimental results suggest that, in addition to the general discomfort, shortness of breath in the frequency band between 1 and 4 Hz and chest pain in the frequency band between 3 and 10 Hz were somewhat more prominent (Goldman and Gierke, 1961).

Several earthquake intensity scales contain some partial characterizations of different earthquake intensity levels which are related to the nature of the response of the human body. Due to the fact that the variability of natural frequencies characterizing response of the human body to strong shaking is much smaller than the variability of natural frequencies of buildings and other man-made structures, it would seem logical that earthquake intensity scales should emphasize more the precise description of response of the human body to strong shaking rather than that of the surrounding objects and buildings only. It seems, however, that this possible improvement would not significantly alter the accuracy nor the qualitative reliability of an earthquake intensity scale.

Some Suggested Relationships Between Peak Ground Accelerations and Modified Mercalli Intensity

From the very beginning of instrumental seismology, numerous attempts have been made to correlate earthquake intensity scales with peak ground accelerations. One of the first such attempts was carried out by Ishimoto (1932), who correlated the horizontal components of peak ground acceleration with the six levels of the intensity scale used by the Japanese Central Meteorological Observatory. The average curve for his data converted to the equivalent Modified Mercalli Intensity Scale is shown in Figure 3. This conversion is performed by matching equivalent descriptions of human response or the behavior of small structures (Barosh, 1969).

In 1951, Kawasumi proposed the following relation between the average peak acceleration, $\bar{a}$, in centimeters per second per second and the intensity, I, on the Japanese intensity scale

$$\log \bar{a} = -0.35 + 0.5\text{I}.$$

This relation, converted to the Modified Mercalli Intensity Scale, is also shown in Figure 3.

In 1942, Gutenberg and Richter (also see Richter, 1958) correlated the peak accelerations with the Modified Mercalli Intensity Scale and proposed the following relation

$$\log a = -0.5 + 0.33\text{I}.$$

In 1956, Hershberger derived another relation given by

$$\log a = -0.90 + 0.43\text{I}.$$

Savarensky and Kirnos (1955) pointed out that it is possible to determine only roughly the maximum acceleration corresponding to various intensity levels. Their minimum estimates for peak acceleration versus the Modified Mercalli intensity are also shown in Figure 3.

For an average epicentral distance of about 15 miles, Neumann (1954) proposed the relation

$$\log a = -0.041 + 0.308\text{I},$$

which is valid for epicentral distances of up to 25 miles only.

For the MKS intensity scale (Medvedev and Sponheuer, 1969) and for the Japanese JMA scale (Okamoto, 1973), the range of possible peak accelerations is presented in Figure 3 and Table 1.

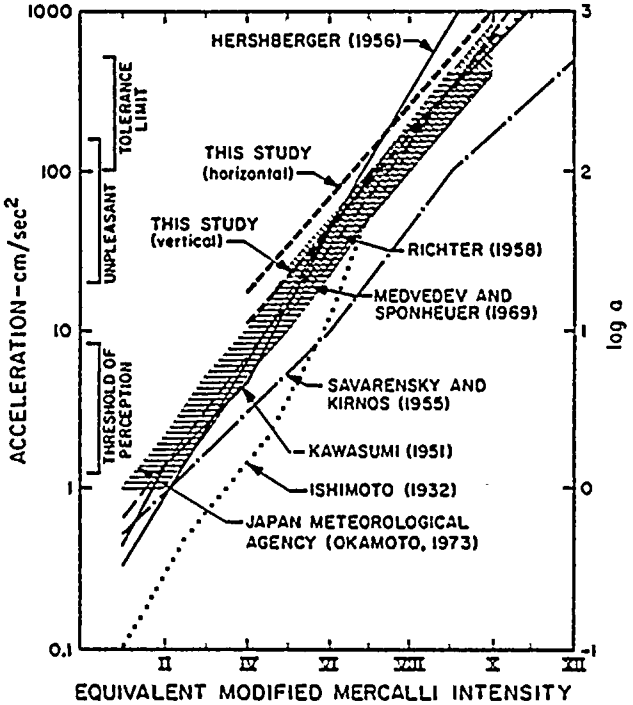

FIG. 3. Relationships between peak ground acceleration and Modified Mercalli intensity, or equivalent intensity when applicable.

TABLE 1

COMPARISON OF NUMERICAL VALUES FOR SOME SUGGESTED RELATIONSHIPS BETWEEN PEAK GROUND ACCELERATION AND MODIFIED MERCALLI INTENSITY, OR EQUIVALENT*

Mod. Mercalli Int. or equivalent	Ishimoto (1932) Ave. Accel.	Kawasumi (1951) Ave. Accel.	Hershberger (1956) Ave. Accel.	Richter (1958) Ave. Accel.	Neumann (1954)	Medvedev and Sponheuer (1969)	Japan Meterological Agency (Okamoto, 1973)	Savarensky and Kirnos (1955)	This Study - Horiz. Ave. Accel.	This Study - Vert. Ave. Accel.
I	0.1	0.5	0.3	0.7	2.		<1.	>0.5		
II	0.3	1.4	0.9	1.4	4.		1-2			
III	0.7	2.5	2.5	3.1	8.		2.1-5			
IV	1.5	4.5	6.6	6.6	16		5.0-10.		16.6	11.
V	3.6	14.	17.8	14.	32.	12-25	10.-21.		34.	17.
VI	12.	44.	47.9	30.	64	25-50	21-44	≥10.	66.	45.
VII	50.	89	128.8	64.	130.	50-100	44-94		126.	83.
VIII	144.	190.	346.7	138.	265.	100-200	94-202		251	166.
IX	302.	331.	933.3	295.	538.	200-400	202-432	≥100.	501	331.
X	616.	616.	2512.	631.	1094.	400-800			1000.	676.
XI	1122.	1000.								
XII								≥500		

* Acceleration is measured in centimeters per second per second.

Strong Motion Data

Since 1969 the Earthquake Engineering Research Laboratory of the California Institute of Technology has been engaged in massive processing of strong-motion data. At this time, routine analysis for about 1000 acceleration components has been completed. These data have been compiled in four volumes: Volume I contains the raw uncorrected accelerograms (Hudson *et al.*, 1969), Volume II presents accelerograms corrected for instrument response (Trifunac, 1972) and for base line (Trifunac, 1971), Volume III presents the response spectra (Hudson *et al.*, 1972a), and Volume IV contains the Fourier amplitude spectra (Hudson *et al.*, 1972b). This data-set contains 187 records or a total of 561 acceleration components from various free-field sites or the basements of tall buildings and other structures and has been recorded during 57 strong earthquakes which are listed in Table 2. As may be seen from this table, these data are representative of strong earthquake ground motions in the Western United States only.

Volume II (Hudson *et al.*, 1971) of the strong-motion data processing is particularly suitable for use in this paper since it contains corrected accelerograms and the integrated velocity and displacement curves. These data can be readily used to correlate the peak values of strong ground motion with the observed earthquake intensity levels.

It may be noted here that some processing errors are inevitable throughout the entire data analysis procedures that lead ultimately to double integration of accelerograms. To diminish these errors the accelerograms have been band-pass filtered between 0.07 Hz (or 0.125 Hz, Trifunac *et al.*, 1973) and 25 Hz (Hudson *et al.*, 1971). While the digital filtering diminishes most of the adverse effects introduced by digitization and processing noise, it systematically decreases the exact peak values, since the D.C. and the high-frequency components of ground motion have been filtered out. Although present in all data used in this paper, these errors are important for only several per cent of all the peak values presented, since only a few strong-motion accelerograms have been recorded close enough to the causative faults to experience significant D.C. contributions to the ground motion. At intermediate and large distances, diffraction around the fault plane rapidly diminishes the relative contribution of the static D.C. displacement field and the band-pass filtered velocity and displacement are essentially the same as the exact unfiltered ground motions (Trifunac and Lee, 1974).

Correlations of Peak Acceleration, Velocity, and Displacement with Modified Mercalli Intensities

The physical basis for correlating an earthquake intensity scale with the recorded levels of strong ground motion is dubious indeed. The descriptive nature of an intensity scale in terms of broken dishes, cracked windows, damaged buildings, landslides, or tsunamis generated, to name only a few terms often used, is qualitative and descriptive at best, but certainly not quantitative and accurate from the point of view of the dynamics of structural response. It is quite clear, however, that this type of descriptive scaling of earthquake effects on man and his environment will have to stay with us for quite some time. Even though we are at present witnessing rapid expansion of strong-motion accelerograph networks in seismically active areas of the world, it will take many years before these networks are completed and many more years before adequate data are collected for future analysis. In the meantime, however, earthquake engineers will have to use information that is now available, but with an understanding of its poor accuracy, the wide scatter of available data points, and sometimes the lack of a physical basis for the correlations which are employed.

TABLE 2

DATA FOR EARTHQUAKES PROVIDING RECORDS USED IN THIS STUDY*

No.	Earthquake Area	Mo. Day Year	Time	Time Zone	Lat. (N) ° ' "	Long. (W) ° ' "	Depth (km)	Mag.	Max. Int.
1	Long Beach, Cal.	Mar. 10, 1933	1754	PST	33 37 00	117 58 00	16.0	6.3	9
2	Southern Cal.	Oct. 2, 1933	0110	PST	33 47 00	118 08 00	16.0	5.4	6
3	Eureka, Cal.	Jul. 6, 1934	1449	PST	41 42 00	124 36 00			5
4	Lower Cal.	Dec. 30, 1934	0552	PST	32 15 00	115 30 00	16.0	6.5	9
5	Helena, Mt.	Oct. 31, 1935	1138	MST	46 37 00	111 58 00		6.0	8
6	Helena, Mt.	Oct. 31, 1935	1218	MST	46 37 00	111 58 00			3
7	Helena, Mt.	Nov. 21, 1935	2058	MST	46 36 00	112 00 00			6
8	Helena, Mt.	Nov. 28, 1935	0742	MST	46 37 00	111 58 00			6
9	Humboldt Bay, Cal.	Feb. 6, 1937	2042	PST	40 30 00	125 15 00			5
10	Imperial Valley, Cal.	Apr. 12, 1938	0825	PST	32 53 00	115 35 00	16.0	3.0	
11	Imperial Valley, Cal.	Jun. 5, 1938	1842	PST	32 54 00	115 13 00	16.0	5.0	
12	Imperial Valley, Cal.	Jun. 6, 1938	0435	PST	32 15 00	115 10 00	16.0	4.0	
13	Northwest Cal.	Sep. 11, 1938	2210	PST	40 18 00	124 48 00		5.5	6
14	Imperial Valley, Cal.	May 18, 1940	2037	PST	32 44 00	115 30 00	16.0	6.7	10
15	Northwest Cal.	Feb. 9, 1941	0145	PST	40 42 00	125 24 00		6.4	
16	Santa Barbara, Cal.	Jun. 30, 1941	2351	PST	34 22 00	119 35 00	16.0	5.9	8
17	Northern Cal.	Oct. 3, 1941	0813	PST	40 36 00	124 36 00			7
18	Torrance-Gardena, Cal.	Nov. 14, 1941	0042	PST	33 47 00	118 15 00	16.0	5.4	8
19	Borrego Valley, Cal.	Oct. 21, 1942	0822	PST	32 58 00	116 00 00	16.0	6.5	7
20	Northern Cal.	Mar. 9, 1949	0429	PST	37 06 00	121 18 00		5.3	7
21	Western Wash.	Apr. 13, 1949	1156	PST	47 06 00	122 42 00		7.1	8
22	Imperial Valley, Cal.	Jan. 23, 1951	2317	PST	32 59 00	115 44 00	16.0	5.6	7
23	Northwest Cal.	Oct. 7, 1951	2011	PST	40 17 00	124 48 00		5.8	7
24	Kern County, Cal.	Jul. 21, 1952	0453	PDT	35 00 00	119 01 00	16.0	7.7	11
25	Kern County, Cal.	Jul. 23, 1952		PDT	35 17 00	118 39 00			
26	Northern Cal.	Sep. 22, 1952	0441	PDT	40 12 00	124 25 00		5.5	7
27	Southern Cal.	Nov. 21, 1952	2346	PST	35 50 00	121 10 00			7
28	Imperial Valley, Cal.	Jun. 13, 1953	2017	PST	32 57 00	115 43 00	16.0	5.5	7
29	Wheeler Ridge, Cal.	Jan. 12, 1954	1534	PST	35 00 00	119 01 00	16.0	5.9	8
30	Central Cal.	Apr. 25, 1954	1233	PST	36 48 00	121 48 00		5.3	7
31	Lower Cal.	Nov. 12, 1954	0427	PST	31 30 00	116 00 00	16.0	6.3	5
32	Eureka, Cal.	Dec. 21, 1954	1156	PST	40 47 00	123 52 00		6.5	7
33	San Jose, Cal.	Sep. 4, 1955	1801	PST	37 22 00	121 47 00		5.8	7
34	Imperial County, Cal.	Dec. 16, 1955	2117	PST	33 00 00	115 30 00	16.0	4.3	
35	Imperial County, Cal.	Dec. 16, 1955	2142	PST	33 00 00	115 30 00	16.0	3.9	
36	Imperial County, Cal.	Dec. 16, 1955	2207	PST	33 00 00	115 30 00	16.0	5.4	7
37	El Alamo, Baja Cal.	Feb. 9, 1956	0633	PST	31 42 00	115 54 00	16.0	6.8	
38	El Alamo, Baja Cal.	Feb. 9, 1956	0725	PST	31 42 00	115 54 00		6.4	
39	Southern Cal.	Mar. 18, 1957	1056	PST	34 07 06	119 13 12	13.8	4.7	6
40	San Francisco, Cal.	Mar. 22, 1957	1048	PST	37 40 00	122 28 00		3.8	5
41	San Francisco, Cal.	Mar. 22, 1957	1144	PST	37 40 00	122 29 00		5.3	7
42	San Francisco, Cal.	Mar. 22, 1957	1515	PST	37 39 00	122 27 00		4.4	5
43	San Francisco, Cal.	Mar. 22, 1957	1627	PST	37 39 00	122 29 00		4.0	5
44	Central Cal.	Jan. 19, 1960	1926	PST	36 47 00	121 26 00		5.0	6
45	Northern Cal.	Jun. 5, 1960	1718	PST	40 49 00	124 53 00		5.7	6
46	Hollister, Cal.	Apr. 8, 1961	2323	PST	36 30 00	121 13 00	11.0	5.7	7
47	Northern Cal.	Sep. 4, 1962	0917	PST	40 58 00	124 12 00		5.0	6
48	Puget Sound, Wash.	Apr. 29, 1965	0729	PST	47 24 00	122 18 00		6.5	8
49	Southern Cal.	Jul. 15, 1965	2346	PST	34 29 06	118 31 18	15.1	4.0	6
50	Parkfield, Cal.	Jun. 27, 1966	2026	PST	35 57 18	120 29 54	6.0*	5.6	7
51	Gulf of Cal.	Aug. 7, 1966	0936	PST	31 48 00	114 30 00	16.0	6.3	6
52	Northern Cal.	Sep. 12, 1966	0841	PST	39 24 00	120 06 00		6.3	7
53	Northern Cal.	Dec. 10, 1967	0407	PST	40 30 00	124 36 00		5.8	6
54	Northern Cal.	Dec. 18, 1967	0925	PST	37 00 36	121 47 18		5.2	6
55	Borrego Mtn., Cal.	Apr. 8, 1968	1830	PST	33 11 24	116 07 42	11.1	6.4	7
56	Lytle Creek, Cal.	Sep. 12, 1970	0630	PST	34 16 12	117 32 24	8.0	5.4	7
57	San Fernando, Cal.	Feb. 9, 1971	0600	PST	34 24 42	118 24 00	13.0	6.4	11

* Blanks indicate unavailable information. Many Southern California earthquakes have an assumed depth of 16 km.

Perhaps one of the most important omissions in the majority of available correlations of peak ground acceleration with earthquake intensity is that insufficient stress is put upon the broad scatter of data points. By the time some of the empirical correlations reach an earthquake engineering office they are presented in the form of a mathematical curve that gives no indication of the possible degree of scatter and uncertainty in the predicted values. Even though the mean trends of the peak values of strong ground motion increase exponentially with respect to earthquake intensity, the observed scatter of data is so large that one peak estimate of a ground motion amplitude could be associated with several different intensity levels.

TABLE 3

MEAN VALUES AND STANDARD DEVIATIONS OF PEAK ACCELERATION, VELOCITY AND DISPLACEMENT FOR DIFFERENT MODIFIED MERCALLI INTENSITIES IN THE WESTERN UNITED STATES

M. M. Intensity	Component	Acceleration - cm/sec^2		Velocity - cm/sec		Displacement - cm		No. of data points used
		$\bar{a}$	σ	$\bar{v}$	σ	$\bar{d}$	σ	
I								
II								
III	Vert.	12.50	-	1.25	-	1.00	0.50	2
	Horiz.	12.50	-	1.25	-	1.25	0.83	4
IV	Vert.	12.50	-	1.25	-	1.83	0.47	3
	Horiz.	16.67	9.32	2.50	1.25	1.83	0.75	6
V	Vert.	18.56	10.71	1.63	1.09	1.29	0.77	33
	Horiz.	37.12	29.35	3.48	2.89	1.92	2.18	66
VI	Vert.	38.99	34.25	3.23	2.46	1.92	1.27	67
	Horiz.	82.46	77.67	7.57	5.98	3.69	3.08	134
VII	Vert.	68.17	34.78	7.15	4.24	3.54	2.00	75
	Horiz.	131.29	61.30	16.48	8.46	8.41	4.48	150
VIII	Vert.	116.67	99.39	9.17	10.45	7.17	8.75	6
	Horiz.	166.67	84.06	18.95	9.65	8.58	6.46	12
IX								
X	Vert.	687.50	-	58.75	-	19.50	-	1
	Horiz.	1087.50	50.0	86.25	27.50	24.0	13.50	2
XI								
XII								

Although 187 ground acceleration records (374 horizontal and 187 vertical components) now available at the Earthquake Engineering Research Laboratory represent the largest uniformly processed set of strong-motion data ever collected, the number of peak values that can now be used for correlation with the Modified Mercalli Intensity Scale is still not adequate to cover the low intensity levels from I to IV and the high intensity levels from IX to XII. This is shown in Table 3 which gives the number of data points used in computing the mean and the standard deviations for different intensity levels. The intensity levels at the recording stations were obtained from *United States Earthquakes*, published annually by the Seismic Engineering Branch of the U.S. Geological Survey (formerly the Seismological Field Survey of the U.S. Coast and Geodetic Survey).

Figures 4, 5, and 6, based on the data summarized in Table 3, present the logarithms of peak acceleration, velocity, and displacement plotted versus the Modified Mercalli intensity. Mean values of the peak amplitudes are presented by full circles for horizontal and by empty circles for vertical components. The spread of data between one standard deviation below and above the mean is indicated by the vertical error bars. Where necessary, the lower limits of these error bars have been terminated at -1 for convenience in plotting.

A detailed study of Figures 4, 5, and 6 shows that even on the logarithmic scales the spread of the measured peak values of strong ground motion is quite large, about one order of magnitude. This spread is also much larger for those intensities for which more data points have been available for analysis, indicating that the real spread is probably even larger than indicated by the presently available data.

For comparison with the correlation formulas proposed by other investigators (Figure 3), we approximated the average trends of the data presented in this paper by making the usual assumption that the logarithm of peak values increases linearly with intensity. For a limited range of Modified Mercalli intensities (I_{MM}), these trends are as follows:

1. Peak accelerations in centimeters per second per second for IV $\leqq I_{MM} \leqq$ X

$$\log a_V = -0.18+0.30\, I_{MM}$$
$$\log a_H = 0.014+0.30\, I_{MM} \tag{1}$$

2. Peak velocities in centimeters per second for IV $\leqq I_{MM} \leqq$ X

$$\log v_V = -1.10+0.28\, I_{MM}$$
$$\log v_H = -0.63+0.25\, I_{MM} \tag{2}$$

3. Peak displacements in centimeters for V $\leqq I_{MM} \leqq$ X

$$\log d_V = -1.13+0.24\, I_{MM}$$
$$\log d_H = -0.53+0.19\, I_{MM} \tag{3}$$

where subscripts "V" and "H" designate vertical and horizontal components, respectively.

While interpreting the data in Figure 5 and the meaning of the average trends given by equations (2), it is interesting to mention here the work of Neumann (1958) and the results of damage of residences from blasting vibrations summarized by Duvall and Fogelson (1962). By correlating the levels of damage with the peak velocity of ground motion, they found that the safe motions are characterized by peak velocities less than about 5 cm/sec, that minor damage occurs for peak ground velocities between 5 and about 14 cm/sec, while the major damage takes place for peak velocities of about 19 cm/sec and larger. These velocity amplitudes would correspond to the Modified Mercalli intensities of about V to VI, VII to VIII, and VIII to IX, respectively (Figure 5). The associated degree of damage is in good agreement with the damage described in the corresponding Modified Mercalli intensity levels.

As may be seen in Figure 6, for low intensities the trend of the observed peak displacements tends to level off at a displacement amplitude of about 2 cm. This results from the fact that at these low peak displacement amplitudes the true ground displacements are indistinguishable from the recording and processing noise. It has been estimated (Trifunac and Lee, 1974; Trifunac *et al.*, 1973) that the maximum displacement amplitudes that can result from the recording and processing noise alone in the frequency band between 0.07 to 25 Hz are on the average about 2 cm. For this reason, in calculating the average trends for the peak displacements versus Modified Mercalli intensity, we consider only intensities V or greater.

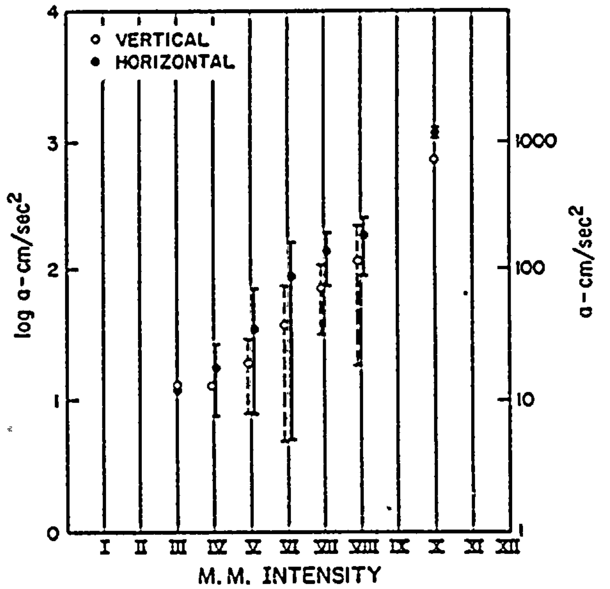

FIG. 4. Mean values and standard deviation error bars of peak ground accelerations plotted against Modified Mercalli intensity.

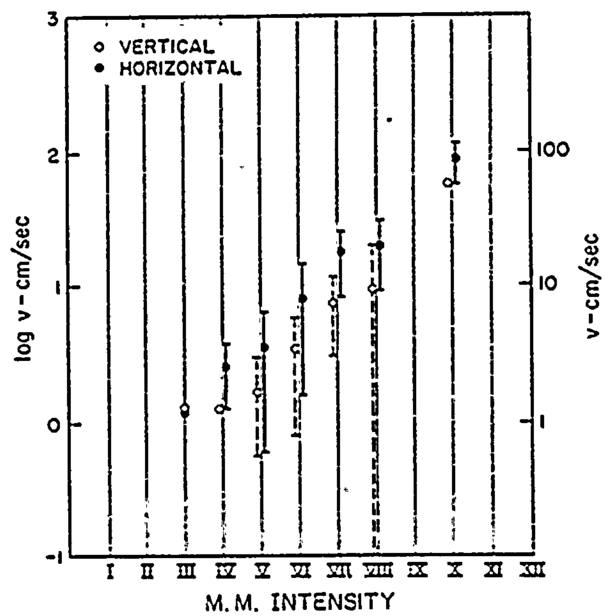

FIG. 5. Mean values and standard deviation error bars of peak ground velocity plotted against Modified Mercalli intensity.

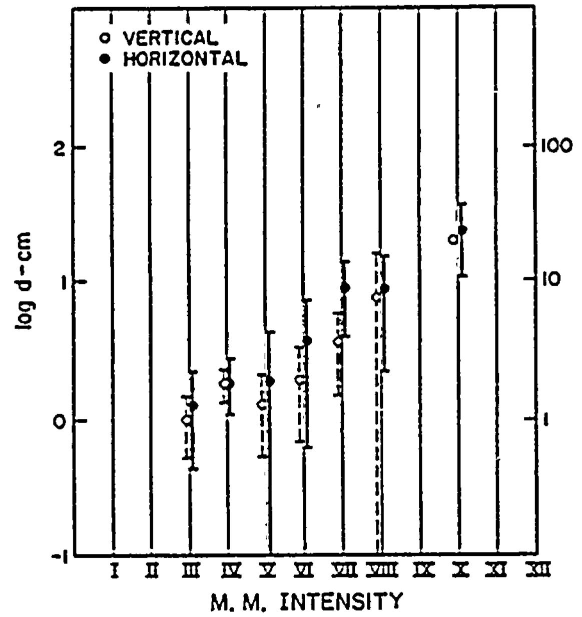

FIG. 6. Mean values and standard deviation error bars of peak ground displacement plotted against Modified Mercalli intensity.

Comparison of our results in (1) with those in Figure 3 and Table 1 shows that equations (1) define accelerations that are among the highest ever reported. Our results for horizontal peak acceleration agree favorably with the trend proposed by Neumann (1954). It is further interesting to note that the slope of the Japanese JMA (Okamoto, 1973) and the MKS (Medvedev and Sponheuer, 1969) proposed relationships are essentially the same as ours. Our average trend is, however, higher by a factor of about two relative to the center of the ranges proposed for the JMA and MKS scales. This discrepancy might be associated with the type of instruments used to measure peak accelerations in Russia and Japan. To explain this possible cause we note that the peak ground accelerations are typically associated with high-frequency components of ground motion, say 5 Hz and higher. Only a few strong-motion accelerographs, however, have a flat frequency response up to several tens of Hertz (Trifunac and Hudson, 1970) and many have a diminished high-frequency response. For example, a peak ground acceleration associated with the frequency of 10 Hz would be reduced by a factor of 2 if it were to be recorded by the Japanese SMAC accelerograph (Hudson, 1972; Trifunac and Hudson, 1970).

We have presented the average trends of peak values of ground motion [equations (1), (2), and (3)] only for their comparison with previous results. We do not recommend that these average trends be used to derive the expected peak values of ground motion in terms of Modified Mercalli intensities. If a result of this type is required, however, we do recommend that all data in Figures 4, 5, and 6 be considered and that the peak values be selected on the basis of a pre-defined degree of conservatism.

Variations of Peak Acceleration, Velocity and Displacements for Different Geological Conditions and for a Given Earthquake Intensity

It is generally recognized that the geological setting of a point on or near the ground surface has an important influence on the nature of the strong motions recorded there.

Numerous studies have been carried out to explain and characterize these effects, but their review and detailed discussion are well beyond the scope of this paper. We refer the reader to the review papers by Barosh (1969) and Duke (1958) and to a recent analysis of recorded ground motions by Trifunac and Udwadia (1974).

To determine the extent to which the geological conditions at a site might affect earthquake ground motion recorded there, the relationships of peak motion to intensity were calculated for three separate site classifications. The groupings were made on the basis of the hardness of the material at the instrument location together with a general knowledge of some of the individual sites in the following way.

Eight members of the Earthquake Engineering Research Laboratory of the California Institute of Technology participated in the estimation of site hardness. Two lists were available to them, one describing briefly the site geology as prepared by the Seismic Engineering Branch of the U.S. Geological Survey (previously the Seismological Field Survey of the U.S. Coast and Geodetic Survey) and the other describing the surface geology read from geological maps (in California, using the Geologic Atlas of California, published by the California Division of Mines and Geology). Coordinates of the accelerograph stations were available from the USGS. These two lists are reproduced in Table 4 with the corresponding estimates of the site classification, where 0 represents soft alluvium deposits, 1 represents hard sedimentary rock, or an intermediate site between 0 and 2, and 2 represents basement or crystalline rock. Also included in this table is a column labeled "U" where the site classifications of Duke *et al.* (1972) have been included where available. Their classifications 3 and 4, for shallow and deep alluvium, are combined here into the grouping 0, their sedimentary rock classification (2) becomes 1, and igneous or metamorphic rock (1) becomes 2.

It should be noted here that we did not make an attempt to describe our site classification in detail and precisely. We believe that it is virtually impossible to do this unequivocally and to satisfy all important constraints at the same time. This point is perhaps best illustrated by the perusal of the eight different estimates for the "Abbreviated Site Geology" and by the seven estimates for the "Data from Geological Map" which are both presented in Table 4. What is meant by "base rock" or "deep alluvium," for example, varies widely from one "expert" to another. The staff of the California Institute of Technology that participated in this simple site evaluation consisted of seismologists, geologists, and earthquake engineers. They are all well aware of what is meant by local geological conditions of a strong-motion accelerograph site and have all thought about the problem on many occasions. Yet their assignments of 0's, 1's, or 2's to the same brief description on the local geological conditions is perhaps the best example of the ambiguities associated with such a simple classification.

All estimates, including those in column "U", were averaged for each site with the result shown in the column "Ave.", with the following exceptions. In the Los Angeles area eight groups of stations are sufficiently closely spaced that within each group one would expect the site classification to be the same. However, in several instances, indicated in the "Ave." column with a superscript ([4]), this was not the case mainly because of the effects of changed wording in the abbreviated site geology listing. The "Ave." column contains seven such adjustments of site classification to ensure consistency across small geographical areas.

Figures 7, 8, and 9 present the histograms for the peak acceleration, velocity, and displacement of the vertical and horizontal components of recorded ground motions for the three Modified Mercalli intensities V, VI, and VII. The small number of data points available did not call for construction of such histograms for the other intensity levels. To show the relative contributions to these histograms from the data recorded at "soft,"

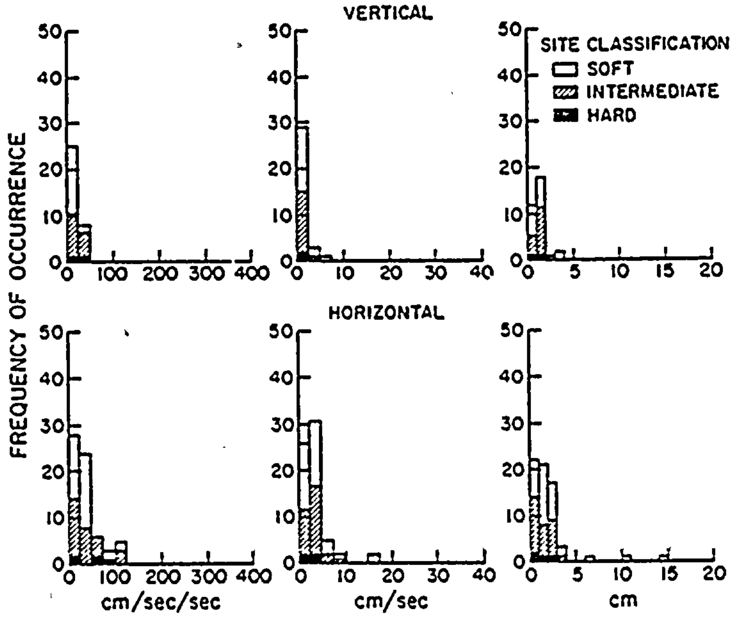

FIG. 7. Histograms of peak acceleration, velocity, and displacement for both vertical and horizontal components of recorded ground motion where the Modified Mercalli intensity of shaking was V.

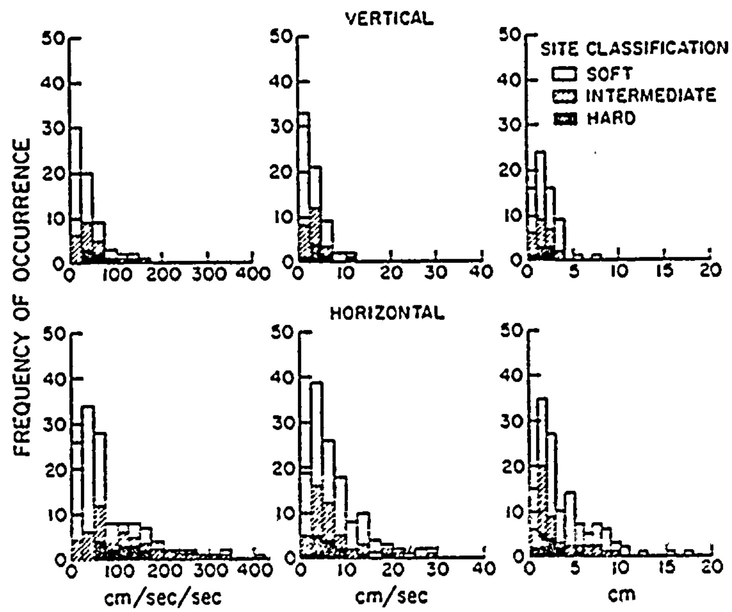

FIG. 8. Histograms of peak acceleration, velocity, and displacement for both vertical and horizontal components of recorded ground motion where the Modified Mercalli intensity of shaking was VI.

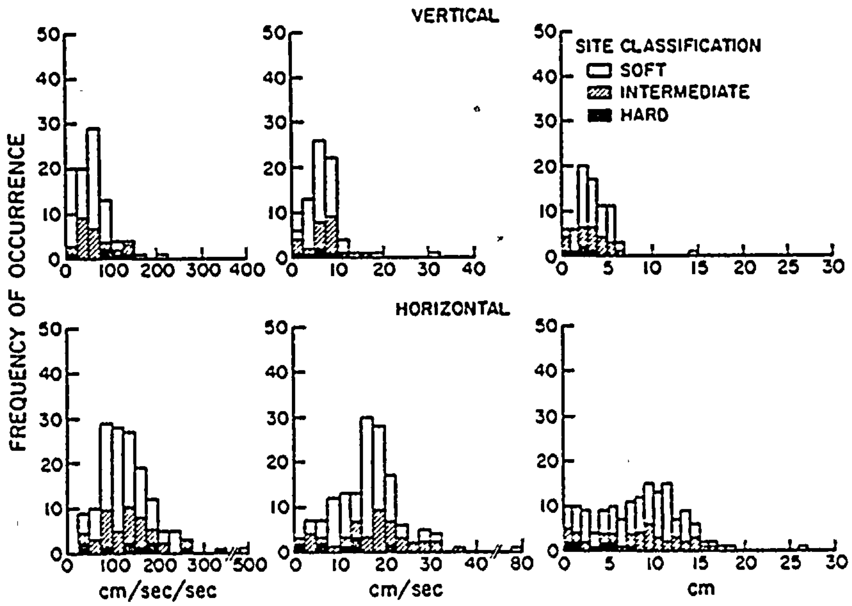

FIG. 9. Histograms of peak acceleration, velocity, and displacement for both vertical and horizontal components of recorded ground motion where the Modified Mercalli intensity of shaking was VII.

TABLE 4

GEOLOGICAL DATA OF TWO TYPES AND ESTIMATES OF SITE CLASSIFICATION FOR STATIONS PROVIDING RECORDS USED IN THIS STUDY.

Rec.	Station Location	Abbreviated Site Geology (with 8 estimates[a] of site classification[b])	Data from Geological Map (with 7 estimates of site classification)	U[A]	Ave.
A001	El Centro	Alluvium, several 1000' (00000001)	Quaternary lake deposits (0000010)	-	0
A002	Ferndale City Hall	1500' of Plio-Pleistocene loosely consolidated massive conglomerate, sandstone, and claystone (02111122)	Recent Quaternary alluvium (0000010)	-	1
A005	Santa Barbara	Approx. 600' of Pleistocene cemented alluvium over sand, silt and clay (10101001)	Recent Quaternary alluvium bounded by Quaternary nonmarine terrace deposits (0100011)	-	0
A010	San Jose (Bank of America)	Unconsolidated alluvium and estuarine deposits (00000000)	Recent Quaternary alluvium (0000010)	-	0
A015	San Francisco (Golden Gate Park)	Outcropping of Franciscan chert and thin interbedded shale (22212221)	Recent Quaternary dune sand (0002010)	-	1
A016	San Francisco (State Bldg.)	Dune sand over clay, sand and gravel. 200' to Franciscan bedrock - shale interbedded with fine-grained sandstone (10101000)	Boundary of recent Quaternary dune sand, alluvium and Mesozoic ultrabasic intrusive rocks (1111011)	-	1
A017	Oakland City Hall	Approx. 250' of unconsolidated Quaternary terrace deposits (10110002)	Pleistocene marine and marine terrace deposits (0100111)	-	1
A020	San Diego Light & Power	Shallow alluvium (50-100') over sedimentary rock (01000000)	Recent Quaternary alluvium bonded by Pleistocene marine and marine terrace deposits (0100011)	-	0
B028	Seattle, Washington	Sand, silt, and gravel over blue clay hardpan (10101000)	Narrow strip of recent Quaternary alluvium bounded by Puget Sound and Pleistocene glacial drift: till, outwash, and associated deposits (0100001)	-	0
B031	Taft (Lincoln School)	Quaternary alluvium, sand, and gravel veneer over 2000' of consolidated gravel, sand and clay (00101001)	Recent Quaternary, Great Valley fan deposits (0001000)	-	0

TABLE 4—*Continued*

Rec.	Station Location	Abbreviated Site Geology	Data from Geological Map	U	Ave.
B032	Olympia, Washington (Materials Lab. - State Dept. of Hwys.)	Sand and silt fill over recent alluvium - unconsolidated clay, silt, sand, and gravel (00100000)	Pleistocene glacial drift: till, outwash, and associated deposits (0100001)	-	0
B033	Cholame-Shandon #2	Alluvium (00000000)	Recent Quaternary alluvium (0000010)	-	0
B034	Cholame-Shandon #5	Unconsolidated shallow soil and alluvium, overlying Plio-Pleistocene loosely consolidated sand, gravel, silt, and clay (00000000)	Boundary of recent Quaternary alluvium and Plio-Pleistocene nonmarine (0100110)	-	0
B035	Cholame-Shandon #8	Alluvium (00000000)	Recent Quaternary alluvium (0000010)	-	0
B036	Cholame-Shandon #12	Unconsolidated shallow soil and alluvium, overlying Plio-Pleistocene loosely consolidated sand, gravel, silt, and clay (00000000)	Quaternary nonmarine terrace deposits (1100121)	-	0
B037.	Temblor	Indeterminate age serpentine and hard, severely fractured ultrabasic complex (22222211)	Boundary of Plio-Pleistocene nonmarine and upper Miocene marine (1101121)	-	2
B038	San Luis Obispo (City Rec. Bldg.)	Thin veneer of alluvium and stream gravels over Franciscan sandstone, conglomerate, and shale (22101022)	Recent Quaternary alluvium (0000010)	-	1
B039	Eureka City Hall	Pleistocene non-marine, loosely consolidated beds of gravel, sand, silt, and clay. Total thickness 200-400' (10100001)	Pleistocene nonmarine deposits (1101121)	-	1
C041	Pacoima Dam, Pacoima	Highly jointed diorite gneiss (22222222)	On the boundary of pre-Cretaceous metamorphic rocks and Mesozoic granitic rocks: granodiorite (2222222)	-	2
C048	8244 Orion Blvd., L.A.	Alluvium (00000001)	Recent Quaternary alluvium (0000010)	0	0
C051	250 E. First, L.A.	Alluvium (01000001)	Recent Quaternary alluvium (0000010)	0	0
C054	445 Figueroa St., L.A.	Shale (01112102)	On the borders of upper and middle Pliocene marine, and Pleistocene nonmarine sedimentary rocks (1111-21)	1	0
D056	Castaic	Sandstone (12111112)	Upper Miocene marine sedimentary rock (1111122)	1	1
D057	Hollywood Storage Building, L.A.	700±, of alluvium (00000001)	Pleistocene nonmarine sedimentary rock (111-121)	0	0
D058	Hollywood Storage Building, L.A.	700±, of alluvium (00000001)	Pleistocene nonmarine sedimentary rock (111-121)	0	0
D059	1901 Avenue of Stars, L.A.	Silt and sand layers. Water table at 70-80' (00100000)	Pleistocene nonmarine sedimentary rock (1111121)	0	0
D062	1640 S. Marengo, L.A.	Pleistocene alluvium. Water level at 35' (00000000)	Pleistocene nonmarine sedimentary rock bordering recent Quaternary alluvium (0111121)	0	0
D065	3710 Wilshire Blvd., L.A.	Alluvium (00000001)	Pleistocene nonmarine sedimentary rock (1111121)	0	1
D068	7080 Hollywood Blvd., L.A.	Alluvium (00000001)	Recent Quaternary alluvium (0000010)	0	0
E071	Wheeler Ridge	Alluvium, 200-300' (10000000)	Recent Quaternary Great Valley fan deposits bordered by Plio-Pleistocene nonmarine sedimentary rock (1101100)	0	0
E072	4680 Wilshire Blvd., L.A.	Alluvium (00000001)	Pleistocene nonmarine sedimentary rock (1111121)	0	1
E075	3470 Wilshire Blvd., L.A.	Alluvium (00000001)	Pleistocene nonmarine sedimentary rock (1111121)	0	0*
E078	L.A. Water & Power, L.A.	Miocene siltstone (01111111)	Border of recent Quaternary alluvium and upper Pliocene marine sedimentary rock (0111011)	1	1
E081	Santa Felicia Dam (Piru)	Sandstone - shale complex (12112112)	Upper Miocene marine sedimentary rock (1111122)	1	1

TABLE 4—*Continued*

Reg.	Station Location	Abbreviated Site Geology	Data from Geological Map	U	Ave.
E083	3407 Sixth St., L.A.	Alluvium (00000001)	Pleistocene nonmarine sedimentary rock (1111121)	0	0*
F086	Vernon	Greater than 1000' of alluvium. Water table > 300' (00000001)	Recent Quaternary alluvium (0000010)	0	0
F087	Orange County Eng. Bldg., Santa Ana	Alluvium (00000001)	Recent Quaternary alluvium (0000010)	0	0
F088	633 E. Broadway, Glendale	Alluvium (00000001)	Pleistocene nonmarine sedimentary rock (1111121)	0	1
F089	808 S. Olive, L.A.	Alluvium (00000001)	Recent Quaternary alluvium (0000010)	0	0
F092	2011 Zonal, L.A.	Shale at east end of bldg. 8' of fill at west end (01111101)	Upper Miocene marine sedimentary rock bordering on Pleistocene nonmarine (1111121)	1	1
F095	120 N. Robertson, L.A.	Alluvium (00000001)	Recent Quaternary alluvium (0000010)	0	0
F098	646 S. Olive, L.A.	Alluvium (00000001)	Recent Quaternary alluvium (0000010)	0	0
F101	Southern Calif. Edison, Colton	Alluvium > 500' (00000001)	Recent Quaternary alluvium (0000010)	0	0
F102	Fort Tejon, Tejon	Granitic (22222222)	Mesozoic granitic rocks: granite and adamellite, and tonalite and diorite (2222222)	0	2
F103	Pumping Plant, Pearblossom	400' of alluvium over 14,000' of sedimentary rock (10000010)	Recent Quaternary alluvium and Pleistocene nonmarine bordered by Mesozoic granitic rock: granite and adamellite (0100111)	0	0
F104	Oso Pumping Plant, Gorman	Alluvium (10000010)	Pleistocene nonmarine sedimentary rock (1112111)	0	1
F105	U.C.L.A. (Boelter Hall), L.A.	70' of alluvium over 5000' of sedimentary rock (01000000)	On the boundary between Pleistocene nonmarine sedimentary rock and recent Quaternary alluvium (0111011)	0	0
G106	Seis. Lab., C.I.T., Pasadena	Weathered granitic (22122222)	Mesozoic granitic rock: tonalite diorite (2222222)	2	2
G107	Athenaeum, C.I.T., Pasadena	Approx. 1000' of alluvium upon granite (00000000)	Pleistocene nonmarine sedimentary rock (1110121)	0	0
G108	Millikan Library, C.I.T., Pasadena	Approx. 1000' of alluvium upon granite (00000001)	Pleistocene nonmarine sedimentary rock (1110121)	0	0*
G110	J.P.L., Pasadena	Sandy-gravel (21110011)	Upper Miocene marine sedimentary rock (1111121)	0	1
G112	611 W. Sixth St., L.A.	Alluvium (00000001)	Recent Quaternary alluvium bordered by upper Pliocene marine sedimentary rock (0101011)	0	0
G114	Fire Station, Palmdale	Alluvium (10000001)	Recent Quaternary alluvium (0000010)	0	0
H115	15250 Ventura Blvd., L.A.	Alluvium, water table at 55' (00000000)	Recent Quaternary alluvium (0000010)	0	0
H118	8639 Lincoln, L.A.	Terrace deposits - sand (01110010)	Recent Quaternary dune sand (0000010)	0	0
H121	900 S. Fremont Ave., Alhambra	Few 100 feet of alluvium over siltstone (00100000)	Pleistocene nonmarine sedimentary rock (1111121)	0	0
H124	2600 Nutwood, Fullerton	Alluvium (00000001)	Recent Quaternary alluvium (0000010)	0	0
I128	435 N. Oakhurst, Beverly Hills	Alluvium, water table at 22' (00000000)	Recent Quaternary alluvium (0000010)	-	0
I131	450 N. Roxbury, Beverly Hills	Alluvium (00000001)	Recent Quaternary alluvium (0000010)	0	0
I134	1800 Century Park East, L.A.	Silt and sand layers. Water table at 70-80' (00100001)	Pleistocene nonmarine sedimentary rock bordered by recent Quaternary alluvium (0111111)	0	0
I137	15910 Ventura Blvd., L.A.	Alluvium, water table at 35' (00000001)	Recent Quaternary alluvium (0000010)	0	0
J141	Array Station 1, Lake Hughes	Granitic (22222222)	Mesozoic granitic rock: granite and adamellite (22222222)	0	2
J142	Array Station 4, Lake Hughes	Weathered granitic (22122222)	Pre-Cambrian metamorphic rocks (gneiss) (22222222)	2	2
J143	Array Station 9, Lake Hughes	Gneiss (22222222)	Pre-Cambrian metamorphic rocks (gneiss) (22222222)	2	2
J144	Array Station 12, Lake Hughes	Eocene sandstone below a shallow (10'±) layer of alluvium (12112112)	Paleocene marine sedimentary rock (1112222)	0	1
J145	15107 Vanowen St., L.A.	Alluvium 500', water table at 70' (00000001)	Recent Quaternary alluvium (0000010)	0	0
J148	616 S. Normandie Ave., L.A.	Alluvium. Siltstone at 25' (01110000)	Border of recent Quaternary alluvium and Pleistocene nonmarine sedimentary rock (0111011)	0	1
L166	3838 Lankershim Blvd., L.A.	Interlayered soft sandstone and shale (01111101)	Border of upper Miocene marine and recent Quaternary alluvium (0101011)	0	1
L171	Southern Calif. Edison, San Onofre	Lightly cemented Pliocene sandstone, > 325' depth (02111111)	Tertiary marine sedimentary rock bordered by Pleistocene marine and marine terrace deposits (1112111)	1	1

TABLE 4—*Continued*

Rec.	Station Location	Abbreviated Site Geology	Data from Geological Map	U	Ave.
M176	1150 S. Hill St., L.A.	500' of gravelly sand over shale (00110000)	Recent Quaternary alluvium (0000010)	0	0
M179	Tehachapi Pumping Plant, Grapevine	15' of alluvium over gneiss (22112010)	On the boundary of Oligocene nonmarine and recent Quaternary Great Valley fan deposits, and bounded by Eocene marine and Mesozoic granitic rocks: tonalite and diorite (1102111)	2	1
M180	4000 W. Chapman Ave., Orange	Alluvium > 300' over shale (00000001)	Recent Quaternary alluvium (0000010)	0	0
M183	6074 Park Drive, Wrightwood	Alluvium veneer on igneous metamorphic complex (22112012)	Recent Quaternary alluvium bordered by pre-Cambrian igneous and metamorphic rock complex (0102110)	2	1
N185	Carbon Canyon Dam, Brea	Thin alluvium over poorly cemented siltstone (01111012)	Narrow strip of recent Quaternary alluvium between upper Pliocene marine sedimentary rock (0101111)	1	1
N186	Whittier Narrows Dam, Whittier	More than 1000' of alluvium (00000001)	Recent Quaternary alluvium (0001010)	-	0
N187	San Antonio Dam, Upland	Up to 150' of alluvium over granitics (20001010)	Recent Quaternary alluvium bordered by Pleistocene nonmarine sedimentary rock (0101010)	-	0
N188	1880 Century Park East, L.A.	Silt and sand layers. Water table at 70-80' (00110000)	Pleistocene nonmarine sedimentary rock bounded by recent Quaternary alluvium (0111111)	0	0
N191	2516 Via Tejon, Palos Verdes Estates	Shallow Pleistocene sands over shale-volcanic complex (21111001)	Narrow strip of Quaternary nonmarine terrace deposits between upper Miocene marine and middle Miocene sedimentary rocks (1101111)	1	1
N192	2500 Wilshire Blvd., L.A.	Alluvium. Siltstone at 20-30'. Water table at 35' (01100000)	Pleistocene nonmarine sedimentary rock (1111121)	0	1
N195	San Juan Capistrano	Alluvium (00000001)	Recent Quaternary alluvium (0000010)	0	0
N196	Long Beach State College, Long Beach	Unconsolidated silt-sand-clay (00100000)	Quaternary nonmarine terrace deposits bordering recent Quaternary alluvium (0100110)	0	0
N197	Anza Post Office, Anza	Alluvium (10000011)	Recent Quaternary alluvium, bordered by pre-Cenozoic granitic and metamorphic rocks (0100110)	-	0
O198	Griffith Park Observatory, L.A.	Granitic (22222222)	Mesozoic granitic rock bordered by Miocene volcanic (2222222)	2	2
O199	1525 Olympic Blvd., L.A.	Alluvium (00000001)	On an approximately located contact between Pleistocene nonmarine sedimentary rock and recent Quaternary alluvium (0011011)	0	0
O204	205 W. Broadway, Long Beach	Alluvium. Water table at 15'. (00000000)	Quaternary nonmarine terrace deposits (1100110)	0	0
O205	Terminal Island, Long Beach	Alluvium. Water table < 20'. (00000000)	Recent Quaternary alluvium (0000010)	0	0
O206	Hall of Records, San Bernardino	Alluvium - 1000'. Water table at 30' (00000001)	Recent Quaternary alluvium (0000010)	0	0
O207	Fairmont Reservoir, Fairmont	Granitic (22222222)	Mesozoic granitic rocks: granite and adamellite, bordered by Pleistocene nonmarine sedimentary rock (22222222)	2	2
O208	University of Calif., Santa Barbara	Alluvium veneer over sandstone (12111011)	Quaternary nonmarine terrace deposits (1001110)	0	1
O210	Fire Station, Hemet	Alluvium (0000001)	Recent Quaternary alluvium (0000010)	-	0
O213	1215 Gallery, Hoover Dam	Several 100' of volcanic breccia over basalt (22211222)	Cretaceous volcanic rocks, predominantly andesitic flows and tuffs (2122222)	-	2
P214	4867 Sunset Blvd., L.A.	Shallow alluvium over Miocene siltstone (01101010)	Pleistocene nonmarine bordered by upper Miocene marine sedimentary rocks (1101121)	0	1
P217	3345 Wilshire Blvd., L.A.	Alluvium (00000001)	Pleistocene nonmarine sedimentary rock (1111121)	0	0*
P220	666 W. 19th St., Costa Mesa	Terrace deposits (01110012)	Quaternary nonmarine terrace deposits (1100120)	0	1
P221	Santa Anita Reservoir, Arcadia	Granite diorite complex (22222222)	Mesozoic granitic rocks: tonalite and diorite (22222222)	2	2
P222	Navy Lab., Port Hueneme	Alluvium > 1000' (00000001)	Recent Quaternary alluvium (0000010)	0	0
P223	Puddingstone Reservoir, San Dimas	Volcanic clastics and intrusions with associated shales (12121212)	Miocene volcanic rock, bordered by Pleistocene nonmarine sedimentary rock (2121122)	1	2
P231	9841 Airport Blvd., L.A.	Alluvium (00000001)	Quaternary nonmarine terrace deposits (1100120)	0	0
Q233	14724 Ventura Blvd., L.A.	Alluvium (00000001)	Recent Quaternary alluvium (0000010)	0	0
Q236	1760 N. Orchid Ave., L.A.	Alluvium (00000001)	Recent Quaternary alluvium bordered by middle Miocene marine sedimentary rock (0101010)	-	0
Q239	9100 Wilshire Blvd., L.A.	Alluvium. Water table at 40' (00000000)	Recent Quaternary alluvium (0000010)	-	0
Q241	800 W. First St., L.A.	Pliocene siltstone (01111101)	On the boundary of upper Miocene marine, middle and/or lower Pliocene marine, and recent Quaternary alluvium (0101011)	1	1

TABLE 4—*Continued*

Rec.	Station Location	Abbreviated Site Geology	Data from Geological Map	U	Ave.
R244	222 Figueroa St., L.A.	25' of alluvium over shale. Water at 20' (01101000)	On the boundary of upper Miocene marine, middle and/or lower Pliocene marine, and recent Quaternary alluvium (0000010)	0	1[4]
R246	6464 Sunset Blvd., L.A.	Alluvium. Water table at 55' (00000000)	Recent Quaternary alluvium (0000010)	0	0
R248	6430 Sunset Blvd., L.A.	Alluvium. Water table at 55' (00000000)	Recent Quaternary alluvium (0000010)	0	0
R249	1900 Avenue of the Stars, L.A.	Silt and sand layers. Water level at 70' (00110000)	Pleistocene nonmarine bordered by Pleistocene marine and marine terrace deposits (0101110)	0	0
R251	234 S. Figueroa St., L.A.	25' of alluvium over shale. Water at 20' (01101000)	On the boundary of upper Miocene marine, Pleistocene nonmarine and middle and/or lower Pliocene marine sedimentary rock (0111121)	0	1
R253	533 S. Fremont Ave., L.A.	Alluvium (00000001)	On the boundary of Pleistocene nonmarine sedimentary rock and recent Quaternary alluvium (0111011)	0	0
S255	6200 Wilshire Blvd., L.A.	Thin layer of alluvium over asphaltic sands (01100000)	Pleistocene nonmarine sedimentary rock (1111121)	1	1
S258	3440 University Ave., L.A.	400' of alluvium over clay and shale. Water table at 375' (0000000-)	Recent Quaternary alluvium (0000010)	0	0
S261	1177 Beverly Dr., L.A.	Alluvium (00000001)	Pleistocene marine and marine terrace deposits (0100110)	0	0
S262	5900 Wilshire Blvd., L.A.	Alluvium - asphaltic sands (01000001)	Pleistocene nonmarine sedimentary rock (1111121)	1	1
S265	3411 Wilshire Blvd., L.A.	Siltstone. Water table at basement level (01111101)	Pleistocene nonmarine sedimentary rock (1111121)	1	1
S266	3550 Wilshire Blvd., L.A.	Alluvium. Water table at 35' (00000000)	Border of Pleistocene non-marine sedimentary rock and recent Quaternary alluvium (0111111)	0	0
S267	5260 Century Blvd., L.A.	Alluvium (000[illegible]001)	Quaternary nonmarine terrace deposits (1100120)	0	0
U297	Helena, Montana (Federal Building)	Limestone bedrock (22222122)	Cambrian, bordering with pre-Cambrian Helena limestone, and Tertiary and Quaternary sedimentary deposits (1212121)	-	2
U313	Hollister	Recent unconsolidated alluvium over partly consolidated gravels, and well consolidated marine sandstone and shale. Water table from 85-95' (00100000)	Boundary of Pleistocene River terrace deposits and recent Quaternary alluvium (0100011)	-	0
V317	L.A. (Chamber of Commerce)	Alluvium veneer over late Tertiary unconsolidated marine sediments (01101011)	Recent Quaternary alluvium (0000010)	-	0
V322	San Francisco (So. Pacific Building)	Sand fill over clay, sand, and gravel. 235' to Franciscan bedrock-sandstone and shale (10100000)	Boundary between recent Quaternary alluvium, dune sand and the Franciscan Formation (Jurasic-Cretaceous) (0110011)	-	0
V323	San Francisco (Alexander Bldg.)	Sand and clay over thin bedded shale and sandstone (10100000)	Boundary between recent Quaternary alluvium, dune sand and the Franciscan Formation (Jurasic-Cretaceous) (0111011)	-	1
V329	Port Hueneme	Coarse grained sand and gravel veneer over fine grained silt and clay (00110000)	Recent Quaternary alluvium (0000010)	0	0
V332	Sacramento (Pacific Telphone & Telegraph)	Approx. 40' of inorganic, clayey silt over consolidated sand, gravel, and silt. 8000' to basement rock (00100001)	Recent Quaternary Great Valley fan deposits (0000000)	-	0
W335	Cedar Springs, Allen Ranch	Granitic (22222222)	Mesozoic granitic rocks - tonalite and diorite (2222222)	2	2
W336	Cedar Springs, Pump house on Dam abutment	Shallow gravelly alluvium (22101022)	On the boundary of Mesozoic granitics, Pleistocene nonmarine and Quaternary alluvium (1102111)	1	1
Y377	So. Calif. Edison Bldg. (L.A.)	30' of alluvial clay silt, and sand overlying 365' of Upper Pliocene blue clay (01100000)	Narrow strip of recent Quaternary alluvium bordering with Pleistocene nonmarine, upper Miocene marine and middle and/or lower Pliocene deposits (0101001)	-	0
Y378	Subway Terminal Bldg. (L.A.)	Alluvium veneer over late Tertiary marine sediments (01100002)	Recent Quaternary alluvium bordering with upper Pliocene marine deposits (0101011)	-	0

[1]Modified site classifications of Duke *et al.* (1972).
[2]Estimates in parentheses by staff members of Earthquake Engineering Research Laboratory.
[3]0, 1, and 2 correspond to soft, intermediate, and hard sites (see text).
[4]Adjustments made to classification to ensure consistency across small geographical areas.

"intermediate," and "hard" local geological conditions, their respective contributions have been shaded as indicated in these figures.

One of the first results that emerges from the analysis of Figures 7, 8, and 9 is that the scatter of data points is very large. In fact, for all peak values considered, the data are broadly distributed, the spread increasing for larger Modified Mercalli intensities.

Table 5 and Figures 10, 11, and 12 present the mean and the standard deviation values of the peaks for the three site classifications considered. Table 5 also summarizes the number of data points available in each subgroup. It is seen that the largest number of data, 63 per cent, is available for the soft geological sites, while only 29 and 8 per cent of all data have been recorded at intermediate and hard geological sites.

TABLE 5

MEAN VALUES AND STANDARD DEVIATIONS OF PEAK ACCELERATION, VELOCITY, AND DISPLACEMENT FOR VARIOUS SITE CLASSIFICATIONS DURING SHAKING OF DIFFERENT MODIFIED MERCALLI INTENSITIES

M. M. Int.-Site Classification	Component	Acceleration - cm/sec²		Velocity - cm/sec		Displacement - cm		No. of data points used
		$\bar{a}$	σ	$\bar{v}$	σ	$\bar{d}$	σ	
V-0	Vert.	15.44	8.05	1.84	1.36	1.38	0.96	17
	Horiz.	34.56	26.96	3.82	3.61	2.41	2.82	34
V-1	Vert.	21.43	11.98	1.43	0.64	1.21	0.45	14
	Horiz.	40.18	32.28	3.21	1.81	1.43	0.92	28
V-2	Vert.	25.00	12.50	1.25	0.	1.00	0.50	2
	Horiz.	37.50	25.00	2.50	1.25	1.25	0.83	4
VI-0	Vert.	32.27	29.31	3.05	2.55	2.03	1.42	43
	Horiz.	65.99	71.24	7.70	6.13	4.22	3.36	86
VI-1	Vert.	44.85	39.07	3.01	1.66	1.68	0.98	17
	Horiz.	113.97	92.14	7.57	6.13	2.97	2.48	34
VI-2	Vert.	66.07	33.88	4.82	2.95	1.79	0.70	7
	Horiz.	107.14	35.58	6.79	4.45	2.21	1.28	14
VII-0	Vert.	68.50	34.48	7.35	4.59	3.70	2.14	50
	Horiz.	128.41	60.25	16.50	8.49	8.83	4.39	100
VII-1	Vert.	62.50	31.62	7.12	3.47	3.50	1.67	20
	Horiz.	131.87	53.18	17.81	8.21	8.60	4.40	40
VII-2	Vert.	87.50	41.83	5.25	2.55	2.10	1.02	5
	Horiz.	157.50	89.30	11.00	6.84	3.30	2.28	10

Figure 10 shows that, for ground shaking of a particular Modified Mercalli intensity the average peak acceleration is larger for the solid rock sites than it is for the soft rock or alluvium sites. Although these variations in the peak acceleration do not exceed a factor of about 2 and the large standard deviations indicate that the observed differences are not significant, the trend of increasing peak acceleration for harder local geological conditions is apparent and consistent for all six data subgroups shown in Figure 10. It is interesting to note that this result is in direct contradiction with the common engineering speculations about the effects of local site conditions on the peak amplitudes of strong-motion accelerations (*e.g.*, Coulter *et al.*, 1973; Schnabel *et al.*, 1972).

Figure 11 indicates that with the exception of vertical components for intensity VI, the average peak velocity is larger for the softer local site conditions by up to about 50 per cent. The large spread of data indicated by the long error bars equal to one standard deviation shows, however, that these differences are not significant.

Dependence on local site conditions of the peak ground displacements is shown in Figure 12. It is seen that the expected displacement peaks increase with decreasing stiffness of local site conditions and that this increase is always less than about two-fold. Again,

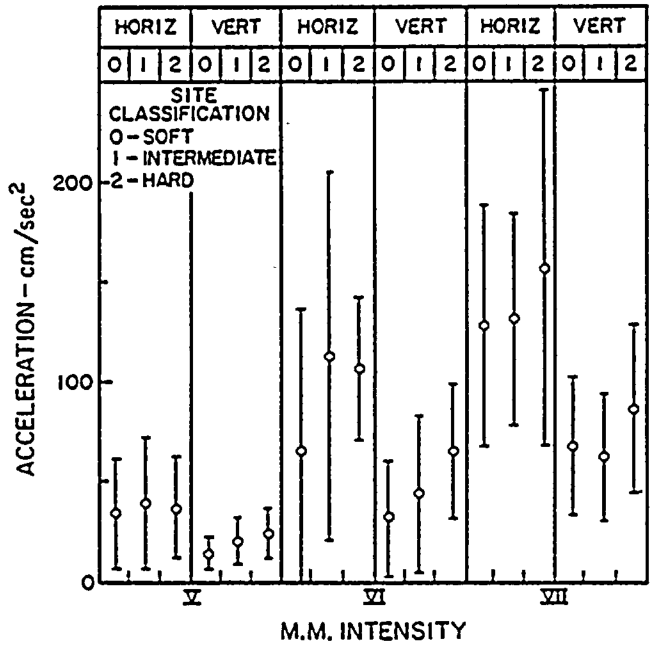

Fig. 10. Mean values and standard deviation error bars of peak ground acceleration, classified by site and component direction, plotted against Modified Mercalli intensity.

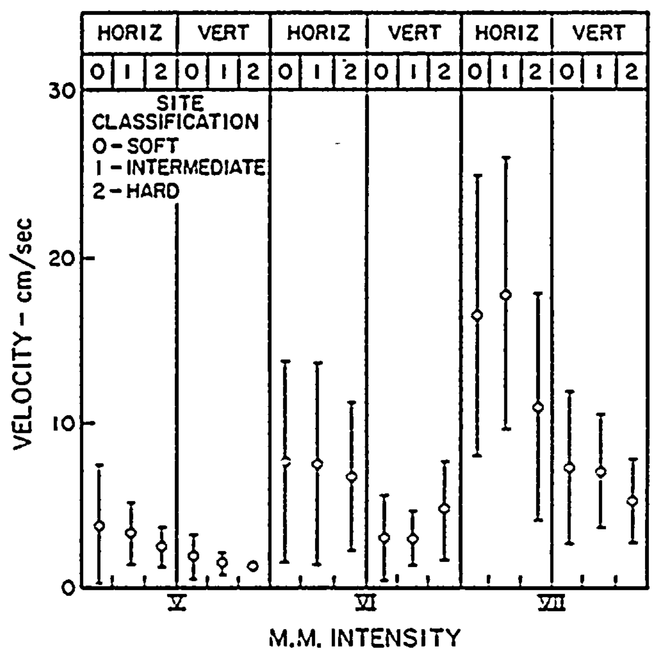

Fig. 11. Mean values and standard deviation error bars of peak ground velocity, classified by site and component direction, plotted against Modified Mercalli intensity.

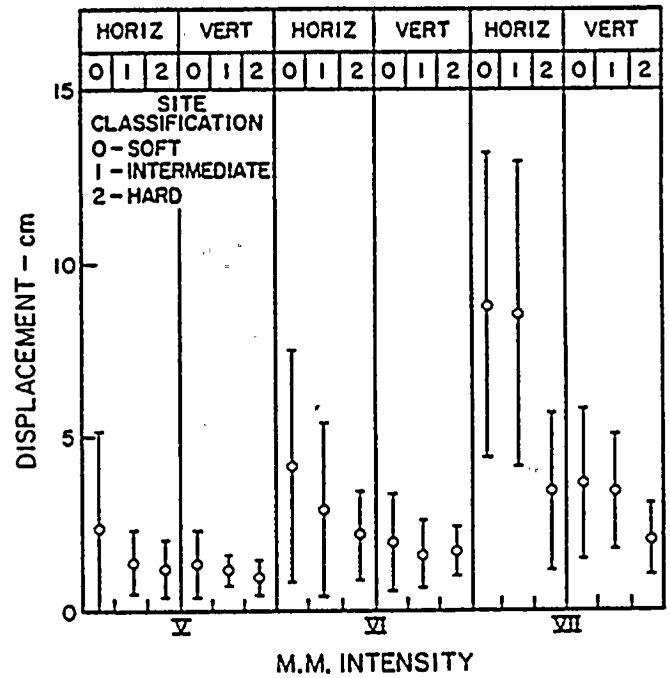

FIG. 12. Mean values and standard deviation error bars of peak ground displacement, classified by site and component direction, plotted against Modified Mercalli intensity.

the spread of data points as measured by the standard deviations shows that these variations are not significant.

In an attempt to explain the observed trends of peak values for different site conditions, it seems that at least two basic phenomena have to be considered. The first deals with the manner in which the earthquake waves are attenuated by propagation away from the source. The second is related to the complicated transfer functions representing the local site effects and the resulting influence on the peaks of a real-time function. The final result, of course, depends on the relative participation of these two factors.

Attenuation with distance of high-frequency waves in the near-field of strong earthquake ground motion is not well understood, partly because there is no adequate data-set to enable systematic studies of the problem. As a first approximation, the attenuation law given by $\exp\{-\omega\Delta/2Q\beta\}$ is frequently used. Here ω is the frequency of the wave motion, Δ is the length of the travel path. β is the wave velocity, and Q is the attenuation constant whose values range from about 50, for weathered soft soils, to about 2000 to 3000 for solid rocks. For typical distances involved in strong-motion seismology, which are less than about 100 km and typically several tens of kilometers. $\exp\{-\omega\Delta/2Q\beta\}$ may be important only for higher frequency waves, say $\omega > 6$ rad/sec. Since the peak accleration and peak velocity sample the high (say $\omega > 30$ rad/sec) and the intermediate frequency band (say $\omega > 6$ rad/sec), attenuation described by $\exp\{-\omega\Delta/2Q\beta\}$ would seem to be important for the peak accelerations only and perhaps just marginal for the peak velocity measurements. Thus, the high-frequency wave amplitudes associated with the peak accelerations may be attenuated by as much as 5 or 10 times, while the intermediate frequencies associated with velocities might be attenuated perhaps only several times.

The local amplification of incident waves by surface topography (*e.g.*, Boore, 1972; Trifunac, 1973; Wong and Trifunac, 1974a) and abrupt changes in medium impedances (*e.g.*, Aki and Larner, 1970; Wong and Trifunac, 1974b) are also highly frequency-dependent. Although only few two-dimensional solutions to such problems are available, with no known solutions for the three-dimensional geometries, some general observations that probably apply to all two- and three-dimensional problems can be summarized as follows. First, for a transient wave amplitude to be significantly amplified, it is essential to amplify a broad and representative frequency band uniformly. This is possible for waves that are long relative to the typical size of the inhomogeneities through which they propagate. While amplification of a given high-frequency component at a given point may be quite high, geometric attenuation of a neighboring frequency point regularly takes place. Thus, while sometimes a peak of a high-frequency wave may be highly amplified, it can also be significantly attenuated. The net effect then is that the resulting peaks of the high-frequency waves have widely scattered amplitudes and are on the average slightly amplified (Wong and Trifunac, 1974a; Wong and Trifunac, 1974b). Combining this with the effect of attenuation by $\exp\{-\omega\Delta/2Q\beta\}$, we find that the observed trend of data in Figures 10, 11, and 12 for different site conditions is quite consistent. Thus, soft soils will amplify low frequencies, and due to attenuation (low Q and low β) the high frequencies will be reduced so that the displacements will be enhanced while accelerations are reduced. For hard soils the high frequencies will be amplified, but the attenuation will not be so important because both Q and β are large. Thus, for hard soils or rock sites the acceleration will be amplified.

Conclusions

The role of this paper has been merely to re-examine some of the well-known correlations between the recorded amplitudes of strong ground motion and existing earthquake intensity scales. Its main contribution to this important subject perhaps lies in the uniformity, accuracy, and number of strong-motion data used in the analysis. Our results are comparable to most of the previously suggested correlations between the peak ground acceleration and the Modified Mercalli intensity or its equivalent. However, our data predict larger peak accelerations than most previous studies. Availability of accurately computed ground velocity and displacement curves has enabled us to derive the expected peak velocity and peak displacement amplitudes for recording sites having different earthquake intensities. Although there is no obvious reason why the correlations developed in this paper could not be used in other parts of the world, the data and the conclusions of our study apply for the Western United States and the State of California in particular. Lomnitz (1970) points out, for example, that in some parts of the world intensity is evaluated by making an average estimate over a region, while in some other parts (e.g., California), the maximum effects are used to determine a particular intensity level.

In the development of the correlations between the peaks of the recorded strong earthquake ground motion and the Modified Mercalli intensities, we emphasized the weaknesses in carrying out such correlations, as well as the wide scatter of the measured peak values. Although we presented the functional relationships between the peak values and the Modified Mercalli intensity to compare the trends of our data with the relationships suggested by previous investigators, we do not recommend the use of these average trends for routine engineering design. However, if there is no better way of deriving the expected peak values of ground acceleration, velocity, and displacements but from the maximum expected Modified Mercalli intensity, we recommend that all broadly-scattered data for each intensity level be considered from the probabilistic viewpoint and with the pre-selected confidence levels appropriate for the particular study. This probabilistic decision process seems to be most suitable, since the peak values for each intensity level have typically a range which is about one order of magnitude.

Systematic, but rough, partitioning of all recording sites into 0 for soft, 1 for intermediate, and 2 for hard, according to the geology surrounding the recording station, has been carried out. Dividing recorded peak values into the three corresponding groups has enabled us to carry out a crude, but simple, test of the possible effects of local site conditions on the amplitudes of the recorded strong ground motion. The results of this analysis suggest that there is no significant difference between the peaks of strong ground motion recorded in different geological conditions. Minor, but consistent, trends have been detected, however, as follows: (1) Recorded peak accelerations are larger on the hard rock sites than on alluvium by a factor which is less than about 2, (2) peak velocities are only marginally higher on the sites located on alluvium, and (3) peak displacements are higher for sites on alluvium than the peaks recorded on the hard rock by a factor which is on the average less than about 2.

Acknowledgments

We thank G. W. Housner, D. E. Hudson, and J. E. Luco for critical reading of the manuscript and offering valuable suggestions. We are indebted to R. Maley of the Seismic Engineering Branch of the United States Geological Survey in Menlo Park and to R. Dielman of the Earthquake Engineering Research Laboratory at Caltech for their help in collecting and completing the geological site descriptions in Table 4. We thank Ms. Barbara Turner for her assistance in compiling the intensity levels corresponding to the 187 accelerograms.

This research was supported in part by a grant from the National Science Foundation and by the Earthquake Research Affiliates program at the California Institute of Technology.

References

Aki, K. and K. Larner (1970). Surface motion of a layered medium having an irregular interface due to incident plane SH waves, *J. Geophys. Res.* 75, 933–954.

Barosh, P. J. (1969). Use of seismic intensity data to predict the effects of earthquakes and underground nuclear explosions in various geologic settings, *U.S. Geol. Surv. Bull. 1279.*

Boore, D. (1972). The effect of simple topography on seismic waves: implications for the recorded accelerations at Pacoima Dam (*Abstract*), Natl. Conf. Earthquake Engr., Los Angeles, Calif.

Coulter, H. W., H. H. Waldron, and J. F. Devine (1973). Seismic and geologic siting considerations for nuclear facilities, *Proc. World Conf. Earthquake Engr., 5th, Rome, Italy.*

Duke, C. M. (1958). *Bibliography of Effects of Soil Conditions on Earthquake Damage*, Earthquake Engr. Res. Inst., 47 pp.

Duke, C. M., K. E. Johnsen, L. E. Larson, and D. C. Engman, Effects of site classification and distance on instrumental indices in the San Fernando earthquake, *UCLA Engineering Report No. UCLA-ENG-7247*, June, 1972.

Duvall, W. I. and D. E. Fogelson (1962). Review of criteria for estimating damage to residences from blasting vibrations, U.S. Dept. of the Interior, Bureau of Mines, *Report of Investigations 5968.*

Goldman, D. E. and H. E. Gierke (1961). Effects of shock and vibration on man, Chapter 44 in *Shock and Vibration Handbook*, C. M. Harris and C. E. Crede, Editors, McGraw-Hill, New York.

Gorshkov, G. P. and G. H. Shenkareva (1958). On correlation of seismic scales, *Tr. Inst. Fiz. Zemli, Akad. Nauk SSR*, 1, (168), Moscow, 44–64.

Gutenberg, B. and C. F. Richter (1942). Earthquake magnitude, intensity, energy, and acceleration, *Bull. Seism. Soc. Am.* 32, 163–191.

Hershberger, J. (1956). A comparison of earthquake accelerations with intensity ratings, *Bull. Seism. Soc. Am.* 46, 317–320.

Hudson, D. E. (1972). Strong motion seismology, *Proc. Intern. Conf. Microzonation Safer Construction Res. Application*, Seattle, Washington.

Hudson, D. E., A. G. Brady, and M. D. Trifunac (1969). Strong motion earthquake accelerograms, digitized and plotted data, Volume I, Part A, *EERL 70-20*, Earthquake Engr. Res. Lab., Calif. Inst. of Tech., Pasadena.

Hudson, D. E., A. G. Brady, M. D. Trifunac, and A. Vijayaraghavan (1971). Strong-motion earthquake accelerograms, corrected accelerograms and integrated ground velocity and displacement curves, Volume II, Part A, *EERL 71–50*, Earthquake Engr. Res. Lab., Calif. Inst. of Tech., Pasadena.

Hudson, D. E., M. D. Trifunac, and A. G. Brady (1972a). Strong-motion earthquake accelerograms, response spectra, Volume III, Part A, *EERL 72–80*, Earthquake Engr. Res. Lab., Calif. Inst. of Tech., Pasadena.

Hudson, D. E., M. D. Trifunac, F. E. Udwadia, A. G. Brady, and A. Vihayaraghavan (1972b). Strong-motion earthquake accelerograms, Fourier Spectra, Volume IV, Part A, *EERL 72–100*, Earthquake Engr. Res. Lab., Calif. Inst. of Tech., Pasadena.

Ishimoto, M. (1932). Echelle d' intensité sismique et acceleration maxima. *Bull. Earthquake Res. Inst., Tokyo Univ.* 10, 614–626.

Kawasumi, H. (1951). Measures of earthquake danger and expectancy of maximum intensity throughout Japan as inferred from the seismic activity in historical times, *Bull. Earthquake Res. Inst., Tokyo Univ.* 29, 469–482.

Lomnitz, C. (1970). Major earthquakes and tsunamis in Chile during the period 1535 to 1955, *Geologishe Rundshau* 59, 938–960.

Medvedev, S. V. (1953). A new seismic scale, *Tr. Geofiz. Inst., Akad. Nauk SSR*, 21, (148).

Medvedev, S. V., W. Sponheuer, and V. Karnik (1963). *Seismiche Scala*, Inst für Bodendynamik und Erdbebenforshung, Jena, 6 pp.

Medvedev, S. V. and W. Sponheuer (1969). Scale of seismic intensity, *Proc. World Conf. Earthquake Engr. A–2, 4th, Santiago, Chile*, 143–153.

Neumann, F. (1954). *Earthquake Intensity and Related Ground Motion*, Univ. Press, Seattle, Washington, 77 pp.

Neumann, F. (1958). Damaging earthquake and blast vibrations in *The Trend in Engineering*, Universtiy of Washington, Seattle, 5–28.

Okamoto, S. (1973). *Introduction to Earthquake Engineering*, John Wiley, New York.

Richter, C. F. (1958). *Elementary Seismology*, Freeman, San Francisco.

Savarensky, Y. F. and D. P. Kirnos (1955). *Elements of Seismology and Seismometry*, Moscow.

Schnabel, P., H. B. Seed and J. Lysmer (1972). Modification of seismograph records for effects of local conditions, *Bull. Seism. Soc. Am.* 62, 1649–1664.

Trifunac, M. D. and D. E. Hudson (1970). Laboratory evaluation and instrument corrections of strong-motion accelerographs, *EERL 70–04*, Earthquake Engr. Res. Lab., Calif. Inst. of Tech., Pasadena.

Trifunac, M. D. (1971). Zero baseline correction of strong-motion accelerograms, *Bull. Seism. Soc. Am.* 61, 343–356.

Trifunac, M. D. (1972). A note on correction of strong-motion accelerograms for instrument response, *Bull. Seism. Soc. Am.* 62, 401–409.

Trifunac, M. D. (1973). A note on scattering of plane *SH* waves by a semi-cylindrical canyon, *Int. J. Earthquake Engr. Struct. Dynamics* 1, 267–281.

Trifunac, M. D., A. G. Brady and D. E. Hudson (1973). Strong-motion earthquake accelerograms, corrected accelerograms and integrated ground velocity and displacement curves, Volume II, Part G, *EERL 73–52*, Earthquake Engr. Res. Lab., Calif. Inst. of Tech., Pasadena.

Trifunac, M. D. and V. W. Lee (1974). A note on the accuracy of computed ground displacements from strong-motion accelerograms, *Bull. Seism. Soc. Am.* 64, 1209–1219.

Trifunac, M. D. and F. E. Udwadia (1974). Variations of strong earthquake ground shaking in the Los Angeles area, *Bull. Seism. Soc. Am.* 64, 1429–1454.

Wong, H. L. and M. D. Trifunac (1974a). Scattering of plane SH waves by a semi-elliptical canyon, *Intern. J. Earthquake Engr. Struct. Dynamics* 3, 157–169.

Wong, H. L. and M. D. Trifunac (1974b). Surface motion of a semi-elliptical alluvial valley for incident plane SH-waves, *Bull. Seism. Soc. Am.* 64, 1389–1408.

Wood, H. O. and F. Neumann (1931). Modified Mercalli Intensity Scale of 1931, *Bull. Seism. Soc. Am.* 21, 277–283.

Earthquake Engineering Research Laboratory
California Institute of Technology
Pasadena, California 91109

Manuscript received May 30, 1974